



TITLE:

Controlling Energy Gaps of pi-Conjugated Polymers by Multi-Fluorinated Boron-Fused Azobenzene Acceptors for Highly Efficient Near-Infrared Emission

AUTHOR(S):

Gon, Masayuki; Wakabayashi, Junko; Nakamura, Masashi; Tanaka, Kazuo; Chujo, Yoshiki

CITATION:

Gon, Masayuki ...[et al]. Controlling Energy Gaps of pi-Conjugated Polymers by Multi-Fluorinated Boron-Fused Azobenzene Acceptors for Highly Efficient Near-Infrared Emission. *Chemistry – An Asian Journal* 2021, 16(6): 696-703

ISSUE DATE:

2021-03

URL:

<http://hdl.handle.net/2433/267495>

RIGHT:

This is the peer reviewed version of the following article: [M. Gon, J. Wakabayashi, M. Nakamura, K. Tanaka, Y. Chujo, *Chem. Asian J.* 2021, 16, 696.], which has been published in final form at <https://doi.org/10.1002/asia.202100037>. This article may be used for non-commercial purposes in accordance with Wiley Terms and Conditions for Use of Self-Archived Versions. This article may not be enhanced, enriched or otherwise transformed into a derivative work, without express permission from Wiley or by statutory rights under applicable legislation. Copyright notices must not be removed, obscured or modified. The article must be linked to Wiley's version of record on Wiley Online Library and any embedding, framing or otherwise making available the article or pages thereof by third parties from platforms, services and websites other than Wiley Online Library must be prohibited.; The full-t ...

Controlling Energy Gaps of π -Conjugated Polymers by Multi-Fluorinated Boron-Fused Azobenzene Acceptors for Highly Efficient Near-Infrared Emission

Masayuki Gon, Junko Wakabayashi, Masashi Nakamura, Kazuo Tanaka and Yoshiki
Chujo*

*Department of Polymer Chemistry, Graduate School of Engineering, Kyoto University
Katsura, Nishikyo-ku, Kyoto 615-8510, Japan*

E-mail: tanaka@poly.synchem.kyoto-u.ac.jp

Key words: boron; conjugated polymer; NIR; solid-state emission; azobenzene

Abstract

We demonstrate that the multi-fluorinated boron-fused azobenzene (BAz) complexes can work as a strong electron acceptor in the electron donor–acceptor (D–A) type π -conjugated polymers. Position-dependent substitution effects were revealed, and the energy level of the lowest unoccupied molecular orbital (LUMO) was critically decreased by fluorination. As a result, the obtained polymers showed near-infrared (NIR) emission ($\lambda_{\text{PL}} = 758\sim 847$ nm) with high absolute photoluminescence quantum yield ($\Phi_{\text{PL}} = 7\sim 23\%$) originating from low-lying LUMO energy levels of the BAz moieties ($-3.94\sim -4.25$ eV). Owing to inherent solid-state emissive properties of the BAz units, deeper NIR emission ($\lambda_{\text{PL}} = 852\sim 980$ nm) was detected in film state. Clear solvent effects prove that the NIR emission is from a charge transfer state originating from a strong D–A interaction. The effects of fluorination on the frontier orbitals are well understandable and predictable by theoretical calculation with density functional theory. This study demonstrates effectiveness of fluorination to the BAz units for producing a strong electron-accepting unit through fine tuning of energy gaps, which can be the promising strategy for designing NIR absorptive and emissive materials.

1. Introduction

Growing demands for high performance and sophisticated materials require finely predictable and controllable design strategies for constructing functional organic compounds. As one of the candidates for designable organic materials, π -conjugated polymers have attracted much attention owing to unique characteristics, such as intense luminescence, high electrical conductivities and good film-formability.^[1] The energy gaps, which are defined as a width of the energy levels between a highest occupied molecular orbital (HOMO) and a lowest unoccupied molecular orbital (LUMO), are critical factors for determining the material properties.^[2] In particular, electron donor–acceptor (D–A) type π -conjugated polymers composed of an alternating array of electron-donor and acceptor moieties have actively studied by feature of easily controllable energy gaps with selecting a donor and an acceptor having desired HOMO and LUMO energy levels as co-monomers, respectively. From these utilities, D–A type π -conjugated polymers have been often applied to organic light-emitting diodes (OLEDs),^[3] organic field effect transistors (OFETs)^[4] and organic photovoltaics (OPVs).^[5] Hence, the development of novel compounds showing electron-donating and accepting abilities is still necessary for preparing D–A type π -conjugated polymers.

Narrow energy gaps of the D–A type π -conjugated polymers can be an origin of absorption and emission in the near-infrared (NIR) region and those were significant for effective use of sun light for organic film solar cells^[6] and bioimaging, optical communication.^[7] In order to construct stable π -conjugated polymers having the narrow energy gaps, reduction of a LUMO energy level of an acceptor unit is required because elevation of a HOMO energy level has a risk of oxidation by air under ambient conditions.^[8] One of the strategies for lowering the LUMO energy level is the

introduction of fluorine substituents to the acceptor.^[9] A fluorine atom intrinsically has high electron negativity and is inactive to chemical substances. Fluorination enhances electron-accepting ability of the organic compounds with good chemical stability.

Recently, we proposed the concept of “element-blocks”, which are structural functional units consisting of various groups of elements, to create advanced materials.^[10] According to the concept, we revealed that boron-fused azobenzene/azomethine (BAz/BAm) complexes, which are “element-blocks” constructed mainly by B, N, O, C and H, worked as a strong acceptor in D–A type π -conjugated polymers with highly efficient emissions including NIR region both in solution and film states.^[11] The film-state emission is valuable because the emission is generally spoiled in a condensed state due to loss of excitation energy via non-radiative pathway mainly by intermolecular π – π interaction.^[12] One of the reasons of the film-state emission could be attributable to the fact that the BAz/BAm complexes potentially enhanced their emission in solid or crystalline states although the emission is critically quenched in the diluted solution state.^[13] These phenomena are known as aggregation-induced emission (AIE)^[14] or crystallization-induced emission enhancement (CIEE) properties.^[15]

Herein, to reinforce electron-accepting ability of the BAz skeleton, we synthesized fluorinated BAz complexes and corresponding D–A type π -conjugated polymers with bithiophene units as a donor. Azobenzene scaffolds were chosen by their inherent higher electron-accepting abilities than azomethine ones to prepare strong acceptors aiming to deeper NIR absorption and emission.^[16] As a result, the LUMO energy levels, which are one of the indexes evaluating the degree of acceptors, were lowered depending on the number of introduced fluorine atoms with the BAz complexes. The obtained D–A type

π -conjugated polymers showed highly-efficient NIR emission ($\lambda_{\text{PL}} = 758\sim 847$ nm) in diluted solution and moderate NIR emission ($\lambda_{\text{PL}} = 852\sim 980$ nm) in film state. The solvent effects evaluated by Lippert-Mataga plots proved that the polymers formed clear D–A interactions. Moreover, the experimental data were in good agreement with the results of theoretical calculations by density functional theory (DFT), and therefore the properties were predictable. We proposed that the high designability of D–A type π -conjugated polymers by fluorination with BAZ complexes was a good example for constructing desired functional materials having controllable energy gaps.

2.1 Synthesis

Scheme 1 shows the syntheses of three types of fluorinated BAz complexes modified with the fluorine atoms at 3,3' positions (**BAz-3F**), 5,5' positions (**BAz-5F**) and both 3,3' and 5,5' positions (**BAz-35F**). The pristine BAz complex, **BAz**, was prepared according to our previous report.^[11b] The fluorinated BAz complexes, **BAz-3F**, **BAz-5F**, and **BAz-35F**, were isolated in high yields by the condensation reaction at 100 °C in toluene between the corresponding azobenzene tridentate ligands, **Az-3F-OH**, **Az-5F-OH** and **Az-35F-OH**, and boron trifluoride diethyl etherate (BF₃·Et₂O), respectively. Next, by using the obtained BAz complexes as monomers, D–A type π-conjugated copolymers with a bithiophene co-monomer were synthesized (Scheme 2 and Table 1). Migita–Kosugi–Stille cross-coupling polymerizations^[17] with **BAz-3F**, **BAz-5F** or **BAz-35F** and 5,5'-bis(trimethylstannyl)-3,3'-didodecyl-2,2'-bithiophene (**BT**) were executed in a catalytic system involving Pd₂(dba)₃ (dba = dibenzylideneacetone) and 2-dicyclohexylphosphino-2',4',6'-triisopropylbiphenyl (**XPhos**) to afford target copolymers, **P-BAz-3F**, **P-BAz-5F** or **P-BAz-35F**, respectively. The synthetic results and polymer data are listed in Table 1. In the case of **P-BAz-5F** and **P-BAz-35F**, high molecular weight polymers were fractionated by high performance liquid chromatography (HPLC) in chloroform as an eluent. In this research, the synthetic polymer data of **P-BAz** were cited or recollected as comparison.^[11b,d,e] All synthesized compounds showed good solubility in common organic solvents such as toluene, chloroform, dichloromethane and tetrahydrofuran, and can be characterized by ¹H, ¹³C, ¹¹B NMR, MS spectra (see Supporting Information). From those characterization data, we concluded that the samples have the objective structures and enough purity for further analyses.

Scheme 1 and 2, Table 1

2.2 Optical measurements

To investigate the position-dependent substituent effect of fluorine atoms on the electronic situation in the ground state, UV–vis absorption measurements were executed in the diluted chloroform solutions (1.0×10^{-5} M) (Figures 1 and S1, Table 2). Interestingly, it was found that the substituent effects worked independently. By substitution at 3,3' positions, the middle transition bands at around 400 nm raised and the energy gaps were preserved (Figures 1A and S1A). On the other hand, the bathochromic shifts of absorption spectra were observed by substitution at 5,5' positions with retaining almost the same spectra shape. Furthermore, the two different effects had additive property and **BAz-35F** showed both substitution effects at 3,3' and 5,5' positions. As a result, **BAz** and **BAz-3F** or **BAz-5F** and **BAz-35F** had the same energy gap, respectively, and the bathochromic shifts of absorption spectra were detected in **BAz-5F** and **BAz-35F** compared to **BAz** and **BAz-3F** (Figures 1A and S1A).

In the D–A type π -conjugated polymers, the absorption bands were located at the longer wavelength regions than those of the corresponding monomers (Figures 1A and 1B). Contrary to the monomers, the value of absorption maximum wavelength (λ_{abs}) was larger in the order of **P-BAz-35F**, **P-BAz-5F**, **P-BAz-3F** and **P-BAz**. Considering that electron-accepting ability of a compound is enhanced by fluorination, the order should be correlated to the strongness of D–A interaction between BAz and bithiophene units. In other words, the ability of BAz acceptors was able to be reinforced by fluorination. Moreover, homogeneous thin films were easily prepared by the commodity spin-coated

method because of good film-formability of the synthesized polymers. The slight bathochromic shifts and broader absorption bands were observed in the film samples compared to those in the diluted solutions (Figures 1B and 1C, Table 1). Owing to the strong D–A interaction leading to a narrow energy gap, the absorption maximum reached a NIR region.

Figure 1 and Table 2

To investigate electronic situations of the BAZ complexes in the excited state, the photoluminescence (PL) properties were evaluated in toluene (1.0×10^{-5} M) and in crystal (Figure 2 and Table 1). It was clearly demonstrated that AIE or CIEE properties were obtained from the complexes. The emission intensity was obviously very weak in solution ($\Phi_{\text{PL}} < 1\%$), whereas intense emission was monitored in crystal ($\Phi_{\text{PL}} = 2\sim 7\%$) (Figure 2A and 2B). Our previous work proposed that the emission quenching in diluted solution should be caused by excitation-driven bending motions which promote non-radiative excitation decay.^[11a,b,13a,18] In solid or crystal packing, those molecular motions are effectively restricted and therefore the emission should be recovered. These situations were often shown in the series of tetracoordinated boron with the azobenzene/azomethine-based tridentate ligands and those compounds also exhibited AIE or CIEE properties.^[11,13]

Contrary to the monomers with environment-sensitive luminescent properties, intense NIR emission was observed from the polymers even in the diluted solution (Figures 2C, 2D and Table 1). The order of the maximum PL wavelength (λ_{PL}) was the same with that of the λ_{abs} . The λ_{PL} and Φ_{PL} were 758~847 nm and 7~23%, respectively,

and it was shown that the BAZ scaffold should be good candidate for NIR-emissive “element-blocks”. Since the excitation-driven molecular motions of the monomeric units would be inhibited by incorporating into the polymer chains,^[11a,b,18] the intense emission should be induced in diluted solution. In the films, the BAZ polymers also showed emission in the NIR region (Figure 2D and Table 1). **P-BAZ** showed intense emission even in the film ($\lambda_{\text{PL}} = 858 \text{ nm}$, $\Phi_{\text{PL}} = 4\%$).^[11b,e] Although the other polymers exhibited weak emission ($\Phi_{\text{PL}} < 1\%$), however the λ_{PLS} were detectable at 916~980 nm. Therefore, it can be said that BAZ unit has potential to targeting to fabricate functional materials showing deeper NIR emission.

Figure 2

2.3 Solvent effects

To obtain more insight about the D–A system originating from strong electron-accepting ability of fluorinated BAZ units, we investigated solvent effects on UV–vis–NIR absorption and PL spectra. All the spectroscopic data are shown in Figures S2 and S3, Tables S1 and S2. From the Lippert–Mataga plot of BAZ monomers in three types of solvents, toluene ($\Delta f = 0.013$, Δf : orientation polarizability), chloroform ($\Delta f = 0.15$) and dichloromethane ($\Delta f = 0.22$), there were almost no correlations between Δf and Stokes shift (ν) ($R^2 < 0.50$, R : correlation coefficient) (Figure 3A). This means that the emission of BAZ monomer is not from a charge transfer (CT) state but from a localized electronic (LE) state. On the other hand, BAZ polymers had good correlations ($R^2 > 0.90$) between Δf and ν by using five types of the solvent including benzene ($\Delta f = 0.003$) and chlorobenzene ($\Delta f = 0.14$) (Figure 3B). Although we also evaluated the

solvent effect in tetrahydrofuran ($\Delta f = 0.21$), the emission band was observed in a position separated from expectation (Figure S4). This might be because nucleophilicity of THF originating from lone pairs of oxygen affected the boron atom in addition to the solvent effect. The slopes of the approximation straight lines in Lippert–Mataga plots were almost the same, while those tended to be decreased by fluorination at 5,5' positions.

Figure 3

During the investigation of the solvent effects, we found generation of the unique absorption band from 700 to 900 nm only from **P-BAz-3F** in benzene/chloroform, toluene/chloroform or dichloromethane/chloroform = 99/1 v/v mixed solutions (Figure S3). From the variable temperature (VT) UV–vis–NIR absorption measurements in toluene/chloroform = 99/1 v/v solution, the band gradually decreased by increasing temperature and subsequently disappeared at 50 °C (Figure S5A). Subsequently, the band was recovered by a cooling process and finally the original spectrum was reproduced at 10 °C (Figure S5B). Interestingly, the hysteresis was observed by holding each temperature for 10 minutes per 10 °C (Figure S5C). The disappearance and reproduction of the band slowly proceeded by monitoring at 40 °C under heating and cooling processes, respectively (Figure S5D). High reversibility was obtained at least five times (Figure S5E) and the hysteresis behavior was reproducible. Furthermore, weak NIR emission at around 950 nm was detectable by excitation at the absorption band (Figure S5F). In the case of the other polymers, **P-BAz**, **P-BAz-5F** and **P-BAz-35F**, there was no unusual temperature dependency regardless of the presence or

absence of fluorine substituents (Figure S6).^[19] The generation of the band in longer wavelength region could be derived from intra- or intermolecular π - π interaction of the polymer chains of **P-BAz-3F** in solution although significant aggregation was not suggested from a dynamic light scattering (DLS) data.^[20] According to the crystal packing structures of **BAz** and **BAz-3F**, it was suggested that the fluorine atom at 3' position is responsible for intermolecular interaction between two molecular fractions of **BAz-3F** (Figures S7~S9, Tables S3 and S4). In particular, there were three short contacts in **BAz-3F** and they were shorter than those of **BAz**, respectively (Figure S9). As a result of the strong binding, the molecules of **BAz-3F** were able to have almost planar conformation in the condensed state. Relatively-planar conformation might be favorable for the formation of assembly followed by the generation of the new absorption band in solution.

2.3 Cyclic voltammetry

To obtain further information on the substituent effect of fluorine atoms on electronic properties, we estimated molecular orbital (MO) energy levels with a cyclic voltammetry (CV). The results are shown in Figure 4 and Table 4. The LUMO energy levels were calculated from the onset of the reduction curve.^[21] In both of **BAz** monomers and polymers, it was found that LUMO energy levels were critically lowered depending on the number of fluorine atoms. In **BAz** monomers, the HOMO energy levels were not able to be estimated from the cyclic voltammograms because the oxidation peaks were out of the potential window. Therefore, we calculated the HOMO energy levels using optical energy gaps ($E_{g,opt}$) obtained from the edge of the UV-vis-NIR absorption spectra (Figure S1). It was shown that fluorination at 3,3' positions,

both HOMO and LUMO energy levels were lowered, whereas at 5,5' positions, only LUMO energy levels were reduced. The similar effect was also monitored in the polymers. The effects had additivity property as shown in the absorption spectra. Accordingly, the electron-accepting ability of BAZ unit in the polymer was enhanced up to -4.25 eV in the LUMO energy level of **P-BAz-35F**. Here, although the oxidation peaks were detectable in the voltammograms of BAZ polymers, the same estimation method as the monomers was adopted because the values should be compared with the same criteria and the substituent effect should be prominently reflected on the LUMO-localized acceptor moiety. The HOMO energy levels evaluated from the oxidation peaks in the voltammograms are shown in Figure S10 and Table S5. In summary, it was confirmed that energy levels of frontier orbitals can be tuned by fluorination at adequate positions.

Figure 4 and Table 3

2.4 Theoretical calculation

To support experimental results, we carried out theoretical calculation with density functional theory (DFT) and time dependent DFT (TD-DFT) at B3LYP/6-311G(d,p) level. The results are summarized in Figures 5, 6, S11, S12 and Tables S6, S7. In monomers, variation tendency of calculated HOMO and LUMO energy levels was precisely matched to the experimental results (Figure 5A). In LUMO, there were little orbital interaction of fluorine atoms both at 3,3' and 5,5' positions, and the only inductive effect of them influenced on energy levels (Figures 5B and S11). Thereby, the step-by-step reduction of LUMO energy levels can be accomplished as increasing the

number of fluorine atoms. On the other hand, in HOMO, the orbital interaction of fluorine atoms existed only at 5,5' positions and electronic donation from the lone pair of fluorine atoms occurred in addition to inductive effect of them (Figure 5B). Hence, elevation of HOMO energy levels was detected in **BAz-5F** and **BAz-35F** (Figure 5A). Consequently, the bathochromic shifts of absorption spectra should be caused by the elevation of HOMO energy levels (Figure 1A and Table S5). We previously reported the similar effect by using bromine atoms as a unique substitution effect at 5,5' positions of BAZ derivatives.^{11d} It was noted the orbital interaction at 3,3' positions was observable in HOMO-2, which led to enhancement of $S_0 \rightarrow S_3$ transition (Figure S11 and Table S6). As a result, rise of the middle absorption band at around 400 nm (Figure 1A) was attributed to the increase of $S_0 \rightarrow S_3$ transition without any disturbance in HOMO-LUMO energy gaps.

Figure 5

To estimate influence of the substituent effect on the electronic structures in polymers, the model compounds having BT units in both sides of the BAZ unit were used for calculations (Figures 6, S12 and Table S7). The calculation with model compounds well helped interpreting the situation of the polymers. Contrary to the monomers, BT units worked as donors and the standard HOMO energy levels were dramatically raised (Figure 6A). In polymers, the orbital interaction of fluorine atoms was still effective as shown in the monomers (Figure 6B and S12) and slight elevation of the HOMO energy levels was detected by fluorination at 5,5' positions (Figure 6A). However, the effect was weakened probably because of large delocalization of HOMO

through the BT units (Figure 6B and S12). Meanwhile, relatively localized LUMO was strongly affected by reduction of energy levels through the inductive effect of fluorine atoms. From those effects, the energy gaps were narrower in the order of **P-BAz-35F**, **P-BAz-5F**, **P-BAz-3F**, **P-BAz** (Figure 6A and Table S7). It can be said that the optical properties of the BAZ polymers can be finely tuned by selecting the substituent positions.

Figure 6

3. Conclusion

Electronic properties of the multi-fluorinated BAZ complexes were evaluated. Distinct and different substitution effects between at 3,3' and 5,5' positions were revealed. Reduction of LUMO energy level was caused by fluorination both at 3,3' and 5,5' positions, whereas elevation of HOMO energy level was brought about only by fluorination at 5,5' positions. The prepared BAZ complexes had a potential to solid-state emission with CIEE properties. Owing to strong D–A interaction of π -conjugated polymers with fluorinated BAZ and BT units, we obtained highly efficient NIR emission. The energy gaps of the π -conjugated polymers were finely tuned depending on fluorinated positions and numbers, as a result, the maximum emission wavelength reached 847 nm in the diluted solution and 980 nm in the film. Additionally, the solvent effect originating from electronic transition attributed to a CT state was clearly shown in the polymers. Interestingly, reversible thermo-responsiveness with generation of the broad absorption band in NIR region was observed in **P-BAz-3F** probably because of interaction between additional fluorine and nitrogen atoms. Furthermore, theoretical calculation well supported the interpretation of the effects gifted by fluorination. Through fluorinated BAZ compounds, it was revealed that the influence of fluorination was systematically understandable and the fluorination was effective in controlling energy gaps of π -conjugated polymers. The study disclosed high potentiality of BAZ compounds as a strong electron acceptor.

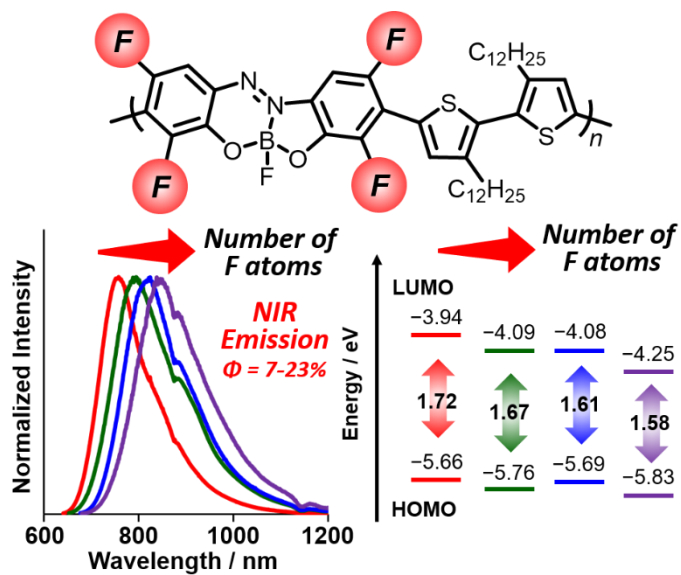
Supporting Information

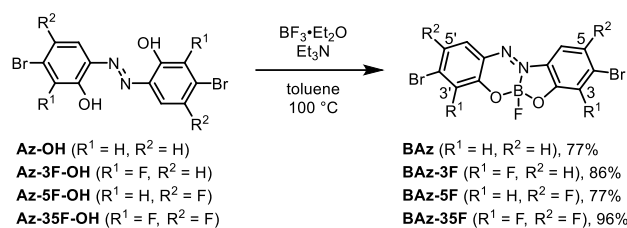
Supporting Information is available from the Wiley Online Library or from the author.

Acknowledgements

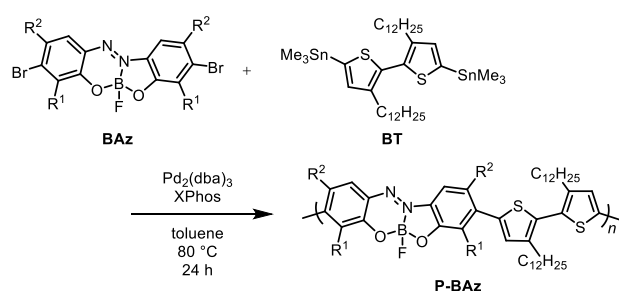
This work was partially supported by the Mizuho Foundation for the Promotion of Sciences, Japan (for M.G.) and a Grant-in-Aid for Early-Career Scientists (for M.G.) (JSPS KAKENHI Grant numbers 20K15334), for Scientific Research (B) (for K.T), (JP17H03067), for Scientific Research on Innovative Areas “New Polymeric Materials Based on Element-Blocks (No.2401)” (JP24102013) and for Challenging Research (Pioneering) (JP18H05356).

TOC





Scheme 1. Syntheses of monomers, **BAz**, **BAz-3F**, **BAz-5F** and **BAz-35F** with the name of substitution positions.



Scheme 2. General procedure for polymer synthesis.

Table 1. Molecular weights and isolated yields of the synthesized polymers

	R^1	R^2	M_n^a /kDa	M_w^a /kDa	M_w/M_n	yield /%
P-BAz-F^b	H	H	21.4	55.6	2.5	85
P-BAz-3F	F	H	13.8	38.8	3.2	54
P-BAz-5F^c	H	F	24.5	48.5	2.0	54
P-BAz-35F^c	F	F	13.4	20.8	1.6	44

^a Determined by a gel permeation chromatography (GPC) with polystyrene standards

^b ref 11b.

^c After fractionated by HPLC.

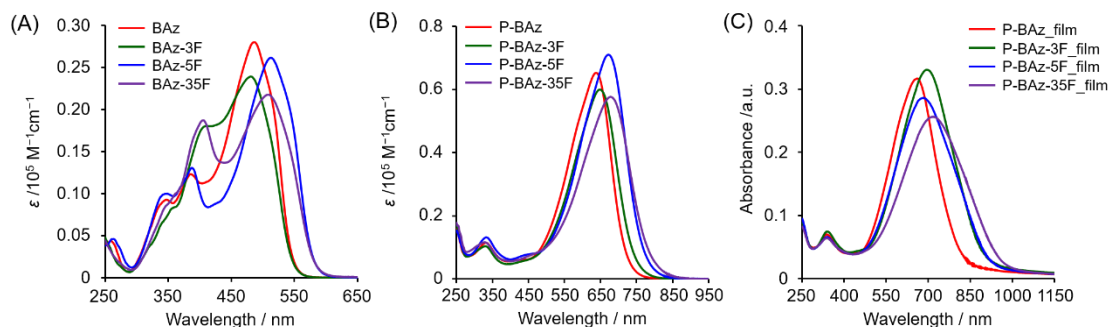


Figure 1. UV-vis absorption spectra of (A) BAZ monomers, (B) polymers in chloroform (1.0×10^{-5} M for monomers, 1.0×10^{-5} M per repeating unit for polymers) and (C) polymer films.

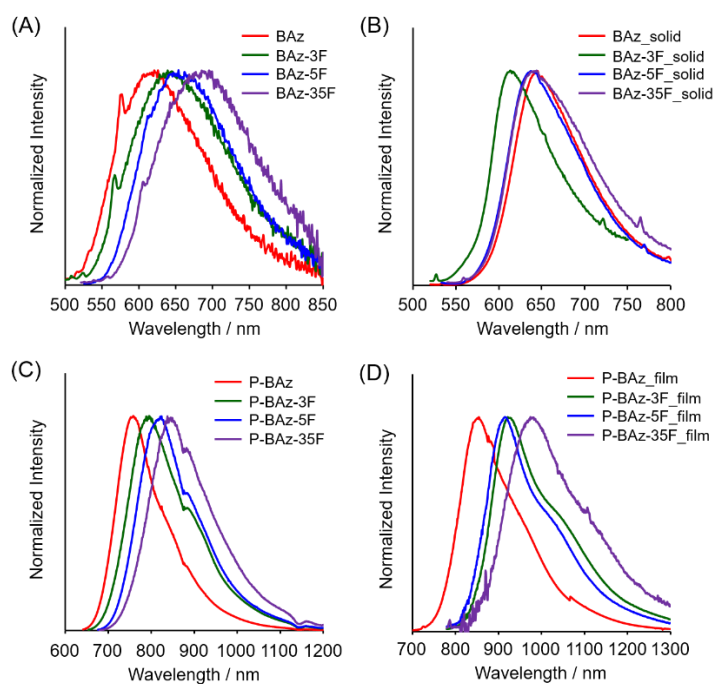


Figure 2. PL spectra of BAZ monomers (A) in chloroform (1.0×10^{-5} M) and (B) in solid state, BAZ polymers (C) in chloroform (1.0×10^{-5} M per repeating unit) and (D) in film state with the excitation light at each absorption maximum.

Table 2. Optical data of the BAz monomers and polymers in solution and solid or film states.

	solution			solid or film		
	λ_{abs}^a /nm	λ_{PL}^b /nm	$\Phi_{\text{PL}}^{b,c}$ /%	λ_{abs}^d /nm	λ_{PL}^d /nm	$\Phi_{\text{PL}}^{c,d}$ /%
BAz	486	621	<1	–	645	7
BAz-3F	480	644	<1	–	613	2
BAz-5F	513	654	<1	–	637	6
BAz-35F	510	688	<1	–	644	2
P-BAz	631	758	23	660	852	4
P-BAz-3F	643	794	8	682	926	<1
P-BAz-5F	666	821	11	698	916	<1
P-BAz-35F	670	847	7	717	980	<1

^a 1.0×10^{-5} M for monomers and 1.0×10^{-5} M per repeating unit for polymers in CHCl_3

^b 1.0×10^{-5} M for monomers and 1.0×10^{-5} M per repeating unit for polymers in toluene, excited at absorption maxima for PL.

^c Absolute PL quantum yield excited at absorption maxima.

^d Solid state for monomers and spin-coated film on the quartz substrate (0.9 cm \times 5 cm) prepared from chloroform solution (0.10 mL, 1000 rpm, concentration: 1.0 mg/0.30 mL) for polymers; excited at absorption maxima for PL.

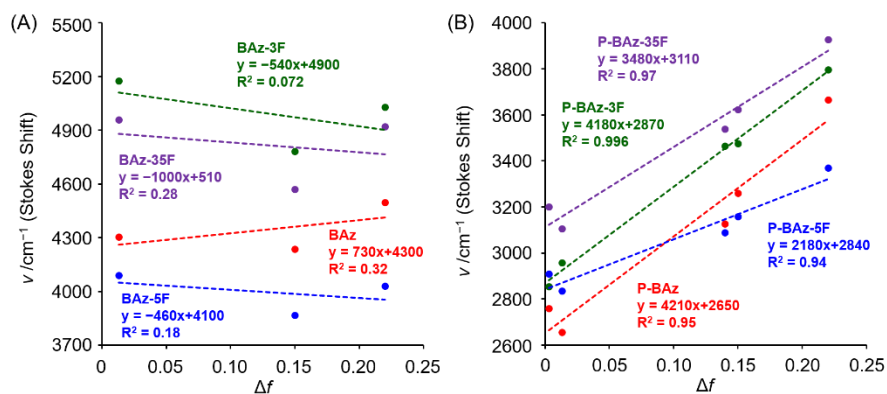


Figure 3. Lippert–Mataga plots of (A) BAz monomers and (B) polymers in the diluted solutions (1.0×10^{-5} M for monomers and 1.0×10^{-5} M per repeating unit for polymers) at room temperature. The formulas of approximate straight lines are described in the same figures. Plotted data are listed in Tables S1 and S2.

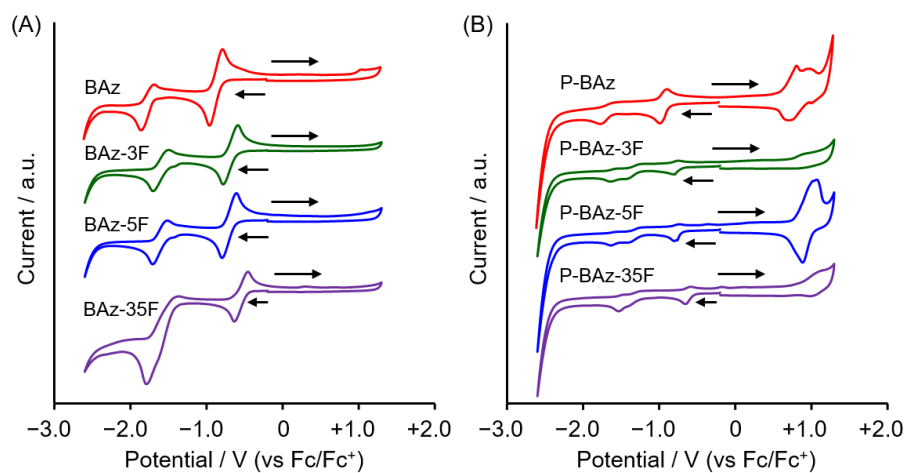


Figure 4. Cyclic voltammograms of (A) BAz monomers and (B) BAz polymers in dichloromethane (1.0×10^{-3} M for monomers, 1.0×10^{-3} M per repeating unit for polymers) containing $n\text{Bu}_4\text{NPF}_6$ (0.10 M) at room temperature with a scan rate of 0.1 V s^{-1} (negative scan). The black arrows denote sweep directions (negative scan).

Table 3. Energy levels of molecular orbitals of BAz monomers and polymers

	$\lambda_{\text{abs,edge}}^a$ /nm	$E_{\text{g,opt}}^b$ /eV	$E_{\text{onset}}^{\text{red}c}$ /V	E_{LUMO}^d /eV	E_{HOMO}^d /eV
BAz	546	2.27	-0.80	-4.00	-6.27
BAz-3F	546	2.27	-0.61	-4.19	-6.46
BAz-5F	579	2.14	-0.63	-4.17	-6.31
BAz-35F	579	2.14	-0.46	-4.34	-6.48
P-BAz	722	1.72	-0.86	-3.94	-5.66
P-BAz-3F	743	1.67	-0.71	-4.09	-5.76
P-BAz-5F	769	1.61	-0.72	-4.08	-5.69
P-BAz-35F	787	1.58	-0.55	-4.25	-5.83

^a In chloroform (1.0×10^{-5} M for monomers, 1.0×10^{-5} M per repeating unit for polymers), estimated from Figure S1.

^b $E_{\text{g,opt}} = 1240/\lambda_{\text{abs,edge}}$.

^c In dichloromethane (1.0×10^{-3} M for monomers, 1.0×10^{-3} M per repeating unit for polymers) containing $n\text{Bu}_4\text{NPF}_6$ (0.10 M) at room temperature with a scan rate of 0.1 V s^{-1} (negative scan).

^d $E_{\text{LUMO}} = -(4.8 - E_{\text{onset}}^{\text{red}})$ (eV),^[21] $E_{\text{HOMO}} = E_{\text{LUMO}} - E_{\text{g,opt}}$.

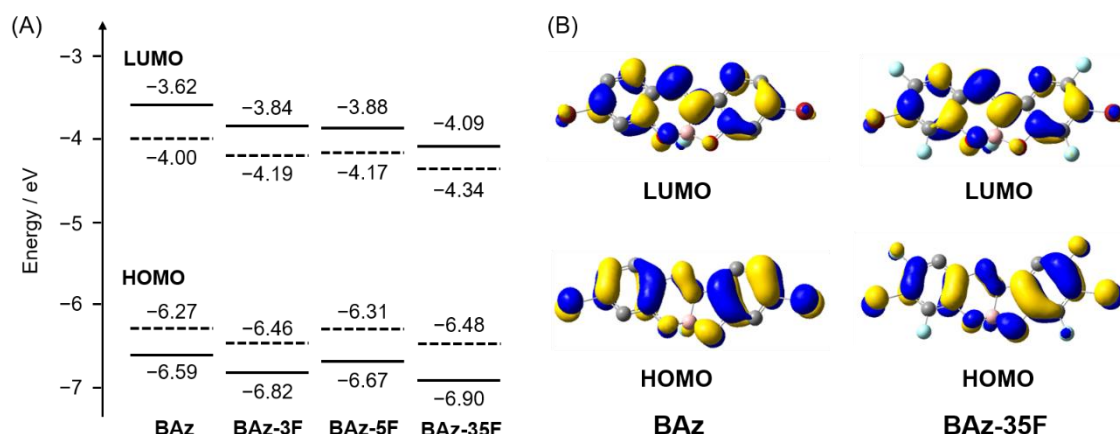


Figure 5. (A) Energy diagrams of BAz monomers (solid line: from DFT calculation, dotted line: from CV and UV-vis absorption spectra, Table 3), (B) HOMO and LUMO of BAz and BAz-35F obtained from DFT calculations (isovalue = 0.03). Hydrogens were omitted for clarity.

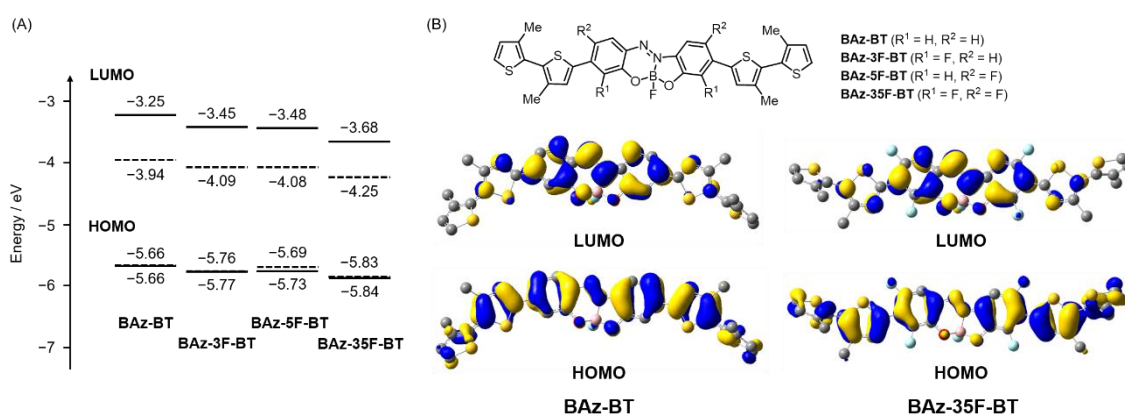


Figure 6. (A) Energy diagrams of model compounds of BAz polymers (solid line: from DFT calculation of model compounds, dotted line: from CV and UV-vis-NIR absorption spectra of BAz polymers, Table 3) and (B) chemical structures of model compounds, and HOMO and LUMO of BAz-BT and BAz-BT-35F with DFT calculations (isovalue = 0.025). Hydrogens were omitted for clarity.

References

- [1] a) A. X. Chen, A. T. Kleinschmidt, K. Choudhary, D. J. Lipomi, *Chem. Mater.* **2020**, *32*, 7582–7601; b) L. Giraud, S. Grelier, E. Grau, G. Hadziioannou, C. Brochon, H. Cramail, E. Cloutet, *J. Mater. Chem. C* **2020**, *8*, 9792–9810; c) R. H. Friend, R. W. Gymer, A. B. Holmes, J. H. Burroughes, R. N. Marks, C. Taliani, D. D. C. Bradley, D. A. D. Santos, J. L. Brédas, M. Lögdlund, W. R. Salaneck, *Nature* **1999**, *397*, 121–128; d) A. C. Grimsdale, K. Leok Chan, R. E. Martin, P. G. Jokisz, A. B. Holmes, *Chem. Rev.* **2009**, *109*, 897–1091; e) A. P. Kulkarni, C. J. Tonzola, A. Babel, S. A. Jenekhe, *Chem. Mater.* **2004**, *16*, 4556–4573; f) H. Zhou, L. Yang, W. You, *Macromolecules* **2012**, *45*, 607–632.
- [2] a) H. Watanabe, K. Tanaka, Y. Chujo, *J. Org. Chem.* **2019**, *84*, 2768–2778; b) H. Watanabe, M. Hirose, K. Tanaka, K. Tanaka, Y. Chujo, *Polym. Chem.* **2016**, *7*, 3674–3680; c) H. Watanabe, J. Ochi, K. Tanaka, Y. Chujo, *Eur. J. Org. Chem.* **2020**, 777–783; d) Z. Genene, W. Mammo, E. Wang, M. R. Andersson, *Adv. Mater.* **2019**, *31*, 1807275; e) P. Cheng, Y. Yang, *Acc. Chem. Res.* **2020**, *53*, 1218–1228; f) B.-G. Kim, X. Ma, C. Chen, Y. Ie, E. W. Coir, H. Hashemi, Y. Aso, P. F. Green, J. Kieffer, J. Kim, *Adv. Funct. Mater.* **2013**, *23*, 439–445.
- [3] B. C. Thompson, L. G. Madrigal, M. R. Pinto, T.-S. Kang, K. S. Schanze, J. R. Reynolds, *J. Polym. Sci. A Polym. Chem.* **2005**, *43*, 1417–1431; b) G. Tregnago, T. T. Steckler, O. Fenwick, M. R. Andersson, F. Cacialli, *J. Mater. Chem. C* **2015**, *3*, 2792–2797; c) T. T. Steckler, M. J. Lee, Z. Chen, O. Fenwick, M. R. Andersson, F. Cacialli, H. Sirringhaus, *J. Mater. Chem. C* **2014**, *2*, 5133–5141; d) T. T. Steckler, O. Fenwick, T. Lockwood, M. R. Andersson, F. Cacialli, *Macromol. Rapid Commun.* **2013**, *34*, 990–996.

- [4] a) H.-H. Liu, S.-L. Chang, K.-H. Huang, F.-Y. Cao, K.-Y. Cheng, H.-S. Sun, Y.-Y. Lai, Y.-J. Cheng, *Macromolecules* **2020**, *53*, 7740–7748; b) D. Shi, Z. Liu, J. Ma, Z. Zhao, L. Tan, G. Lin, J. Tian, X. Zhang, G. Zhang, D. Zhang, *Adv. Funct. Mater.* **2020**, *30*, 1910235; c) C.-H. Chen, Y. Wang, T. Michinobu, S.-W. Chang, Y.-C. Chiu, C.-Y. Ke, G.-S. Liou, *ACS Appl. Mater. Interfaces* **2020**, *12*, 6144–6150; d) S. Jeon, C. Sun, S. H. Yu, S.-K. Kwon, D. S. Chung, Y. J. Jeong, Y.-H. Kim, *ACS Appl. Mater. Interfaces* **2020**, *12*, 2743–2752.
- [5] a) H. L. T. Mai, N. T. T. Truong, T. Q. Nguyen, B. K. Doan, D. H. Tran, L.-T. T. Nguyen, W. Lee, J. W. Jung, M. H. Hoang, H. P. K. Huynh, C. D. Tran, H. T. Nguyen, *New J. Chem.* **2020**, *44*, 16900–16912; b) S. Ma, S. Wu, J. Zhang, Y. Song, H. Tang, K. Zhang, F. Huang, Y. Cao, *ACS Appl. Mater. Interfaces* **2020**, *12*, 51776–51784; c) S. Samson, J. Rech, L. Perdigón-Toro, Z. Peng, S. Shoaee, H. Ade, D. Neher, M. Stolterfoht, W. You, *ACS Appl. Polym. Mater.* **2020**, *2*, 5300–5308; d) R. Zhao, J. Liu, L. Wang, *Acc. Chem. Res.* **2020**, *53*, 1557–1567.
- [6] a) G. Qian, Z. Y. Wang, *Chem. Asian J.* **2010**, *5*, 1006–1029; b) Y. Li, J.-D. Lin, X. Che, Y. Qu, F. Liu, L.-S. Liao, S. R. Forrest, *J. Am. Chem. Soc.* **2017**, *139*, 17114–17119.
- [7] a) H. Xiang, J. Cheng, X. Ma, X. Zhou, J. J. Chruma, *Chem. Soc. Rev.* **2013**, *42*, 6128–6185; b) L. Yuan, W. Lin, K. Zheng, L. He, W. Huang, *Chem. Soc. Rev.* **2013**, *42*, 622–661; c) A. Zampetti, A. Minotto, F. Cacialli, *Adv. Funct. Mater.* **2019**, *29*, 1807623; d) N. Suzuki, M. Wakioka, F. Ozawa, S. Yamaguchi, *Asian J. Org. Chem.* **2020**, *9*, 1326–1332; e) S. Wang, J. Liu, G. Feng, L. G. Ng, B. Liu, *Adv. Funct. Mater.* **2019**, *29*, 1808365; f) C. Rohatgi, T. Harada, E. F. Need, M. Krasowska, D. A. Beattie, G. D. Dickenson, T. A. Smith, T. W. Kee, *ACS Appl.*

- Nano Mater.* **2018**, *1*, 4801–4808; g) L. Chen, D. Chen, Y. Jiang, J. Zhang, J. Yu, C. C. DuFort, S. R. Hingorani, X. Zhang, C. Wu, D. T. Chiu, *Angew. Chem. Int. Ed.* **2019**, *58*, 7008–7012; *Angew. Chem.* **2019**, *131*, 7082–7086; h) G. Deng, X. Peng, Z. Sun, W. Zheng, J. Yu, L. Du, H. Chen, P. Gong, P. Zhang, L. Cai, B. Z. Tang, *ACS Nano* **2020**, *14*, 11452–11462; i) P. R. Neumann, D. L. Crossley, M. Turner, M. Ingleson, M. Green, J. Rao, L. A. Dailey, *ACS Appl. Mater. Interfaces* **2019**, *11*, 46525–46535; j) X. Ma, X. Jiang, S. Zhang, X. Huang, Y. Cheng, C. Zhu, *Polym. Chem.* **2013**, *4*, 4396–4404; k) R. Yoshii, A. Nagai, Y. Chujo, *J. Polym. Sci. A Polym. Chem.* **2010**, *48*, 5348–5356; l) R. Yoshii, A. Nagai, K. Tanaka, Y. Chujo, *J. Polym. Sci. A Polym. Chem.* **2013**, *51*, 1726–1733.
- [8] a) D. M. de Leeuw, M. M. J. Simenon, A. R. Brown, R. E. F. Einerhand, *Synth. Met.* **1997**, *87*, 53–59; b) V. Viswanathan, A. Rao, U. Pandey, A. V. Kesavan, P. Ramamurthy, *Beilstein J. Org. Chem.* **2017**, *13*, 863–873.
- [9] a) F. Babudri, G. M. Farinola, F. Naso, R. Ragni, *Chem. Commun.* **2007**, 1003–1022; b) H. Zhou, L. Yang, A. C. Stuart, S. C. Price, S. Liu, W. You, *Angew. Chem. Int. Ed.* **2011**, *50*, 2995–2998; *Angew. Chem.* **2011**, *123*, 3051–3054; c) H. J. Son, W. Wang, T. Xu, Y. Liang, Y. Wu, G. Li, L. Yu, *J. Am. Chem. Soc.* **2011**, *133*, 1885–1894; d) D. Deng, Y. Zhang, J. Zhang, Z. Wang, L. Zhu, J. Fang, B. Xia, Z. Wang, K. Lu, W. Ma, Z. Wei, *Nat. Commun.* **2016**, *7*, 13740; e) M. Zhang, X. Guo, S. Zhang, J. Hou, *Adv. Mater.* **2014**, *26*, 1118–1123; f) N. Wang, Z. Chen, W. Wei, Z. Jiang, *J. Am. Chem. Soc.* **2013**, *135*, 17060–17068; g) T. Lei, J.-H. Dou, Z.-J. Ma, C.-H. Yao, C.-J. Liu, J.-Y. Wang, J. Pei, *J. Am. Chem. Soc.* **2012**, *134*, 20025–20028; h) T. Lei, X. Xia, J.-Y. Wang, C.-J. Liu, J. Pei, *J. Am. Chem. Soc.* **2014**, *136*, 2135–2141; i) D. Liu, W. Zhao, S. Zhang, L. Ye, Z. Zheng, Y. Cui, Y. Chen, J.

- Hou, *Macromolecules* **2015**, *48*, 5172–5178; j) P. Lei, B. Zhang, Y. Chen, Y. Geng, Q. Zeng, A. Tang, E. Zhou, *ACS Appl. Mater. Interfaces* **2020**, *12*, 38451–38459.
- [10] a) Y. Chujo, K. Tanaka, *Bull. Chem. Soc. Jpn.* **2015**, *88*, 633–643; b) M. Gon, K. Tanaka, Y. Chujo, *Polym. J.* **2018**, *50*, 109–126; c) K. Tanaka, Y. Chujo, *Polym. J.* **2020**, *52*, 555–566.
- [11] a) M. Gon, K. Tanaka, Y. Chujo, *Chem. Rec.* **2021**, *21*, DOI: 10.1002/tcr.202000156; b) M. Gon, K. Tanaka, Y. Chujo, *Angew. Chem. Int. Ed.* **2018**, *57*, 6546–6551; *Angew. Chem.* **2018**, *130*, 6656–6661; c) S. Ohtani, M. Gon, K. Tanaka, Y. Chujo, *Macromolecules* **2019**, *52*, 3387–3393; d) M. Gon, J. Wakabayashi, K. Tanaka, Y. Chujo, *Chem. Asian J.* **2019**, *14*, 1837–1843; e) M. Gon, J. Wakabayashi, M. Nakamura, K. Tanaka, Y. Chujo, *Macromol. Rapid Commun.* **2020**, 2000566. DOI: 10.1002/marc.202000566.
- [12] S. A. Jenekhe and J. A. Osaheni, *Science* **1994**, *265*, 765–768.
- [13] a) S. Ohtani, M. Gon, K. Tanaka, Y. Chujo, *Chem. Eur. J.* **2017**, *23*, 11827–11833; b) S. Ohtani, M. Nakamura, M. Gon, K. Tanaka, Y. Chujo, *Chem. Commun.* **2020**, *56*, 6575–6578; c) S. Ohtani, M. Gon, K. Tanaka, Y. Chujo, *Crystals* **2020**, *10*, 615; d) S. Ohtani, Y. Takeda, M. Gon, K. Tanaka, Y. Chujo, *Chem. Commun.* **2020**, *56*, 15305–15308; e) J. Wakabayashi, M. Gon, K. Tanaka, Y. Chujo, *Macromolecules* **2020**, *53*, 4524–4532.
- [14] a) J. Mei, N. L. C. Leung, R. T. K. Kwok, J. W. Y. Lam, B. Z. Tang, *Chem. Rev.* **2015**, *115*, 11718–11940; b) J. Luo, Z. Xie, J. W. Y. Lam, L. Cheng, H. Chen, C. Qiu, H. S. Kwok, X. Zhan, Y. Liu, D. Zhu, B. Z. Tang, *Chem. Commun.* **2001**, 1740–1741.

- [15] Y. Dong, J. W. Y. Lam, A. Qin, Z. Li, J. Sun, H. H.-Y. Sung, I. D. Williams, B. Z. Tang, *Chem. Commun.* **2007**, 40–42.
- [16] a) C.-L. Liu, F.-C. Tsai, C.-C. Chang, K.-H. Hsieh, J.-L. Lin, W.-C. Chen, *Polymer* **2005**, *46*, 4950–4957; b) Y. Wang, J. Ma, Y. Jiang, *J. Phys. Chem. A* **2005**, *109*, 7197–7206.
- [17] a) M. Kosugi, K. Sasazawa, Y. Shimizu, T. Migita, *Chem. Lett.* **1977**, *6*, 301–302;
b) D. Milstein, J. K. Stille, *J. Am. Chem. Soc.* **1978**, *100*, 3636–3638.
- [18] M. Gon, K. Tanaka, Y. Chujo, *Bull. Chem. Soc. Jpn.* **2019**, *92*, 7–18.
- [19] X. Long, Z. Ding, C. Dou, J. Zhang, J. Liu, L. Wang, *Adv. Mater.* **2016**, *28*, 6504–6508.
- [20] K. Suenaga, K. Uemura, K. Tanaka, Y. Chujo, *Polym. Chem.* **2020**, *11*, 1127–1133.
- [21] a) J. Pommerehne, H. Vestweber, W. Guss, R. F. Mahrt, H. Bässler, M. Porsch, J. Daub, *Adv. Mater.* **1995**, *7*, 551–554; b) C. M. Cardona, W. Li, A. E. Kaifer, D. Stockdale, G. C. Bazan, *Adv. Mater.* **2011**, *23*, 2367–2371.

Supporting Information

**Controlling Energy Gaps of π -Conjugated Polymers by
Multi-Fluorinated Boron-Fused Azobenzene Acceptors for Highly
Efficient Near-Infrared Emission**

Masayuki Gon, Junko Wakabayashi, Masashi Nakamura, Kazuo Tanaka* and Yoshiki Chujo

*Department of Polymer Chemistry, Graduate School of Engineering, Kyoto University Katsura,
Nishikyo-ku, Kyoto 615-8510, Japan*

E-mail: tanaka@poly.synchem.kyoto-u.ac.jp

Contents	page
General	S-3
Materials	S-4
Synthetic procedures and characterization	S-5
Enlarged views of UV-vis-NIR absorption spectra	S-41
Solvent effect of monomers	S-42
Solvent effect of polymers	S-43
Variable temperature absorption spectra and PL spectra	S-46
Single crystal X-ray structure analysis	S-48
Intermolecular interaction in BAz and BAz-3F crystals	S-52
Cyclic voltammerty	S-53
Computational details for theoretical calculation	S-54
Results of representative transitions of BAz complexes	S-54
Molecular orbitals of BAz monomers	S-55
Selected Kohn-Sham orbitals of model compounds	S-56
References	S-57

General

^1H , ^{13}C and ^{11}B NMR spectra were recorded on JEOL EX400 and AL400 instruments at 400, 100 and 128 MHz, respectively. Samples were analyzed in CDCl_3 , CD_2Cl_2 , $\text{DMSO}-d_6$ and $\text{THF}-d_8$. The chemical shift values were expressed relative to Me_4Si for ^1H and ^{13}C NMR as an internal standard in CDCl_3 and $\text{BF}_3\cdot\text{Et}_2\text{O}$ for ^{11}B NMR as a capillary standard. Analytical thin layer chromatography (TLC) was performed with silica gel 60 Merck F254 plates. Column chromatography was performed with Wakogel[®] C-300 silica gel. Recyclable preparative high-performance liquid chromatography (HPLC) was carried out on a Japan Analytical Industry Model LaboACE LC-5060 (JAIGEL-2.5H and 3HH columns) using CHCl_3 as an eluent. High-resolution mass (HRMS) spectrometry was performed at the Technical Support Office (Department of Synthetic Chemistry and Biological Chemistry, Graduate School of Engineering, Kyoto University), and the HRMS spectra were obtained on a Thermo Fisher Scientific EXACTIVE spectrometer for electrospray ionization (ESI) and a Thermo Fisher Scientific EXACTIVE spectrometer for atmospheric pressure chemical ionization (APCI). UV-vis-NIR spectra were recorded on a SHIMADZU UV-3600i plus spectrophotometer, and samples were analyzed at room temperature. Fluorescence emission spectra were recorded on a HORIBA Scientific Fluorolog-3 spectrofluorometer and samples were analyzed at room temperature with PMT P928 (250–810 nm) and DSS-IGA (810–1550 nm) as detectors. Absolute photoluminescence quantum efficiency (Φ_{PL}) was recorded on a Hamamatsu Photonics Quantaaurus-QY Plus C13534-01. Cyclic voltammetry (CV) was carried out on a BASALS-Electrochemical-Analyzer Model 600D with a grassy carbon working electrode, a Pt counter electrode, an Ag/AgCl reference electrode, and the ferrocene/ferrocenium (Fc/Fc^+) external reference at a scan rate of 0.1 V s^{-1} . X-ray crystallographic analysis was carried out by Rigaku R-Axis RAPID-F graphite-monochromated $\text{MoK}\alpha$ radiation diffractometer with imaging plate or Rigaku Saturn 724+ with MicroMax-007HF CCD diffractometer with Varimax Mo optics using graphite-monochromated $\text{MoK}\alpha$ radiation. A symmetry-related absorption correction was carried out by using the program ABSCOR.^[1] The analysis was carried out with direct methods (SHELX-97^[2]) using Yadokari-XG.^[3] The program ORTEP3^[4] and Mercury-4.2.0 were used to generate the X-ray structural diagram.

Materials

Commercially available compounds used without purification:

3-Fluoro-2-methoxyaniline (**3F-a**) (Combi-Blocks, Inc.)

5-Fluoro-2-methoxyaniline (**5F-a**) (Tokyo Chemical Industry Co, Ltd.)

3,5-Difluoro-2-methoxyaniline (**35F-a**) (Fluorochem Ltd.)

N-Bromosuccinimide (NBS) (FUJIFILM Wako Pure Chemical Industries, Ltd.)

Manganese(IV) Oxide, Powder (MnO₂) (FUJIFILM Wako Pure Chemical Industries, Ltd.)

Boron tribromide (17% in CH₂Cl₂, ca. 1 M) (BBr₃ in CH₂Cl₂) (Tokyo Chemical Industry Co, Ltd.)

Boron trifluoride diethyl etherate (≥46% BF₃ basis) (BF₃·Et₂O) (Sigma-Aldrich Co. LLC.)

Pd₂(dba)₃ (dba = dibenzylideneacetone) (Tokyo Chemical Industry Co, Ltd.)

2-Dicyclohexylphosphino-2',4',6'-triisopropylbiphenyl (XPhos) (Strem Chemicals, Inc.)

Commercially available solvents:

MeOH (FUJIFILM Wako Pure Chemical Industries, Ltd.), THF (FUJIFILM Wako Pure Chemical Industries, Ltd.), toluene (deoxidized grade, FUJIFILM Wako Pure Chemical Industries, Ltd.), CH₂Cl₂ (deoxidized grade, FUJIFILM Wako Pure Chemical Industries, Ltd.) used without purification. Et₃N (Kanto Chemical Co., Inc.), purified by passage through solvent purification columns under N₂ pressure.^[5]

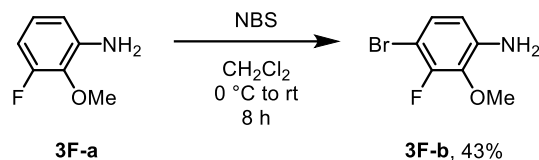
Compounds prepared as described in the literatures:

BAz^[6]

5,5'-Bis(trimethylstannyl)-3,3'-didodecyl-2,2'-bithiophene (**BT**)^{[7],[8]}

Synthetic Procedures and Characterization

Synthesis of 3F-b



A mixture of 3-fluoro-2-methoxyaniline (**3F-a**) (2.13 g, 15.1 mmol), NBS (2.69 g, 15.1 mmol) and dichloromethane (38 mL) was placed in a round-bottom flask equipped with a magnetic stirring bar. The mixture was reacted at room temperature for 8 h. After adding H₂O, the organic layer was extracted with CH₂Cl₂, and washed with brine. The organic layer was dried over MgSO₄. After filtration, the solvent was evaporated. The residue was semi-purified by column chromatography on SiO₂ (hexane/CH₂Cl₂ = 1/2 v/v as an eluent). The residue was purified by reprecipitation by hexane from the CHCl₃ solution at -78 °C to afford **3F-b** (1.42 g, 6.46 mmol, 43%) as a light brown solid.

$R_f = 0.37$ (hexane/CH₂Cl₂ = 1/2 v/v). ¹H NMR (CDCl₃, 400 MHz) δ 7.00 (dd, $J = 8.8, 7.3$ Hz, 1H), 6.41 (dd, $J = 8.8, 1.4$ Hz, 1H), 3.92–3.91 (m, 5H) ppm; ¹³C NMR (CDCl₃, 100 MHz) δ 152.7 (d, $J_{\text{C-F}} = 243$ Hz), 140.6 (d, $J_{\text{C-F}} = 5.8$ Hz), 135.7 (d, $J_{\text{C-F}} = 1.4$ Hz), 126.9 (d, $J_{\text{C-F}} = 1.7$ Hz), 111.3 (d, $J_{\text{C-F}} = 3.3$ Hz), 96.8 (d, $J_{\text{C-F}} = 19.7$ Hz), 60.9 (d, $J_{\text{C-F}} = 5.8$ Hz) ppm. HRMS (APCI) calcd. for C₇H₈BrFN₂O₂ [M+H]⁺: 219.9768, found: 219.9769.

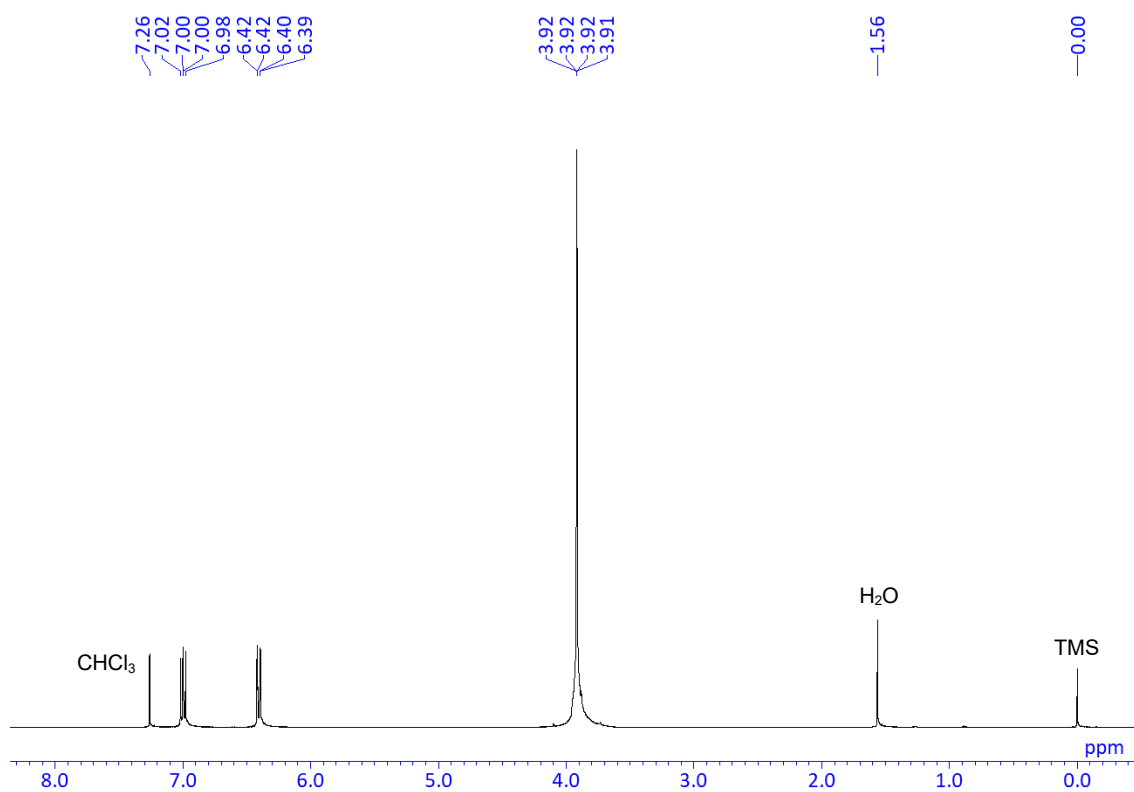


Chart S1. ^1H NMR spectrum of **3F-b** in CDCl_3 , 400 MHz.

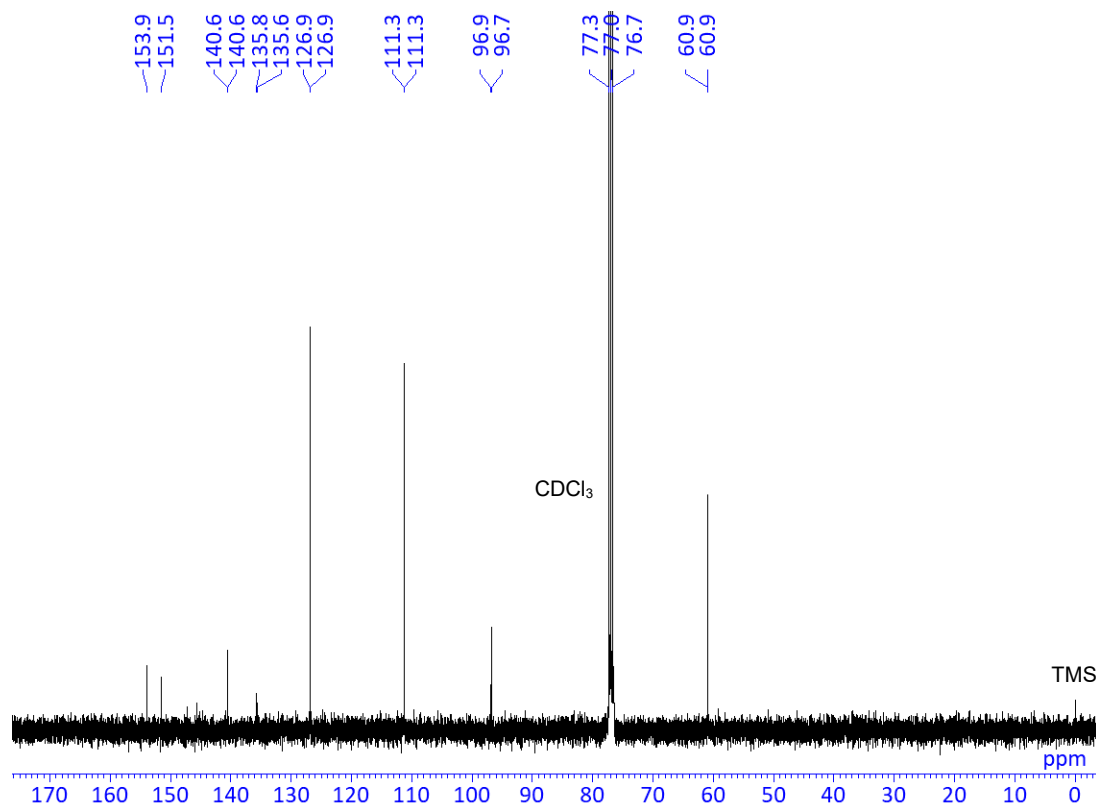
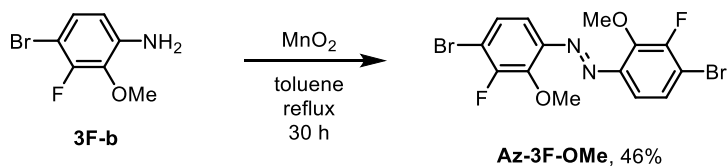


Chart S2. ^{13}C NMR spectrum of **3F-b** in CDCl_3 , 100 MHz.

Synthesis of Az-3F-OMe



A mixture of **3F-b** (1.41 g, 6.40 mmol), MnO_2 (2.23 g, 25.6 mmol) and toluene (30 mL) was placed in a round-bottom flask equipped with a magnetic stirring bar. The mixture was reacted at reflux temperature for 30 h. After the reaction, MnO_2 was removed by filtration and washed with CHCl_3 . The residue was purified by recrystallization with MeOH (poor solvent) and CHCl_3 (good solvent) to afford **Az-3F-OMe** (642 mg, 1.47 mmol, 46%) as an orange solid.

^1H NMR (CDCl_3 , 400 MHz) δ 7.38 (dd, $J = 9.0, 1.7$ Hz, 2H), 7.30 (dd, $J = 9.0, 6.4$ Hz, 2H), 4.18 (d, $J = 1.2$ Hz, 6H) ppm; ^{13}C NMR (CDCl_3 , 100 MHz) δ 153.4 (d, $J_{\text{C-F}} = 247$ Hz), 147.3 (d, $J_{\text{C-F}} = 13.2$ Hz), 145.8 (d, $J_{\text{C-F}} = 2.5$ Hz), 126.7, 113.6 (d, $J_{\text{C-F}} = 18.9$ Hz), 112.9 (d, $J_{\text{C-F}} = 4.1$ Hz), 63.7 (d, $J_{\text{C-F}} = 3.3$ Hz) ppm. HRMS (ESI) calcd. for $\text{C}_{14}\text{H}_{11}\text{Br}_2\text{F}_2\text{N}_2\text{O}_2$ $[\text{M}+\text{H}]^+$: 434.9150, found: 434.9151.

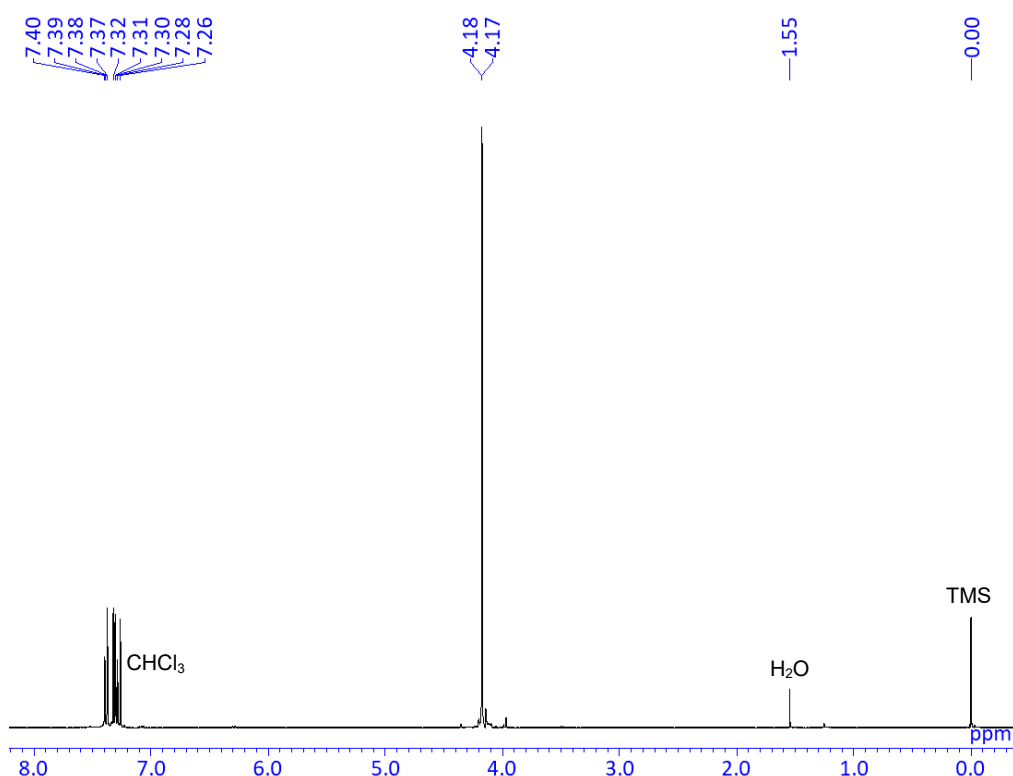


Chart S3. ^1H NMR spectrum of Az-3F-OMe in CDCl_3 , 400 MHz.

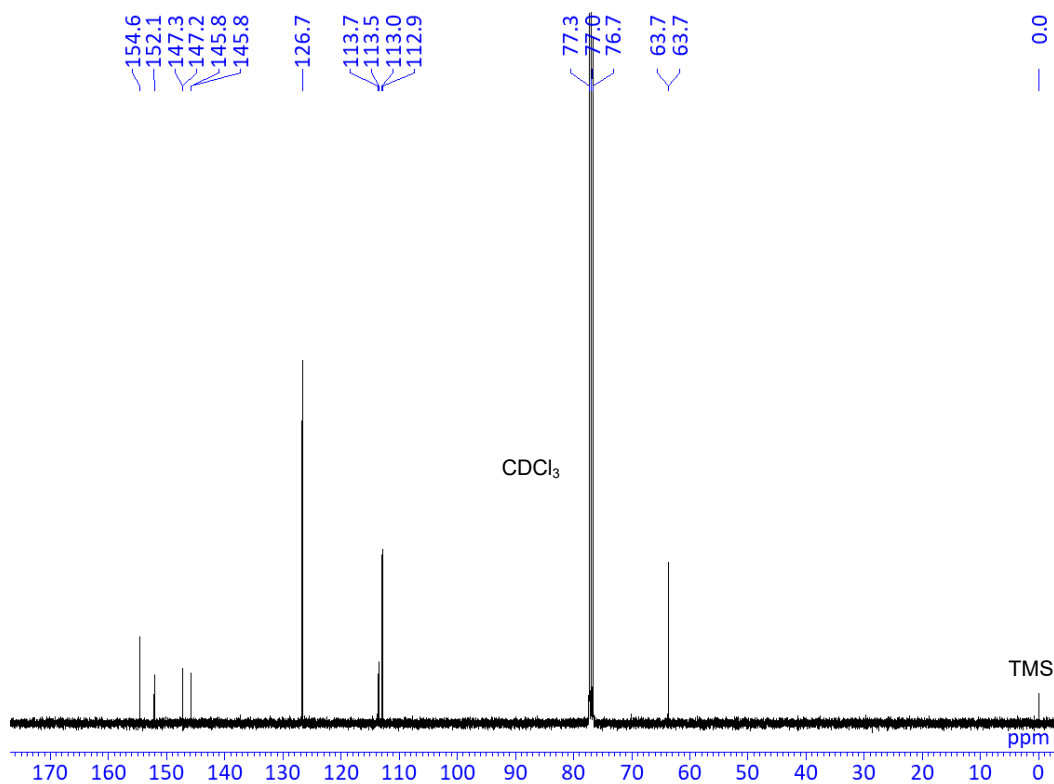
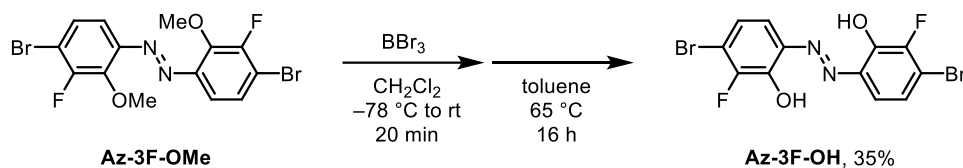


Chart S4. ^{13}C NMR spectrum of Az-3F-OMe in CDCl_3 , 100 MHz.

Synthesis of Az-3F-OH



Az-3F-OMe (626 mg, 1.44 mmol) was placed in a round-bottom flask equipped with a magnetic stirring bar. After degassing and filling N₂ three times, CH₂Cl₂ (36 mL) was added to the flask. After cooling the mixture to -78 °C, BBr₃ (1 M in CH₂Cl₂, 7.18 mL, 7.18 mmol) was dropwise added. The reaction was carried out at room temperature for 20 min. Then toluene (36 mL) was added to the flask and heated to 65 °C for 16 h. After the reaction, MeOH was carefully added at 0 °C for quenching the reaction. Then, the target compound was immediately precipitated. The solid was collected and washed with MeOH and CHCl₃ to afford **Az-3F-OH** (205 mg, 0.502 mmol, 35%) as a yellow solid.

¹H NMR (DMSO-*d*₆, 400 MHz) δ 11.54 (br, 2H), 7.74 (dd, *J* = 8.8, 1.4 Hz 2H), 7.27 (dd, *J* = 9.0, 6.8 Hz, 2H) ppm; ¹³C NMR (DMSO-*d*₆, 100 MHz) δ 149.1 (d, *J*_{C-F} = 241 Hz), 144.8 (d, *J*_{C-F} = 14.0 Hz), 139.8 (d, *J*_{C-F} = 3.3 Hz), 122.0, 115.8 (d, *J*_{C-F} = 3.3 Hz), 112.7 (d, *J*_{C-F} = 18.1 Hz) ppm. HRMS (ESI) calcd. for C₁₂H₅Br₂F₂N₂O₂ [M-H]⁻: 404.8691, found: 404.8796.

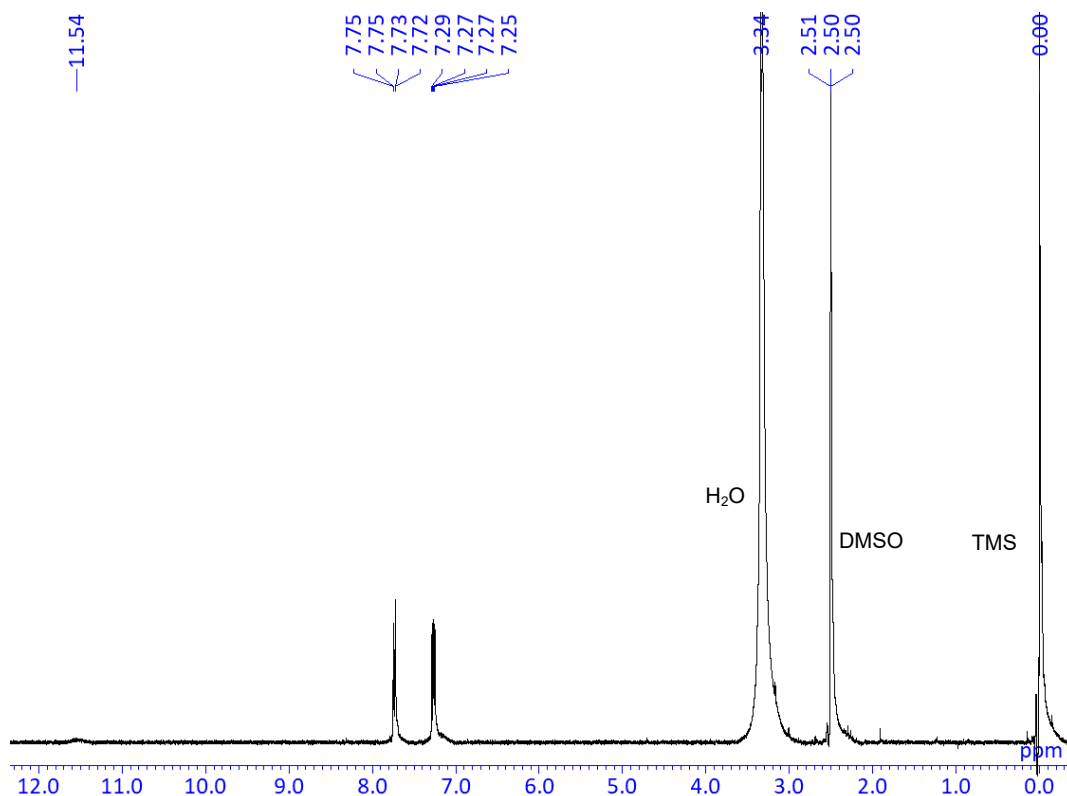


Chart S5. ¹H NMR spectrum of Az-3F-OH in DMSO-*d*₆, 400 MHz.

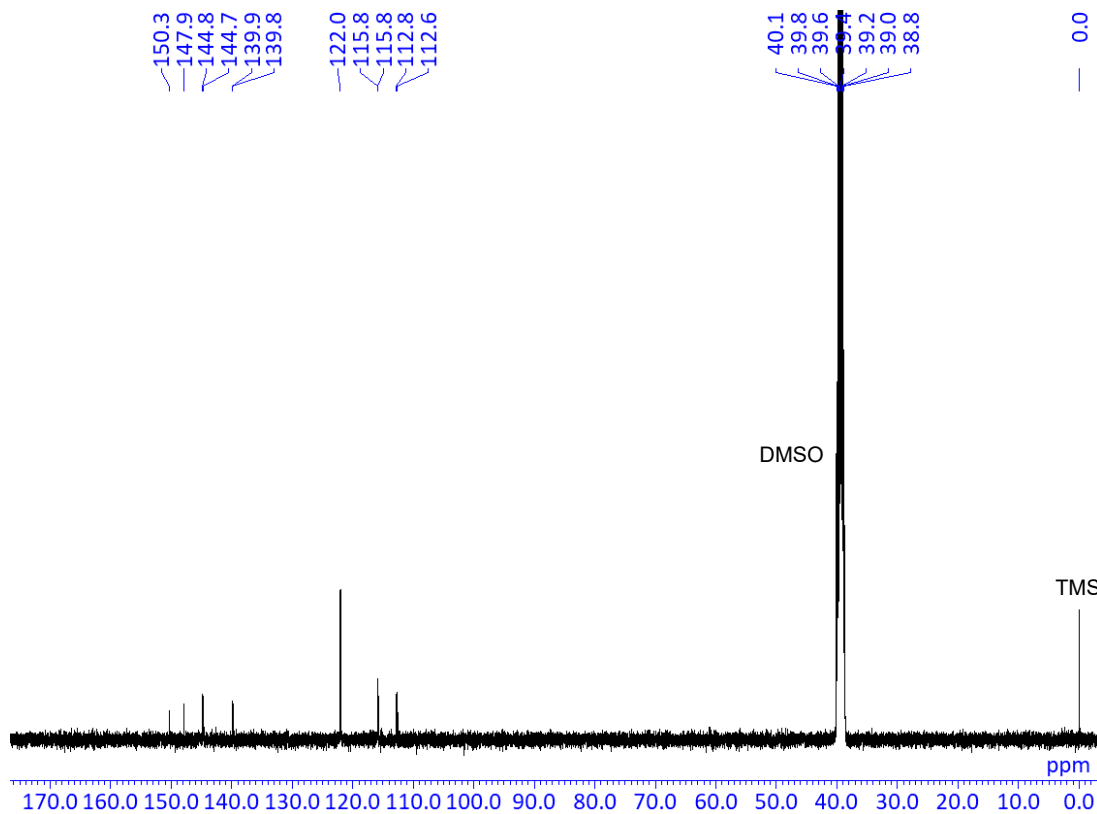
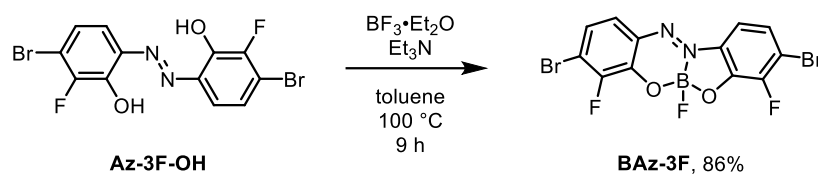


Chart S6. ¹³C NMR spectrum of Az-3F-OH in DMSO-*d*₆, 100 MHz.

Synthesis of BAz-3F



Az-3F-OH (195 mg, 0.478 mmol) was placed in a round-bottom flask equipped with a magnetic stirring bar. After degassing and filling N_2 three times, toluene (5 mL) was added to the flask. $\text{BF}_3 \cdot \text{Et}_2\text{O}$ (0.30 mL, 2.4 mmol) and Et_3N (0.17 mL, 1.2 mmol) were added to the mixture. After finishing the addition, the reaction was carried out at $100\text{ }^\circ\text{C}$ for 9 h. After the reaction, the solvent was removed with a rotary evaporator. The residue was purified by column chromatography on SiO_2 (hexane/ $\text{CH}_2\text{Cl}_2 = 3/2$ v/v as an eluent) to afford **BAz-3F** (179 mg, 0.411 mmol, 86%) as a red crystal.

$R_f = 0.35$ (hexane/ $\text{CH}_2\text{Cl}_2 = 3/2$ v/v). $^1\text{H NMR}$ (CDCl_3 , 400 MHz) δ 7.72 (d, $J = 8.8$ Hz, 1H), 7.55 (d, $J = 8.8$ Hz, 1H), 7.45 (dd, $J = 8.6, 5.9$ Hz, 1H), 7.32 (dd, $J = 8.5, 5.6$ Hz, 1H) ppm; $^{13}\text{C NMR}$ (CDCl_3 , 100 MHz) δ 150.4 (d, $J_{\text{C-F}} = 252$ Hz), 149.7 (d, $J_{\text{C-F}} = 15.4$ Hz), 148.0 (d, $J_{\text{C-F}} = 252$ Hz), 139.7, 135.9 (d, $J_{\text{C-F}} = 14.8$ Hz), 133.4, 126.7 (d, $J_{\text{C-F}} = 4.1$ Hz), 126.0, 125.9 (d, $J_{\text{C-F}} = 1.7$ Hz), 120.0 (d, $J_{\text{C-F}} = 18.1$ Hz), 119.1 (d, $J_{\text{C-F}} = 17.3$ Hz), 112.8 (d, $J_{\text{C-F}} = 4.9$ Hz), ppm. $^{11}\text{B NMR}$ (CDCl_3 , 128 MHz) δ 1.23 (d, $J = 37.1$ Hz) ppm. HRMS (ESI) calcd. for $\text{C}_{12}\text{H}_4\text{BBr}_2\text{F}_3\text{N}_2\text{O}_2$ [M^\bullet] $^-$: 433.8690, found: 433.8685.

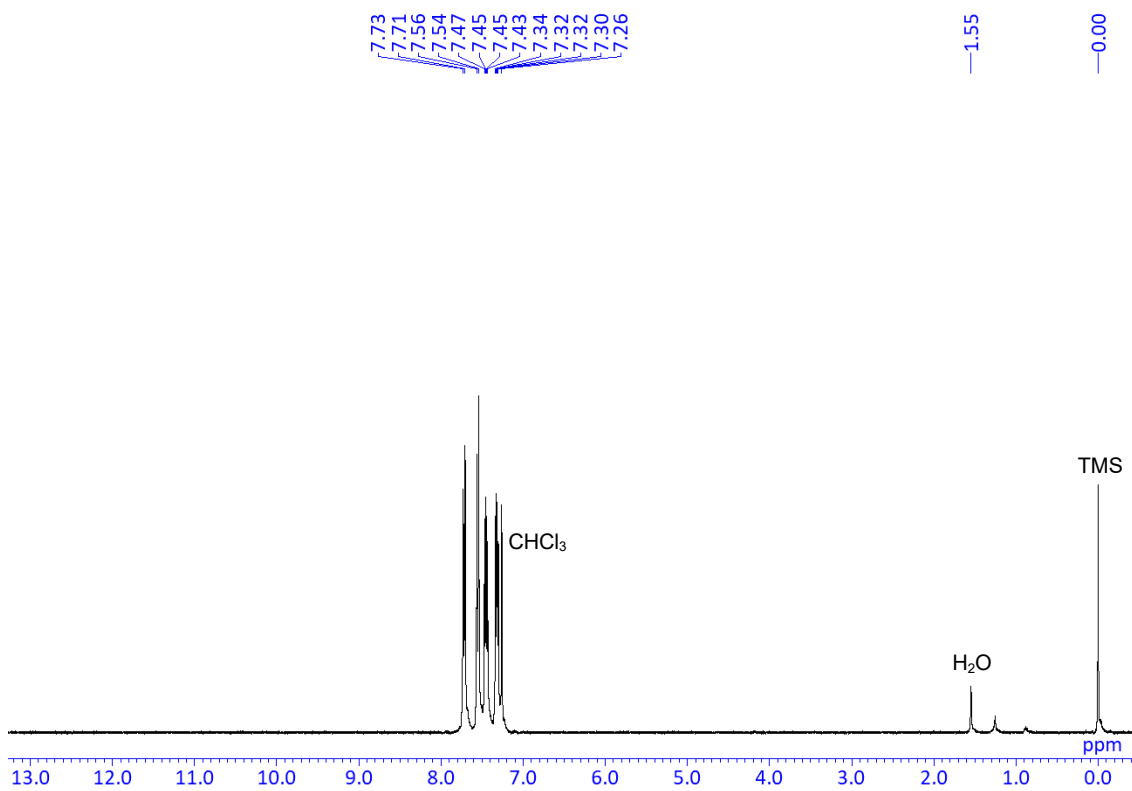


Chart S7. ¹H NMR spectrum of **BAz-3F** in CDCl₃, 400 MHz.

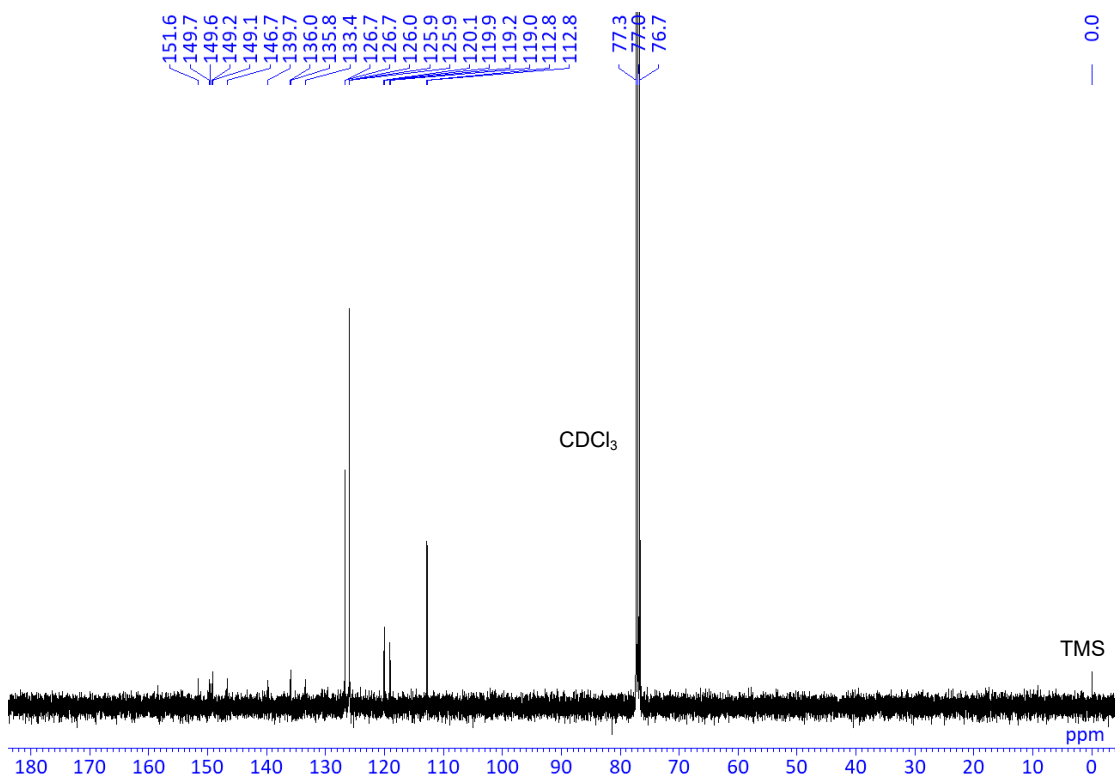


Chart S8. ¹³C NMR spectrum of **BAz-3F** in CDCl₃, 100 MHz.

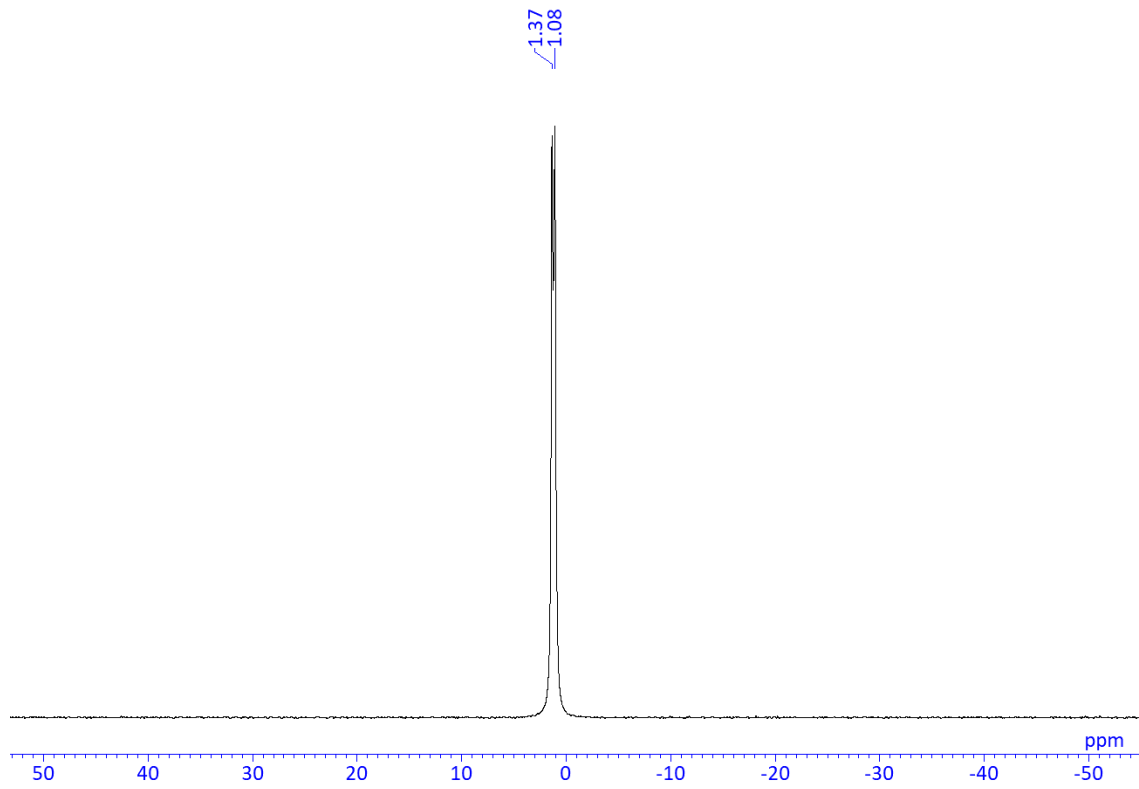
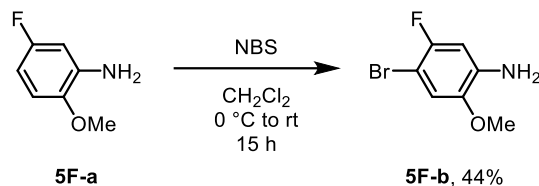


Chart S9. ^{11}B NMR spectrum of **BAz-3F** in CDCl_3 , 128 MHz.

Synthesis of 5F-b



A mixture of 5-fluoro-2-methoxyaniline (**5F-a**) (5.00 g, 35.4 mmol), NBS (6.30 g, 35.4 mmol) and dichloromethane (100 mL) was placed in a round-bottom flask equipped with a magnetic stirring bar. The mixture was reacted at room temperature for 15 h. After adding H₂O, the organic layer was extracted with CH₂Cl₂, and washed with brine. The organic layer was dried over MgSO₄. After filtration, the solvent was evaporated. The residue was semi-purified by column chromatography on SiO₂ (hexane/CH₂Cl₂ = 1/1 v/v as an eluent). The residue was purified by recrystallization with hexane to afford **5F-b** (3.38 g, 15.4 mmol, 44%) as a light brown crystal.

$R_f = 0.25$ (hexane/CH₂Cl₂ = 1/1 v/v). ¹H NMR (CDCl₃, 400 MHz) δ 6.84 (d, $J = 6.4$ Hz, 1H), 6.50 (d, $J = 9.8$ Hz, 1H), 3.91 (s, 2H), 3.82 (s, 3H) ppm; ¹³C NMR (CDCl₃, 100 MHz) δ 153.8 (d, $J_{\text{C-F}} = 236$ Hz), 143.8 (d, $J_{\text{C-F}} = 1.6$ Hz), 136.8 (d, $J_{\text{C-F}} = 9.9$ Hz), 114.2 (d, $J_{\text{C-F}} = 1.6$ Hz), 102.5 (d, $J_{\text{C-F}} = 27.1$ Hz), 94.1 (d, $J_{\text{C-F}} = 23.0$ Hz), 56.1 ppm. HRMS (APCI) calcd. for C₇H₈BrFNO [M+H]⁺: 219.9768, found: 219.9769.

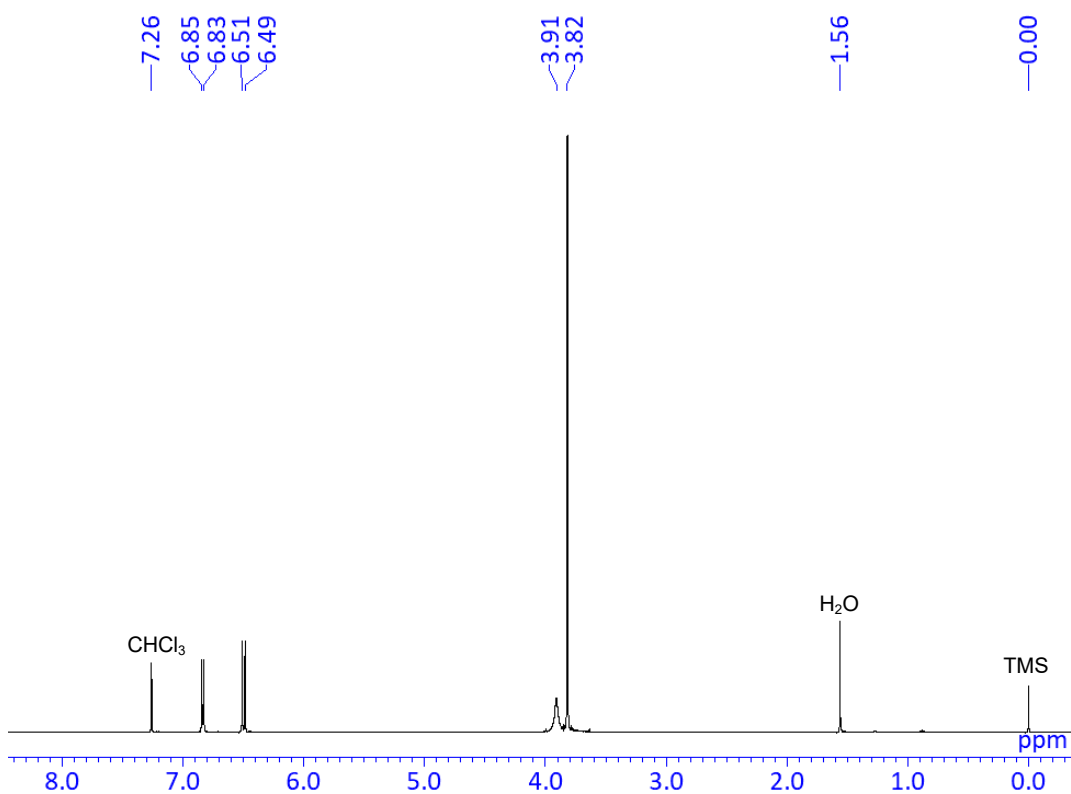


Chart S10. ¹H NMR spectrum of **5F-b** in CDCl₃, 400 MHz.

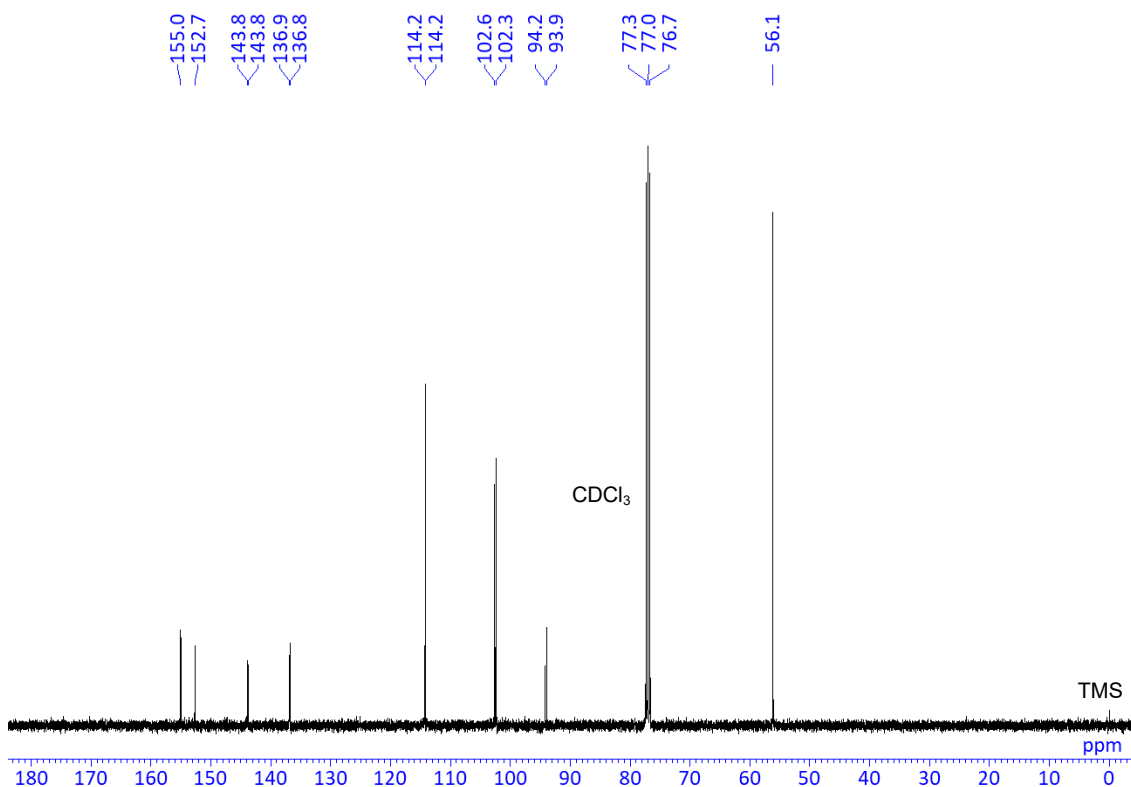
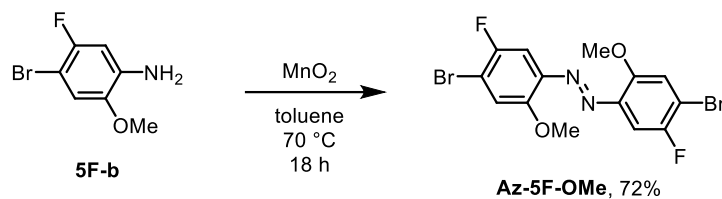


Chart S11. ¹³C NMR spectrum of **5F-b** in CDCl₃, 100 MHz.

Synthesis of Az-5F-OMe



A mixture of **5F-b** (3.27 g, 14.9 mmol), MnO₂ (10.3 g, 119 mmol) and toluene (100 mL) was placed in a round-bottom flask equipped with a magnetic stirring bar. The mixture was reacted at 70 °C for 6 h. After the reaction, MnO₂ was removed by filtration and washed with CHCl₃. The residue was purified by recrystallization with MeOH (poor solvent) and CHCl₃ (good solvent) to afford **Az-5F-OMe** (2.33 g, 5.34 mmol, 72%) as an orange solid.

¹H NMR (CD₂Cl₂ 400 MHz) δ 7.46 (d, $J = 9.3$ Hz, 2H), 7.32 (d, $J = 5.9$, 2H), 4.00 (s, 6H) ppm; ¹³C NMR (CD₂Cl₂, 100 MHz) δ 154.4 (d, $J_{\text{C-F}} = 2.5$ Hz), 154.2 (d, $J_{\text{C-F}} = 241$ Hz), 142.2 (d, $J_{\text{C-F}} = 4.1$ Hz), 118.3, 113.4 (d, $J_{\text{C-F}} = 23.9$ Hz), 104.4 (d, $J_{\text{C-F}} = 24.7$ Hz), 57.6 ppm. HRMS (APCI) calcd. for C₁₄H₁₁Br₂F₂N₂O₂ [M+H]⁺: 434.9150, found: 434.9155.

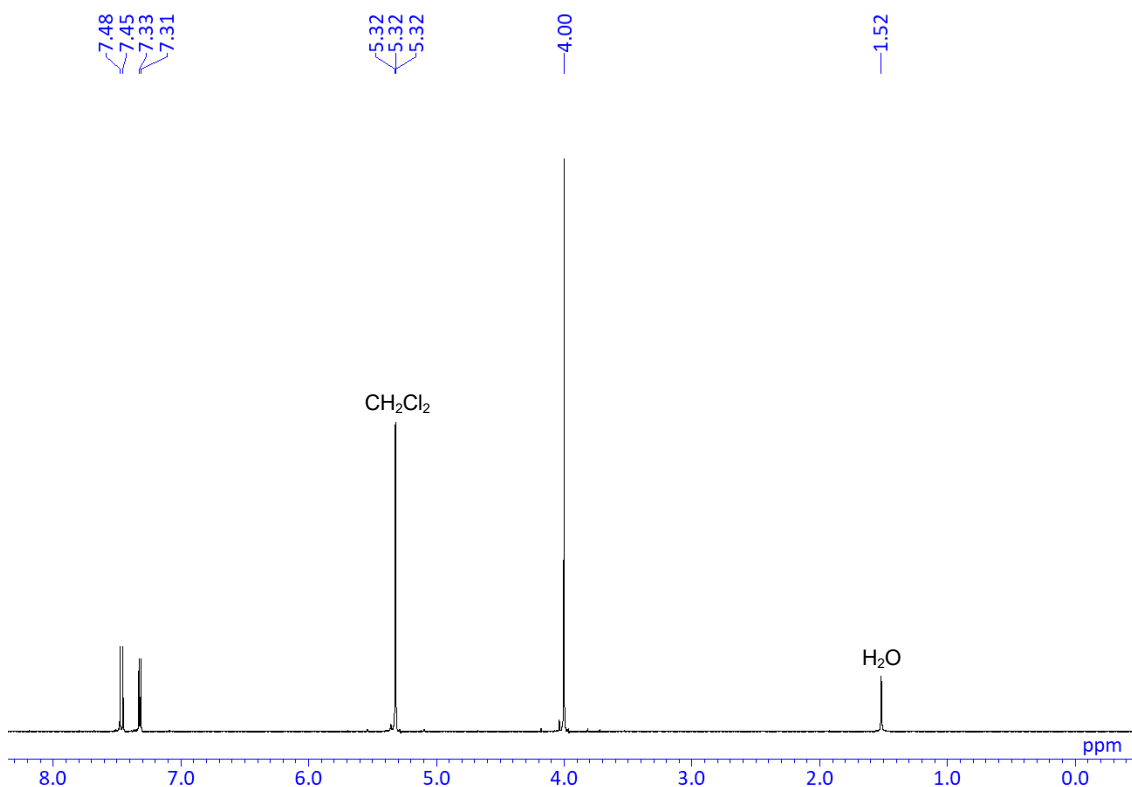


Chart S12. ¹H NMR spectrum of Az-5F-OMe in CD₂Cl₂, 400 MHz.

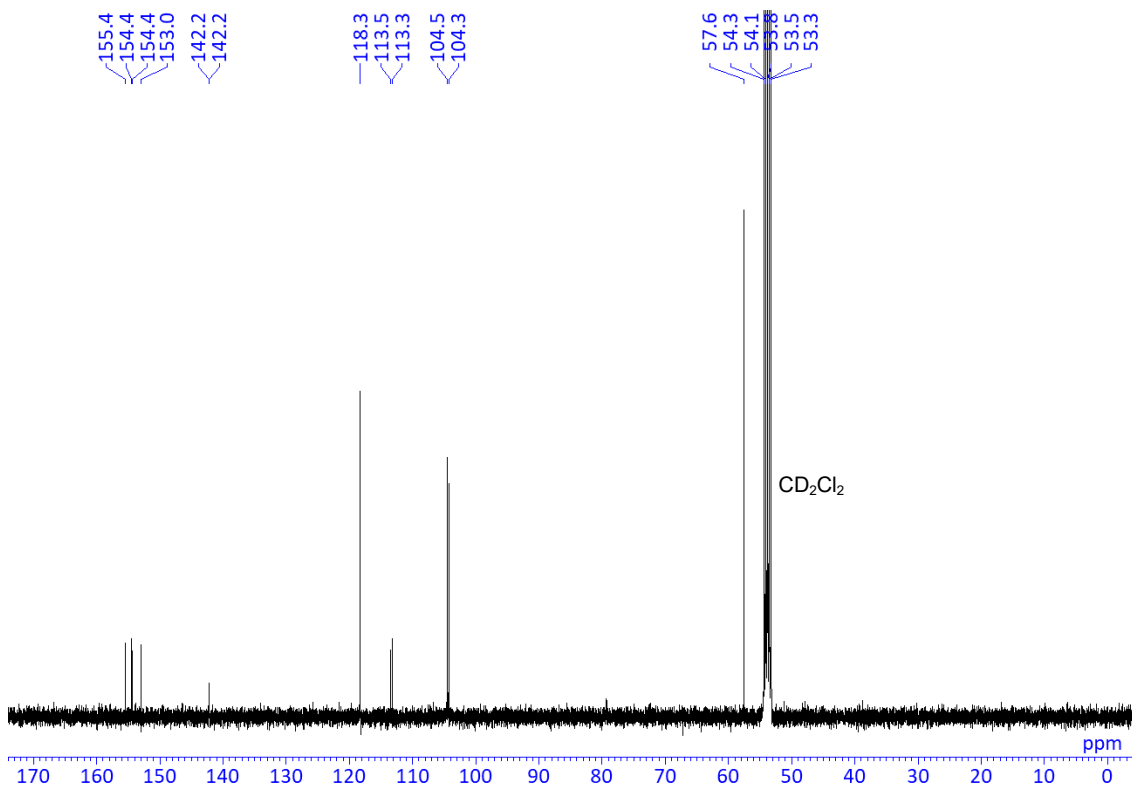
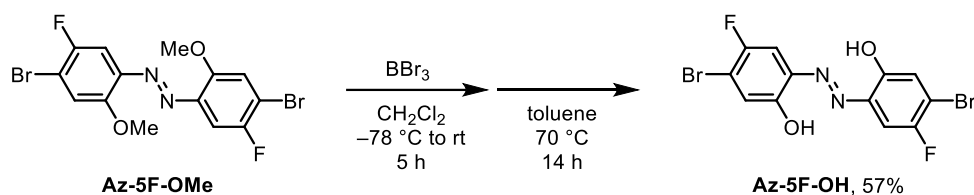


Chart S13. ¹³C NMR spectrum of Az-5F-OMe in CD₂Cl₂, 100 MHz.

Synthesis of Az-5F-OH



Az-5F-OMe (2.42 g, 5.55 mmol) was placed in a round-bottom flask equipped with a magnetic stirring bar. After degassing and filling Ar three times, CH_2Cl_2 (60 mL) was added to the flask. After cooling the mixture to -78°C , BBr_3 (1 M in CH_2Cl_2 , 27.8 mL, 27.8 mmol) was dropwise added. The reaction was carried out at room temperature for 5 h. Then toluene (60 mL) was added to the flask and heated to 70°C for 14 h. After the reaction, MeOH was carefully added at 0°C for quenching the reaction. Then, the target compound was immediately precipitated as an orange solid. The crystal was collected and washed with MeOH to afford **Az-5F-OH** (1.30 g, 3.19 mmol, 57%) as a yellow solid.

^1H NMR (CDCl_3 , 400 MHz) δ 11.69 (s, 2H), 7.48 (d, $J = 8.1$ Hz, 2H), 7.30 (d, $J = 6.1$ Hz, 2H) ppm;
 ^{13}C NMR ($\text{THF}-d_8$, 100 MHz) δ 153.0 (d, $J_{\text{C-F}} = 239$ Hz), 151.7 (d, $J_{\text{C-F}} = 1.6$ Hz), 137.5 (d, $J_{\text{C-F}} = 6.3$ Hz), 122.2, 114.1 (d, $J_{\text{C-F}} = 23.0$ Hz), 108.8 (d, $J_{\text{C-F}} = 24.7$ Hz) ppm. HRMS (ESI) calcd. for $\text{C}_{12}\text{H}_5\text{Br}_2\text{F}_2\text{N}_2\text{O}_2$ $[\text{M}-\text{H}]^-$: 404.8686, found: 404.8764.

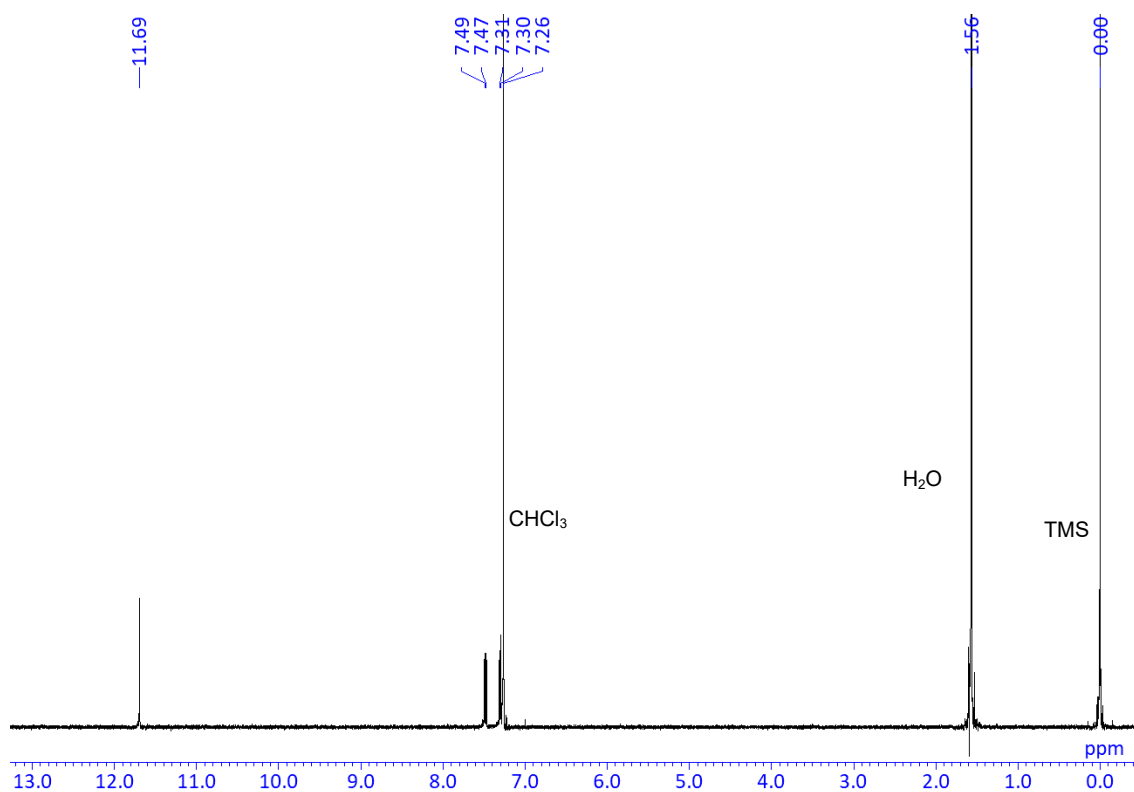


Chart S14. ¹H NMR spectrum of Az-5F-OH in CDCl₃, 400 MHz.

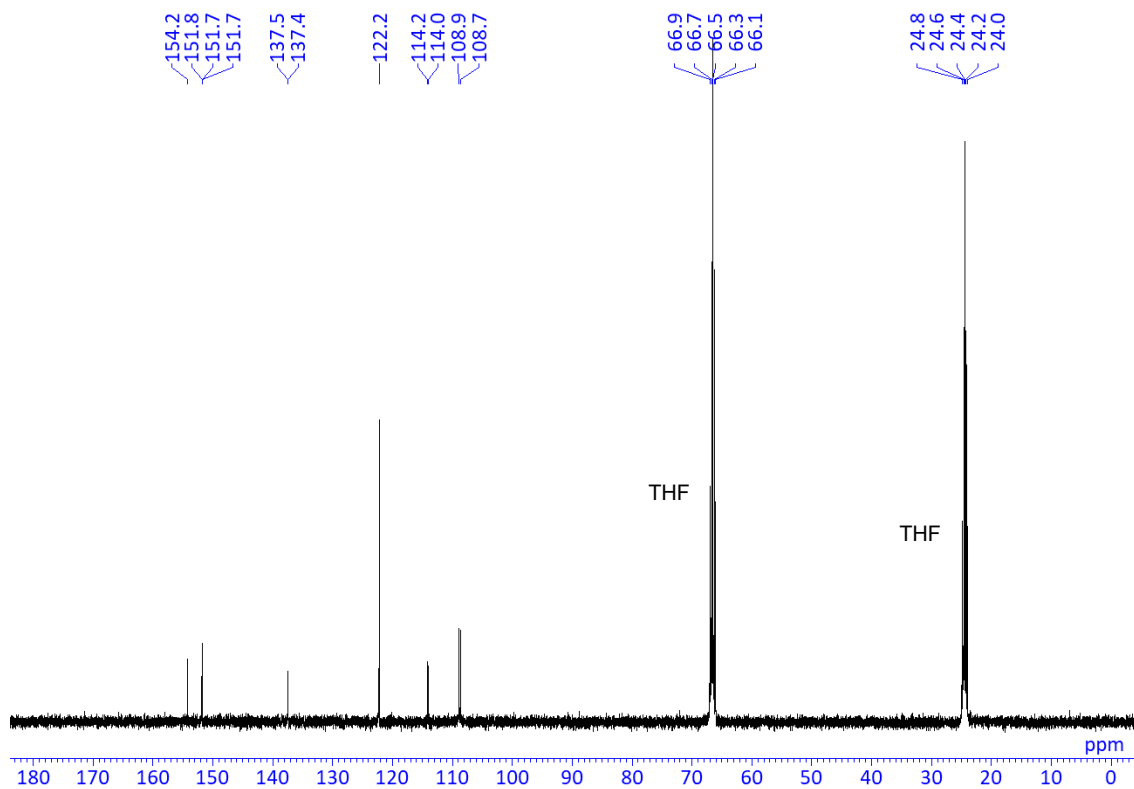
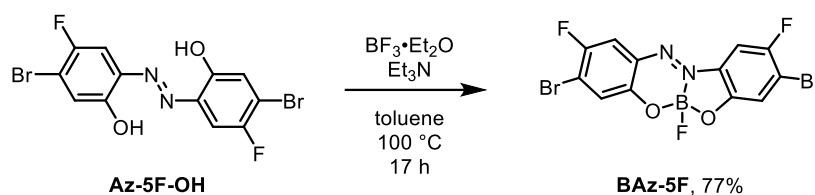


Chart S15. ¹³C NMR spectrum of Az-5F-OH in THF-*d*₈, 100 MHz.

Synthesis of BAz-5F



Az-5F-OH (1.30 g, 3.19 mmol) was placed in a round-bottom flask equipped with a magnetic stirring bar. After degassing and filling Ar three times, toluene (100 mL) was added to the flask. $\text{BF}_3 \cdot \text{Et}_2\text{O}$ (8.0 mL, 63.7 mmol) and Et_3N (4.4 mL, 31.9 mmol) were added to the mixture. After finishing the addition, the reaction was carried out at 100 °C for 17 h. After the reaction, the solvent was removed with a rotary evaporator. The residue was semi-purified by column chromatography on SiO_2 (CHCl_3 as an eluent) and further purification was carried out by recrystallization with hexane to afford **BAz-5F** (1.08 g, 2.46 mmol, 77%) as a dark red crystal.

$R_f = 0.70$ (hexane/ $\text{CH}_2\text{Cl}_2 = 1/1$ v/v). $^1\text{H NMR}$ (CDCl_3 , 400 MHz) δ 7.72 (d, $J = 7.6$ Hz, 1H), 7.60 (d, $J = 2.7$ Hz, 1H), 7.58 (d, $J = 3.4$ Hz, 1H), 7.50 (d, $J = 5.4$ Hz, 1H) ppm; $^{13}\text{C NMR}$ (CDCl_3 , 100 MHz) δ 157.7 (d, $J_{\text{C-F}} = 1.6$ Hz), 154.2 (d, $J_{\text{C-F}} = 246$ Hz), 154.1 (d, $J_{\text{C-F}} = 243$ Hz), 142.4 (d, $J_{\text{C-F}} = 1.6$ Hz), 138.4, 131.1, 125.1, 121.9 (d, $J_{\text{C-F}} = 23.4$ Hz), 121.0, 120.6 (d, $J_{\text{C-F}} = 23.9$ Hz), 115.8 (d, $J_{\text{C-F}} = 24.7$ Hz), 103.5 (d, $J_{\text{C-F}} = 27.4$ Hz) ppm. $^{11}\text{B NMR}$ (CDCl_3 , 128 MHz) δ 1.32 (d, $J = 37.7$ Hz) ppm. HRMS (ESI) calcd. for $\text{C}_{12}\text{H}_4\text{Br}_2\text{F}_3\text{N}_2\text{O}_2$ [M^\bullet] $^-$: 433.8690, found: 433.8693.

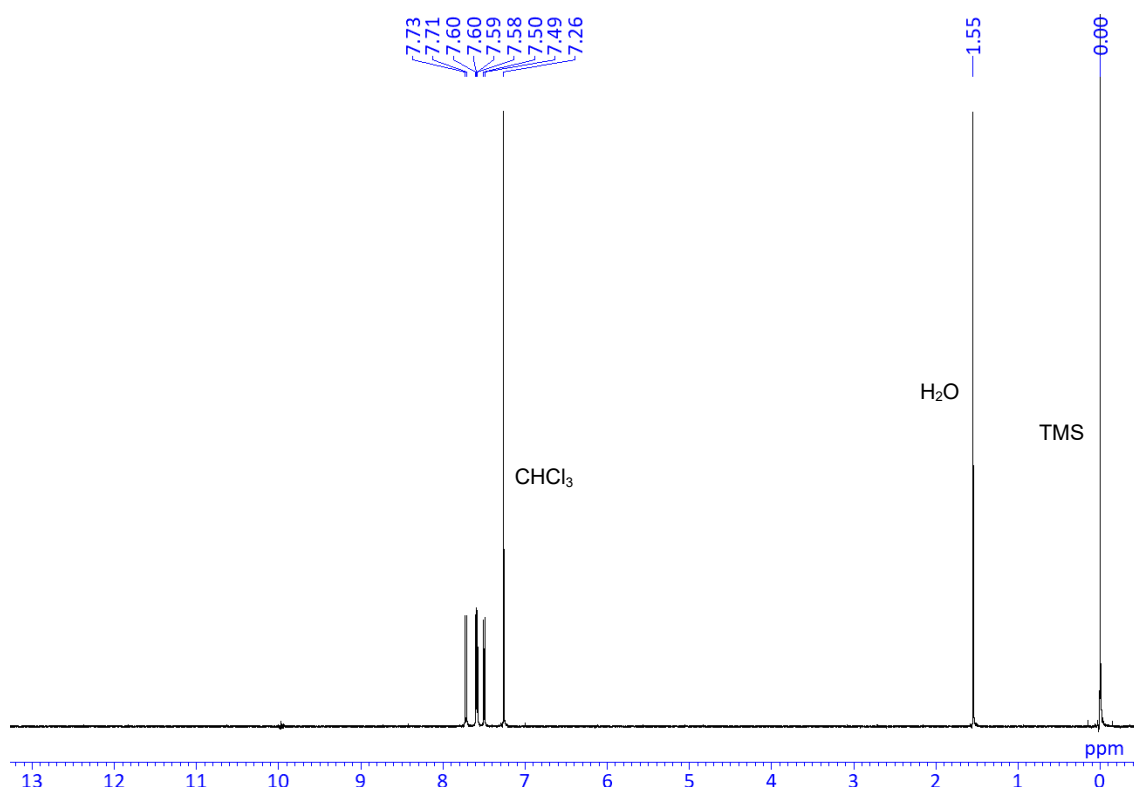


Chart S16. ^1H NMR spectrum of **BAz-5F** in CDCl_3 , 400 MHz.

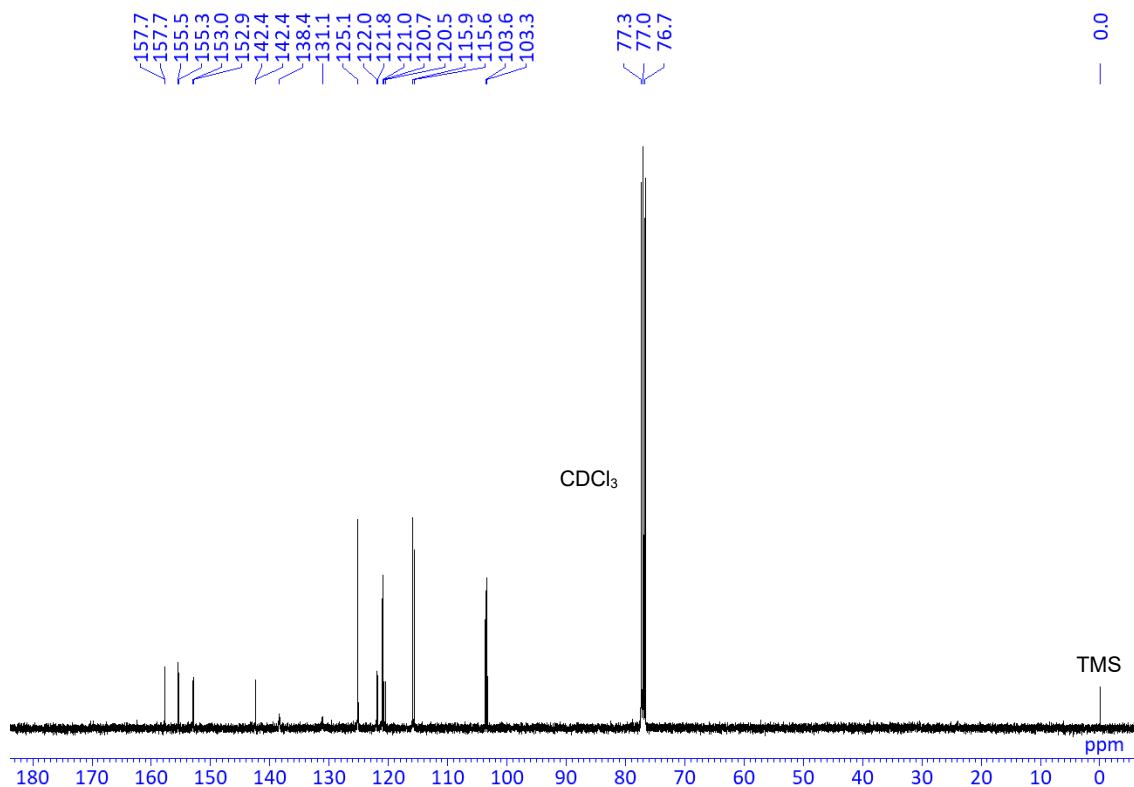


Chart S17. ^{13}C NMR spectrum of **BAz-5F** in CDCl_3 , 100 MHz.

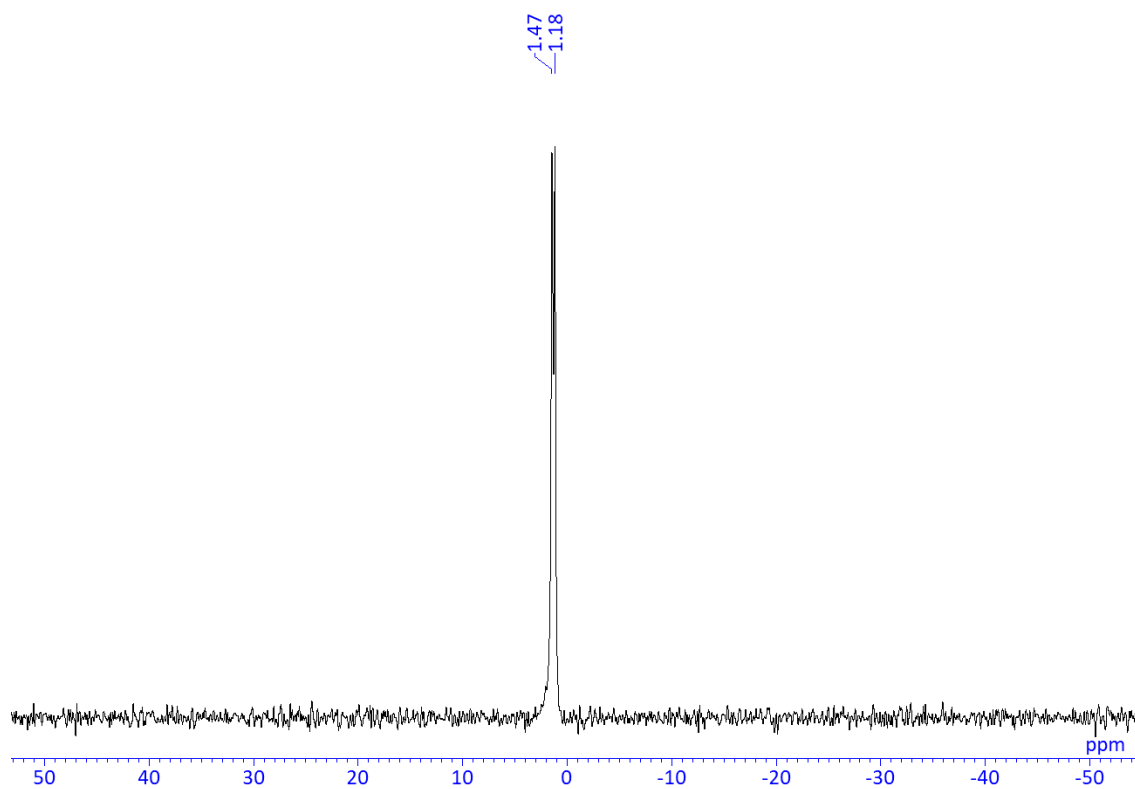
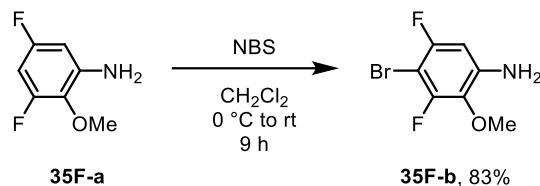


Chart S18. ^{11}B NMR spectrum of BAz-5F in CDCl_3 , 128 MHz.

Synthesis of 35F-b



A mixture of 3,5-difluoro-2-methoxyaniline (**35F-a**) (4.86 g, 30.5 mmol) and CH_2Cl_2 (280 mL) was placed in a round-bottom flask equipped with a magnetic stirring bar. NBS (5.44 g, 30.5 mmol) was slowly added at 0 °C. The mixture was reacted at room temperature for 9 h. After adding H_2O , the organic layer was extracted with CH_2Cl_2 , and washed with brine. The organic layer was dried over MgSO_4 . After filtration, the solvent was evaporated. The residue was purified by recrystallization with hexane to afford **35F-b** (6.06 g, 25.5 mmol, 83%) as a light brown crystal.

^1H NMR (CDCl_3 , 400 MHz) δ 6.34 (dd, $J = 9.8, 2.2$ Hz, 1H), 4.09 (s, 2H), 3.87 (s, 3H) ppm; ^{13}C NMR (CDCl_3 , 100 MHz) δ 155.6 (dd, $J_{\text{C-F}} = 239, 5.8$ Hz), 153.1 (dd, $J_{\text{C-F}} = 243, 7.4$ Hz), 140.5 (dd, $J_{\text{C-F}} = 12.3, 6.6$ Hz), 131.9 (dd, $J_{\text{C-F}} = 14.8, 4.1$ Hz), 97.8 (dd, $J_{\text{C-F}} = 26.3, 2.5$ Hz), 84.7 (dd, $J_{\text{C-F}} = 25.5, 22.2$ Hz), 61.0 (d, $J_{\text{C-F}} = 4.9$ Hz) ppm. HRMS (APCI) calcd. for $\text{C}_7\text{H}_7\text{BrF}_2\text{NO}$ $[\text{M}+\text{H}]^+$: 237.9674, found: 237.9675.

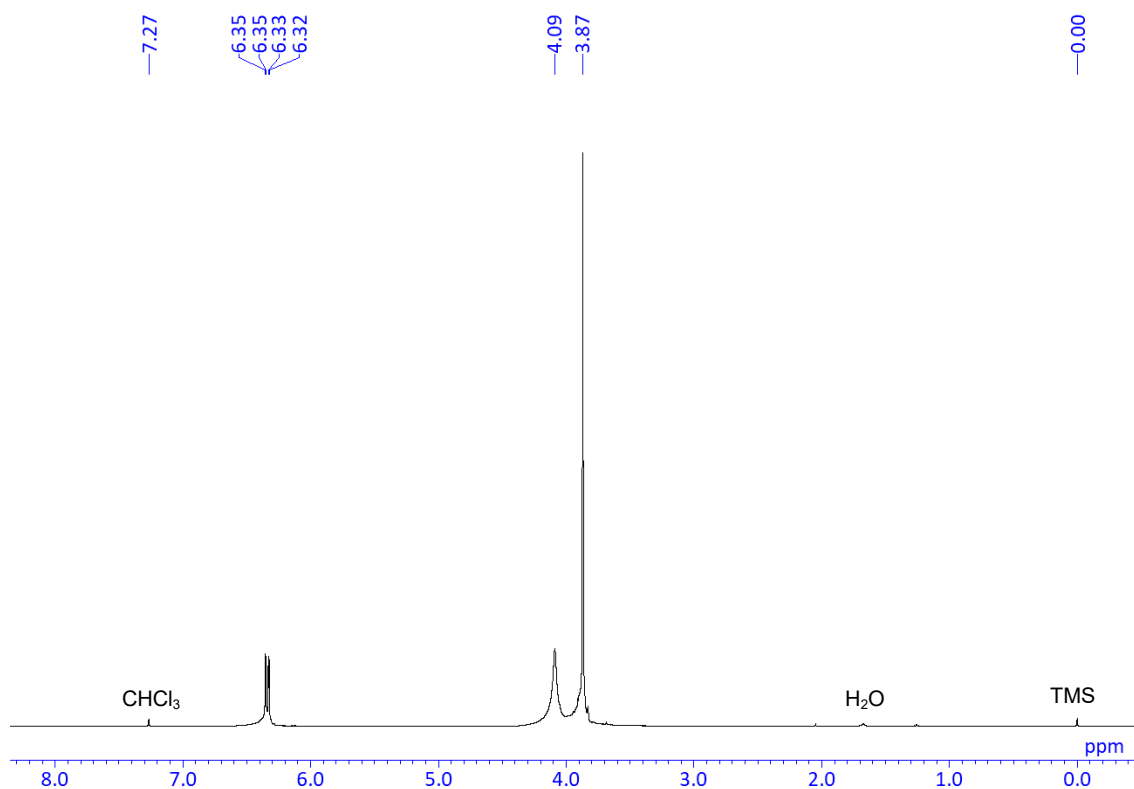


Chart S19. ¹H NMR spectrum of **35F-b** in CDCl₃, 400 MHz.

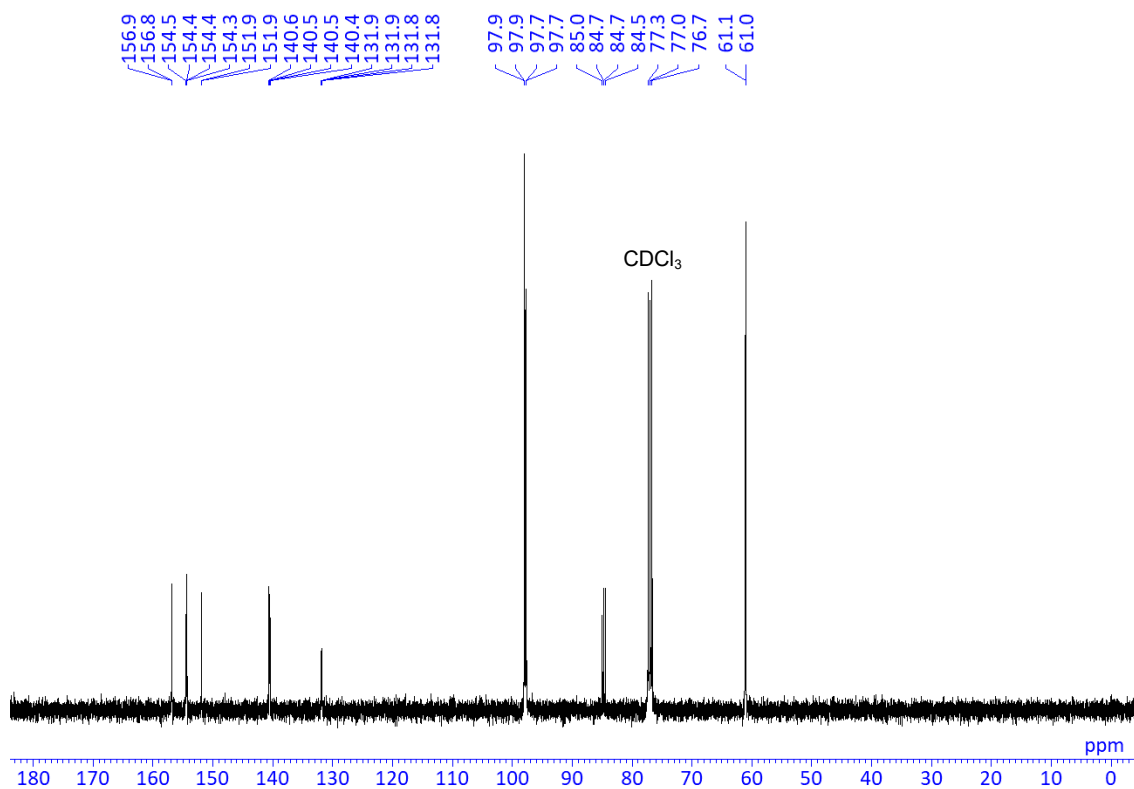
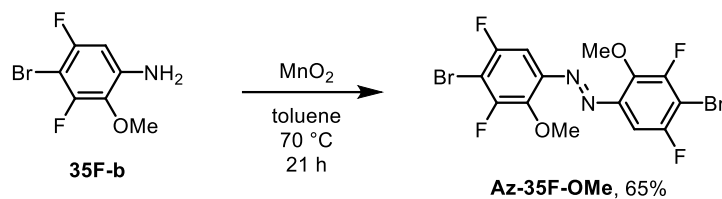


Chart S20. ¹³C NMR spectrum of **35F-b** in CDCl₃, 100 MHz.

Synthesis of Az-35F-OMe



A mixture of **35F-b** (5.65 g, 23.7 mmol), MnO₂ (8.23 g, 94.7 mmol) and toluene (100 mL) was placed in a round-bottom flask equipped with a magnetic stirring bar. The mixture was reacted at 70 °C for 21 h. After the reaction, MnO₂ was removed by filtration and washed with CHCl₃. The residue was purified by recrystallization with MeOH (poor solvent) and CHCl₃ (good solvent) to afford **Az-35F-OMe** (3.64 g, 7.71 mmol, 65%) as an orange crystal.

¹H NMR (CDCl₃, 400 MHz) δ 7.35 (dd, $J = 9.0, 1.4$ Hz, 2H), 4.15 (s, 6H) ppm; ¹³C NMR (CDCl₃, 100 MHz) δ 155.2 (dd, $J_{\text{C-F}} = 246, 4.1$ Hz), 154.3 (dd, $J_{\text{C-F}} = 6.4, 4.9$ Hz), 144.8 (dd, $J_{\text{C-F}} = 248, 3.9$ Hz), 144.2 (dd, $J_{\text{C-F}} = 13.2, 4.1$ Hz), 103.2 (dd, $J_{\text{C-F}} = 27.1, 23.0$ Hz), 98.9 (dd, $J_{\text{C-F}} = 24.7, 3.3$ Hz), 64.1 (d, $J_{\text{C-F}} = 3.3$ Hz) ppm. HRMS (APCI) calcd. for C₁₄H₉Br₂F₄N₂O₂ [M+H]⁺: 470.8961, found: 470.8967.

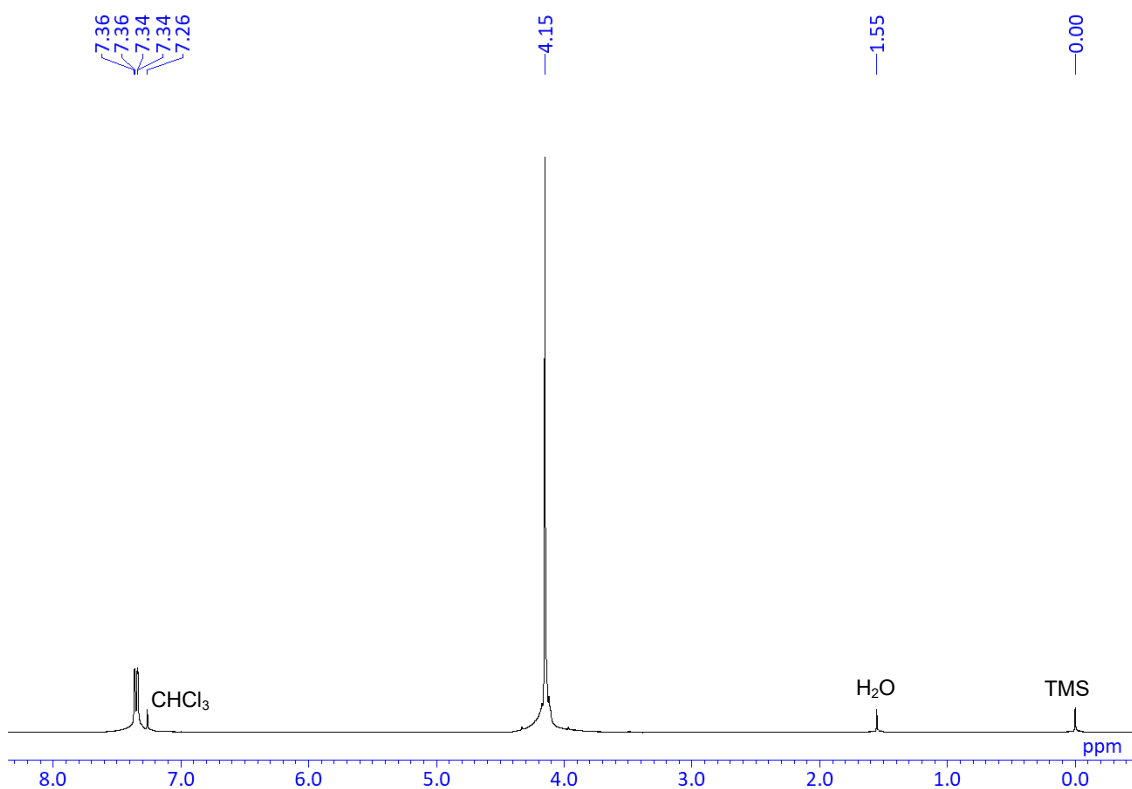


Chart S21. ¹H NMR spectrum of Az-35F-OMe in CDCl₃, 400 MHz.

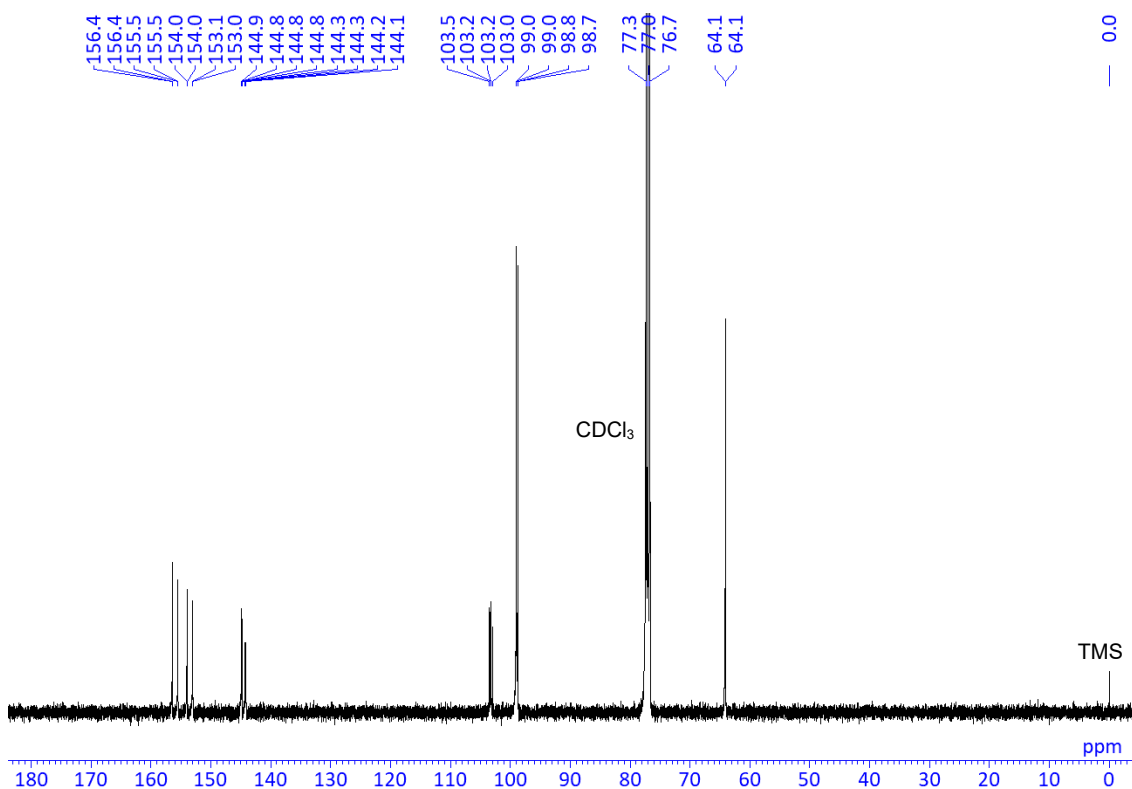
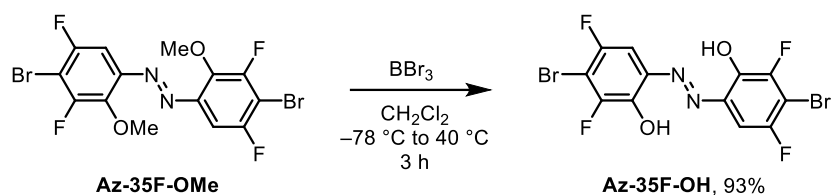


Chart S22. ¹³C NMR spectrum of Az-35F-OMe in CDCl₃, 100 MHz.

Synthesis of Az-35F-OH



Az-35F-OMe (472 mg, 1.00 mmol) was placed in a round-bottom flask equipped with a magnetic stirring bar. After degassing and filling N_2 three times, CH_2Cl_2 (20 mL) was added to the flask. After cooling the mixture to $-78\text{ }^\circ\text{C}$, BBr_3 (1 M in CH_2Cl_2 , 4.0 mL, 4.0 mmol) was dropwise added. The reaction was carried out at $40\text{ }^\circ\text{C}$ for 3 h. After the reaction, H_2O and THF were carefully added at $0\text{ }^\circ\text{C}$ for quenching the reaction. Subsequently, MeOH was added. Then, the target compound was precipitated as a light brown solid. The solid was collected and washed with MeOH to afford **Az-35F-OH** (412 mg, 0.928 mmol, 93%) as a light brown solid.

^1H NMR ($\text{DMSO-}d_6$, 400 MHz) δ 11.19 (s, 2H), 7.95 (dd, $J = 10.0, 2.2$ Hz, 2H) ppm; ^{13}C NMR ($\text{DMSO-}d_6$, 100 MHz) δ 151.5 (dd, $J_{\text{C-F}} = 238, 3.9$ Hz), 149.8 (dd, $J_{\text{C-F}} = 243, 5.4$ Hz), 143.1 (dd, $J_{\text{C-F}} = 13.6, 2.7$ Hz), 138.9 (dd, $J_{\text{C-F}} = 6.2, 5.1$ Hz), 102.5 (dd, $J_{\text{C-F}} = 27.6, 22.0$ Hz), 99.0 (dd, $J_{\text{C-F}} = 24.9, 3.5$ Hz), ppm. HRMS (ESI) calcd. for $\text{C}_{12}\text{H}_3\text{Br}_2\text{F}_4\text{N}_2\text{O}_2$ $[\text{M-H}]^-$: 440.8503, found: 440.8508.

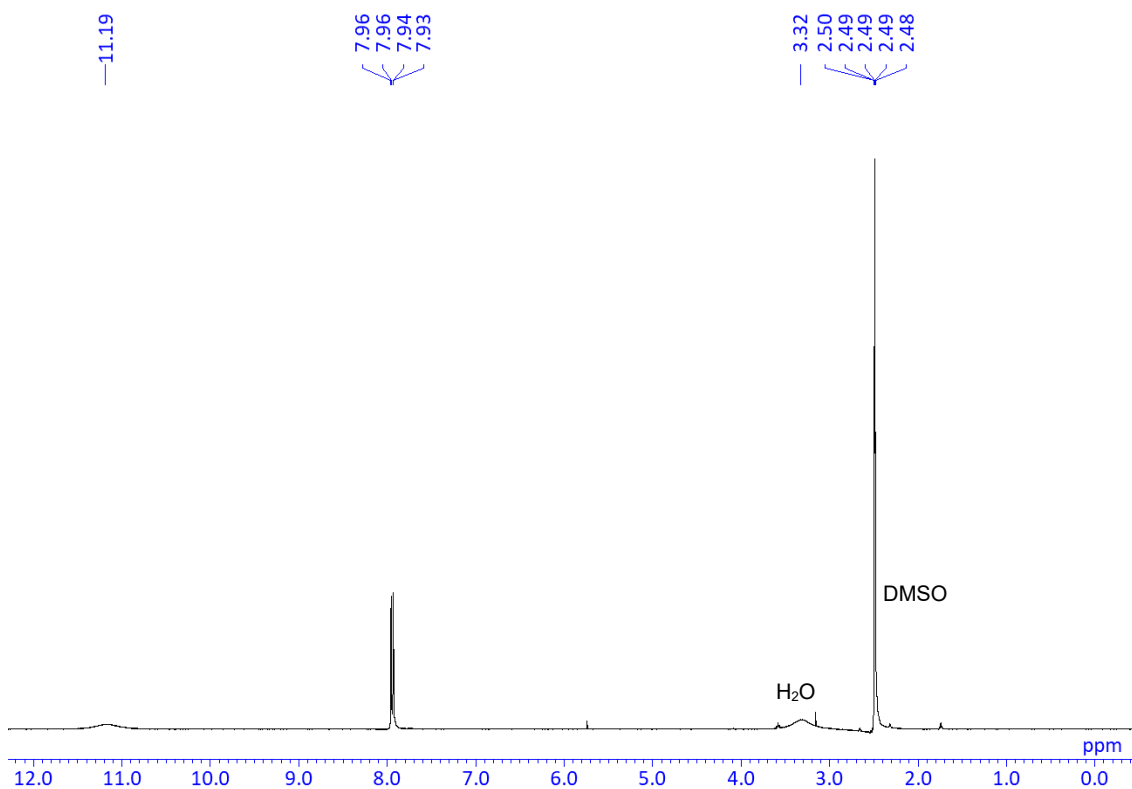


Chart S23. ^1H NMR spectrum of Az-35F-OH in DMSO- d_6 , 400 MHz.

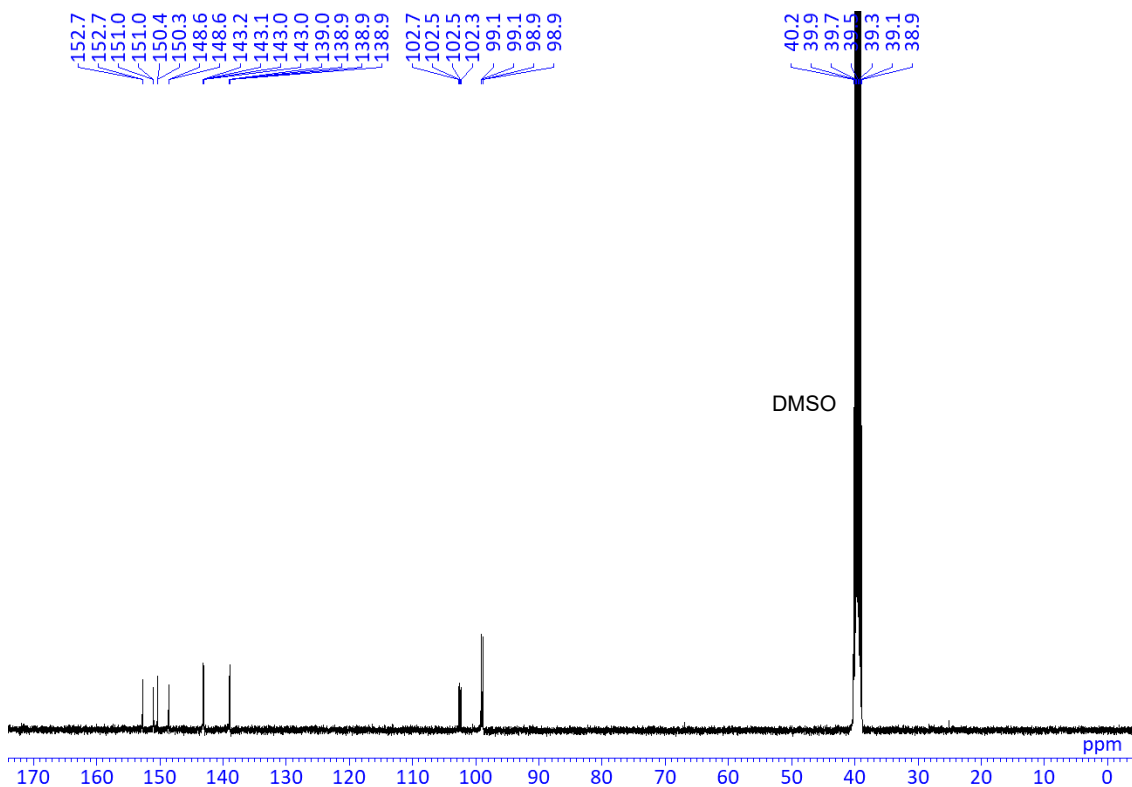
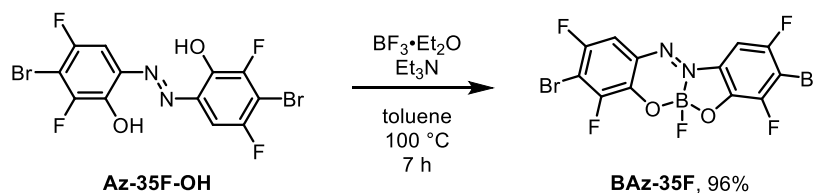


Chart S24. ^{13}C NMR spectrum of Az-35F-OH in DMSO- d_6 , 100 MHz.

Synthesis of BAz-35F



Az-35F-OH (222 mg, 0.500 mmol) was placed in a round-bottom flask equipped with a magnetic stirring bar. After degassing and filling N_2 three times, toluene (10 mL) was added to the flask. $\text{BF}_3 \cdot \text{Et}_2\text{O}$ (0.31 mL, 2.50 mmol) and Et_3N (0.15 mL, 1.10 mmol) were added to the mixture. After finishing the addition, the reaction was carried out at $100\text{ }^\circ\text{C}$ for 7 h. After the reaction, the solvent was removed with a rotary evaporator. The residue was purified by column chromatography on SiO_2 (hexane/ $\text{CH}_2\text{Cl}_2 = 1/1$ v/v as an eluent) to afford **BAz-35F** (226 mg, 0.479 mmol, 96%) as a red crystal.

$R_f = 0.70$ (hexane/ $\text{CH}_2\text{Cl}_2 = 1/1$ v/v). ^1H NMR (CDCl_3 , 400 MHz) δ 7.64 (dd, $J = 7.3, 2.2$ Hz, 1H), 7.49 (dd, $J = 6.2, 2.0$ Hz, 1H) ppm; ^{13}C NMR (CDCl_3 , 100 MHz) δ 154.3 (dd, $J_{\text{C-F}} = 247, 1.4$ Hz), 153.6 (dd, $J_{\text{C-F}} = 245, 2.5$ Hz), 151.0 (dd, $J_{\text{C-F}} = 255, 4.9$ Hz), 148.5 (d, $J_{\text{C-F}} = 256$ Hz), 146.7 (dd, $J_{\text{C-F}} = 15.6, 1.7$ Hz), 138.3, 132.5 (dd, $J_{\text{C-F}} = 15.0, 2.7$ Hz), 131.9, 110.9 (dd, $J_{\text{C-F}} = 25.5, 4.1$ Hz), 110.8 (dd, $J_{\text{C-F}} = 27.1, 21.4$ Hz), 109.8 (dd, $J_{\text{C-F}} = 26.3, 19.7$ Hz), 99.1 (dd, $J_{\text{C-F}} = 28.0, 4.9$ Hz) ppm. ^{11}B NMR (CDCl_3 , 128 MHz) δ 1.28 (d, $J = 25.1$ Hz) ppm. HRMS (ESI) calcd. for $\text{C}_{12}\text{H}_2\text{BBr}_2\text{F}_5\text{N}_2\text{O}_2$ [M^\bullet] $^-$: 469.8502, found: 469.8504.

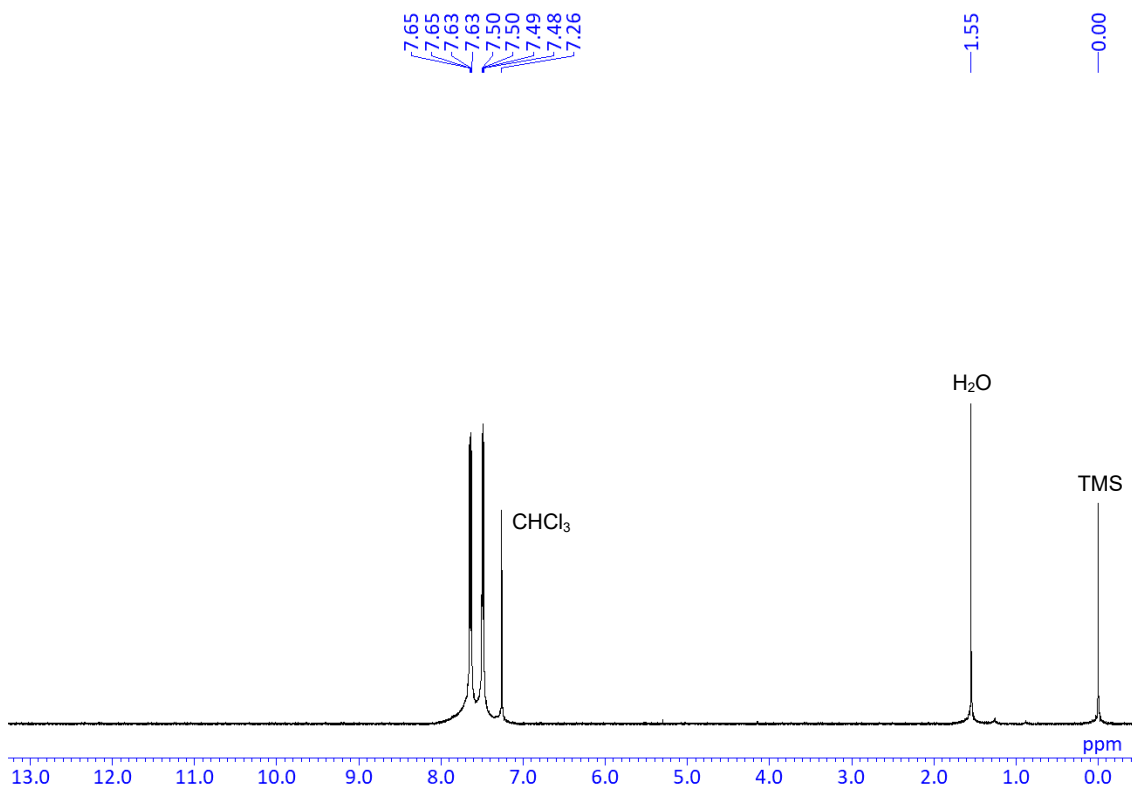


Chart S25. ¹H NMR spectrum of **BAz-35F** in CDCl₃, 400 MHz.

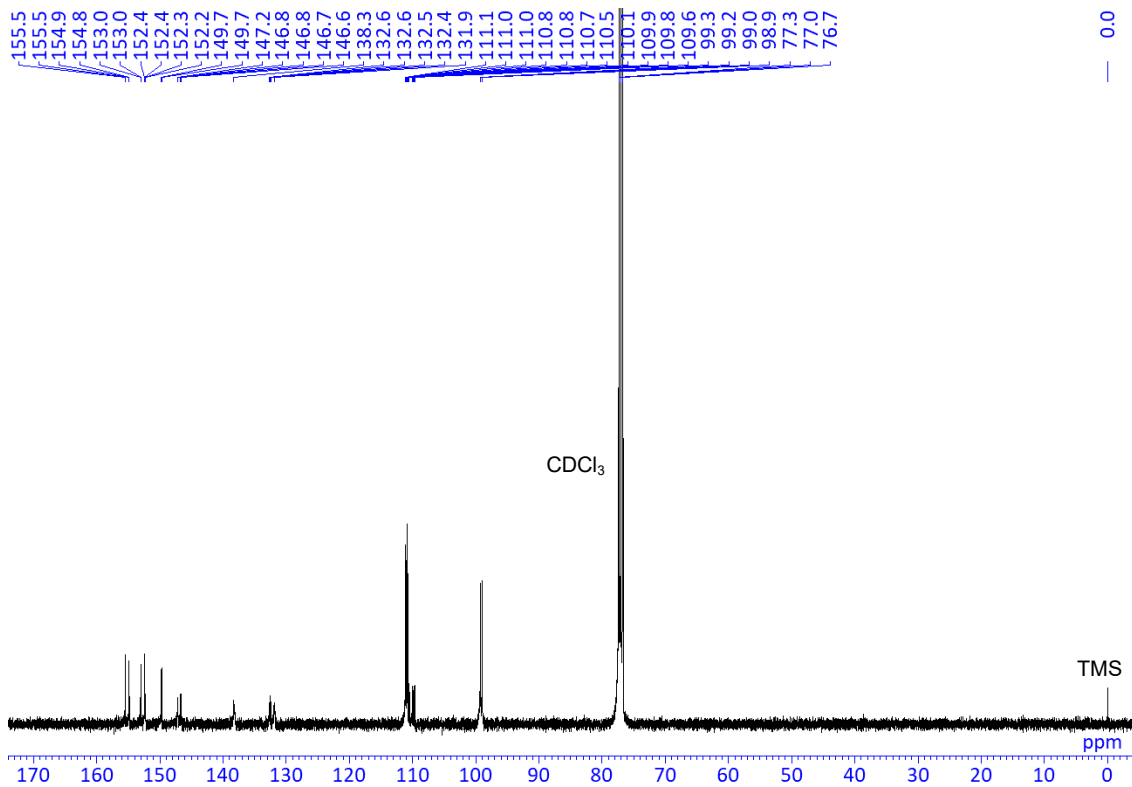


Chart S26. ¹³C NMR spectrum of **BAz-35F** in CDCl₃, 100 MHz.

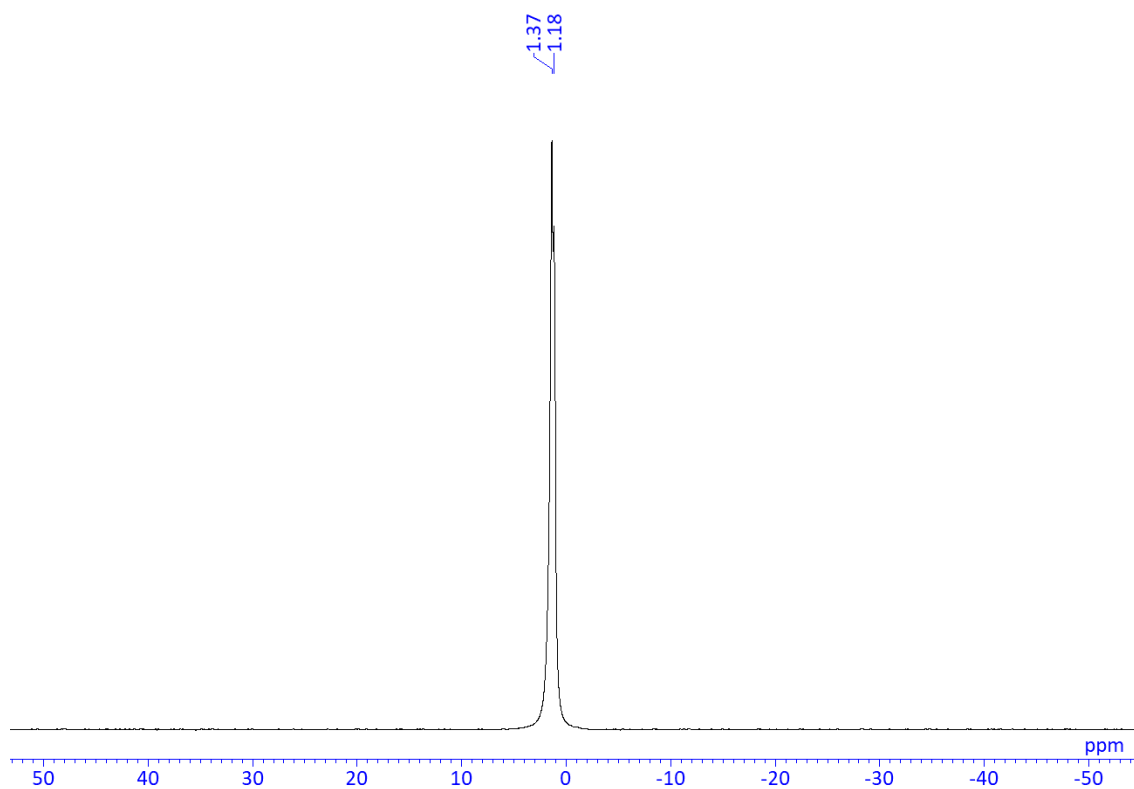
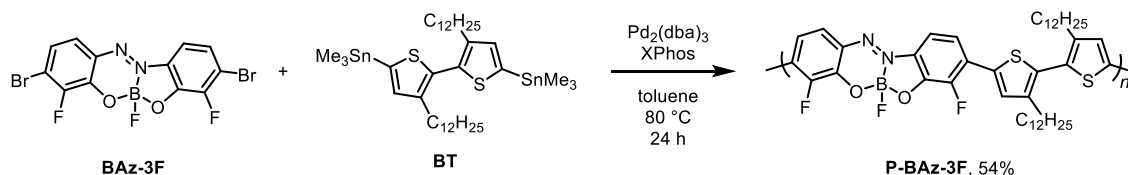


Chart S27. ^{11}B NMR spectrum of **BAz-35F** in CDCl_3 , 128 MHz.

Synthesis of P-BAz-3F



A mixture of **BAz-3F** (43.6 mg, 0.10 mmol), 5,5'-bis(trimethylstannyl)-3,3'-didodecyl-2,2'-bithiophene (**BT**) (82.9 mg, 0.10 mmol), $\text{Pd}_2(\text{dba})_3$ (2.7 mg, 0.0030 mmol), XPhos (2.9 mg, 0.0060 mmol) was placed in a round-bottom flask equipped with a magnetic stirring bar. After degassing and filling Ar three times, toluene (2.0 mL) was added to the mixture. The reaction was carried out at 80 °C for 24 h. After the reaction, the obtained polymer was redissolved in CHCl_3 at 80 °C, and then the product was reprecipitated from CH_3CN . The polymer collected by filtration was dried in vacuo to afford **P-BAz-5F** (42.0 mg, 54%) as a black solid.

$M_n = 13,500$, $M_w = 38,800$, $M_w/M_n = 3.2$. $^1\text{H NMR}$ (CDCl_3 , 400 MHz) δ 7.71 (br, 2H), 7.64 (br, 2H), 7.51 (s, 1H), 7.39 (s, 1H), 2.65 (br, 4H), 1.64 (br, 4H), 1.24 (br, 36H), 0.86 (t, $J = 6.3$ Hz, 6H) ppm; $^{13}\text{C NMR}$ (CDCl_3 , 100 MHz) δ 149.7, 147.5, 144.6, 144.6, 139.8, 136.5, 133.0, 132.0, 131.1, 129.7, 129.2, 126.3, 120.8, 120.3, 112.3, 31.9, 30.7, 29.7, 29.7, 29.6, 29.4, 29.4, 29.2, 22.7, 14.1 ppm; $^{11}\text{B NMR}$ (CDCl_3 , 128 MHz) δ 1.37 ppm.

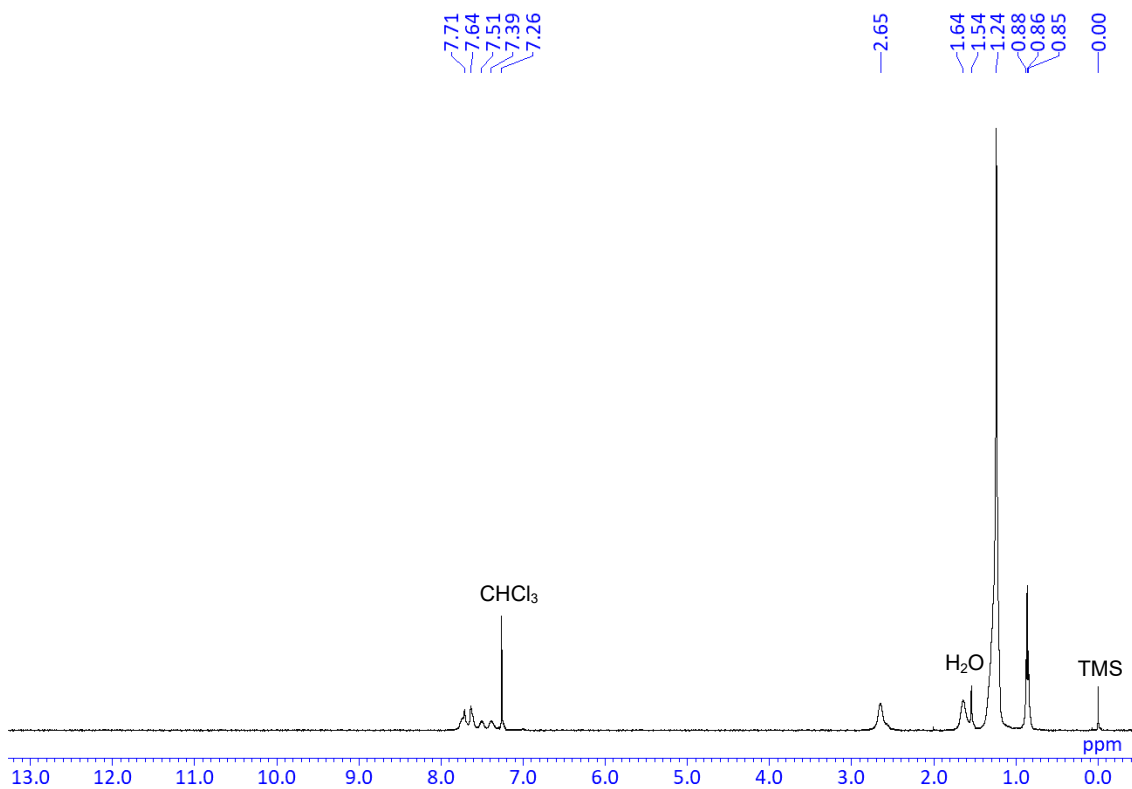


Chart S28. ^1H NMR spectrum of **P-BAz-3F** in CDCl_3 , 400 MHz.

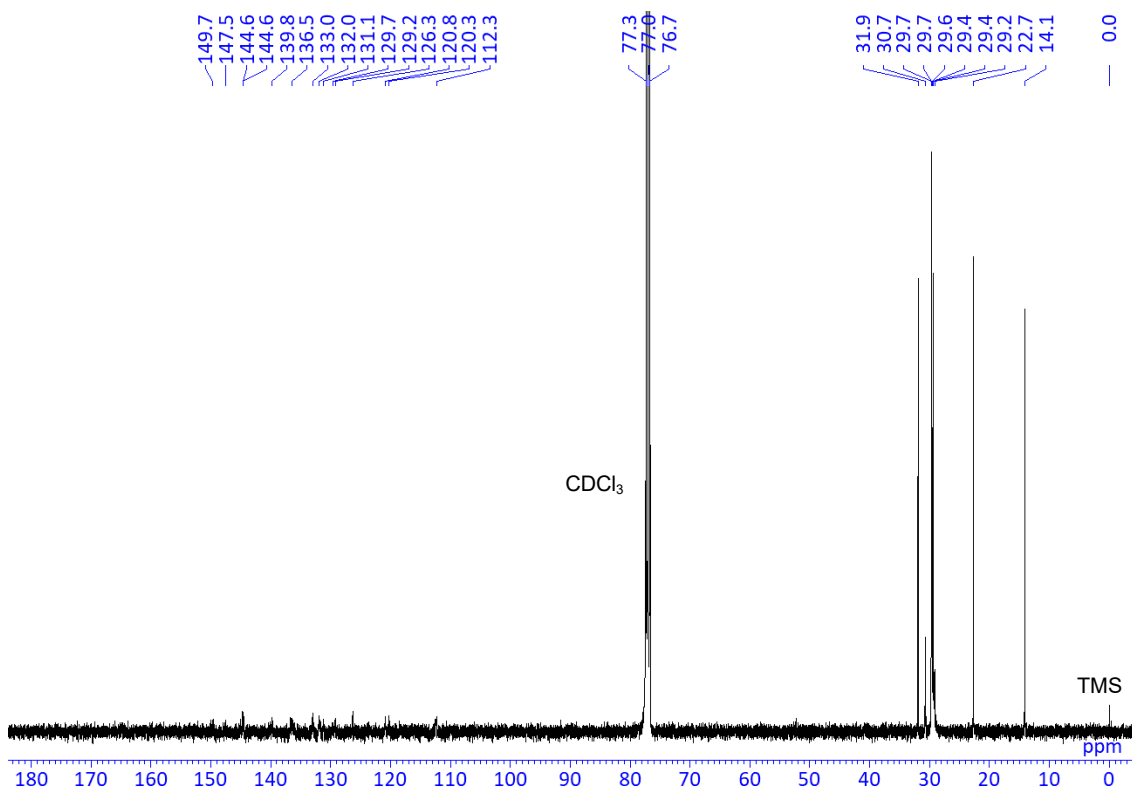


Chart S29. ^{13}C NMR spectrum of **P-BAz-3F** in CDCl_3 , 100 MHz.

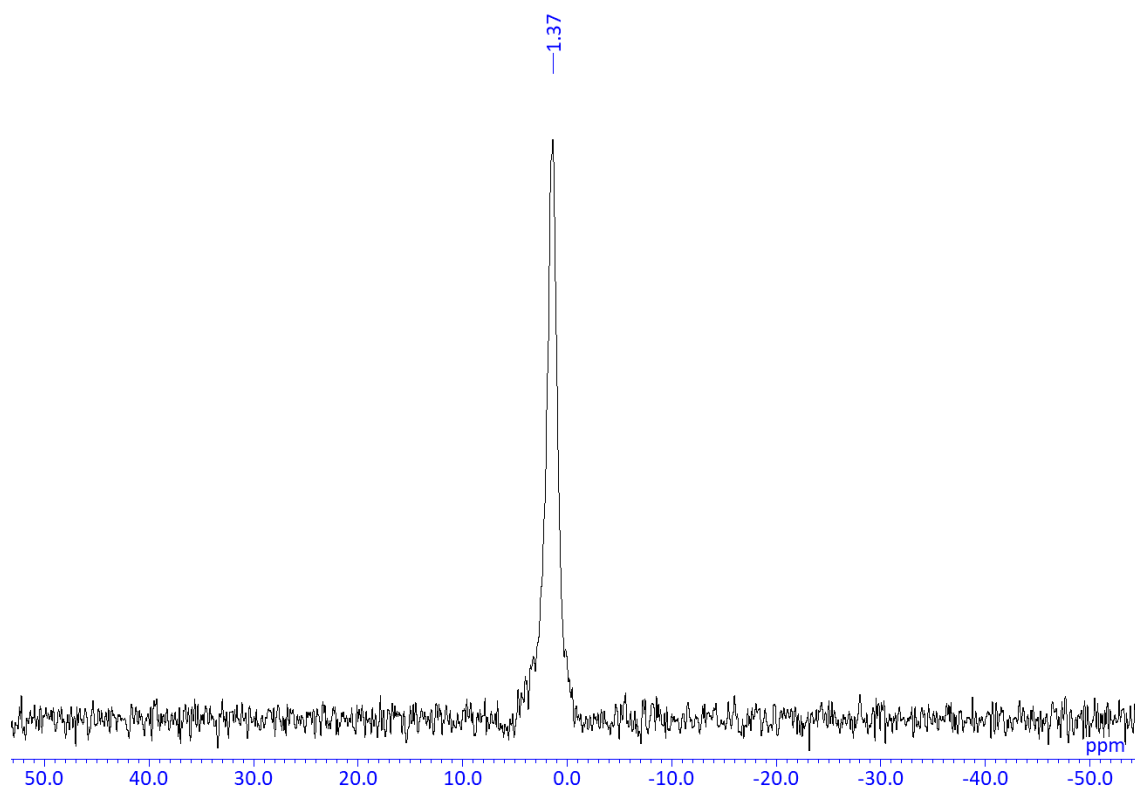
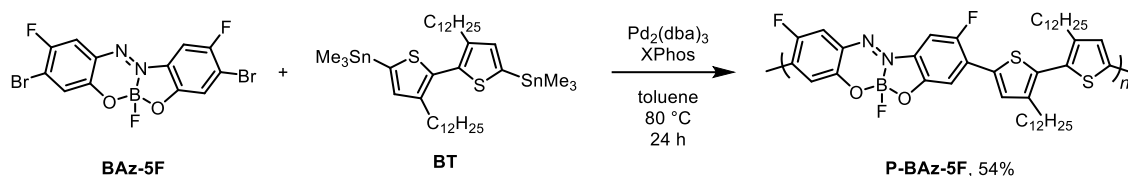


Chart S30. ^{11}B NMR spectrum of **P-BAz-3F** in CDCl_3 , 128 MHz.

Synthesis of P-BAz-5F



A mixture of **BAz-5F** (217 mg, 0.50 mmol), 5,5'-bis(trimethylstannyl)-3,3'-didodecyl-2,2'-bithiophene (**BT**) (414.3 mg, 0.50 mmol), Pd₂(dba)₃ (13.7 mg, 0.015 mmol), XPhos (14.3 mg, 0.030 mmol) was placed in a round-bottom flask equipped with a magnetic stirring bar. After degassing and filling N₂ three times, toluene (10 mL) was added to the mixture. The reaction was carried out at 80 °C for 24 h. After the reaction, the obtained polymer was redissolved in a small amount of CHCl₃, and then the product was reprecipitated from MeOH. The high molecular weight of the polymer was fractionated by HPLC. The obtained fraction was redissolved in a small amount of CHCl₃, and then the product was reprecipitated from MeOH. The polymer collected by filtration was dried in vacuo to afford **P-BAz-5F** (211 mg, 54%) as a black solid.

$M_n = 24,500$, $M_w = 48,500$, $M_w/M_n = 2.0$. ¹H NMR (CDCl₃, 400 MHz) δ 7.71–7.67 (br, 2H), 7.59–7.57 (br, 3H), 7.46 (d, $J = 5.9$ Hz, 1H), 2.65 (br, 4H), 1.64 (br, 4H), 1.24 (br, 36H), 0.86 (t, $J = 6.3$ Hz, 6H) ppm; ¹³C NMR (CDCl₃, 100 MHz) δ 157.4, 155.8, 153.3, 152.8, 144.5, 143.2, 138.5, 136.4, 135.9, 131.8, 130.9, 117.5, 116.2, 113.1, 104.2, 103.7, 31.9, 30.7, 29.7, 29.7, 29.6, 29.4, 29.4, 29.1, 22.7, 14.1 ppm; ¹¹B NMR (CDCl₃, 128 MHz) δ 1.37 ppm.

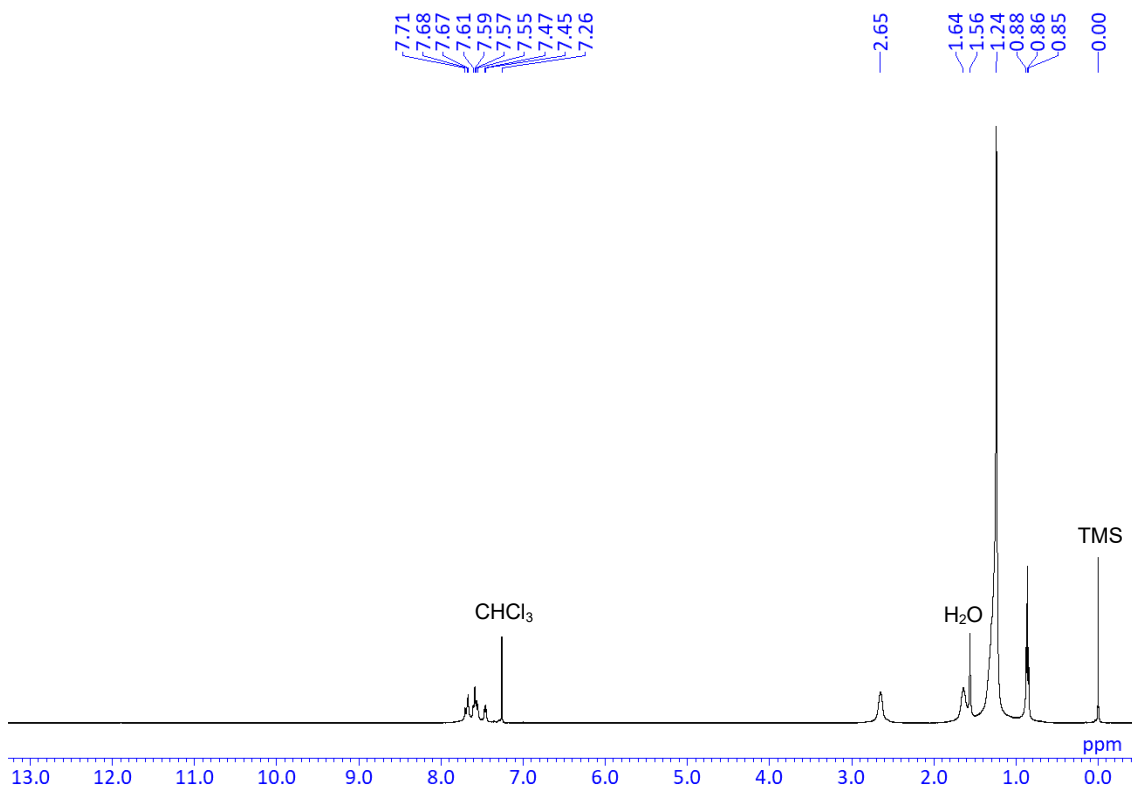


Chart S31. ¹H NMR spectrum of P-BAz-5F in CDCl₃, 400 MHz.

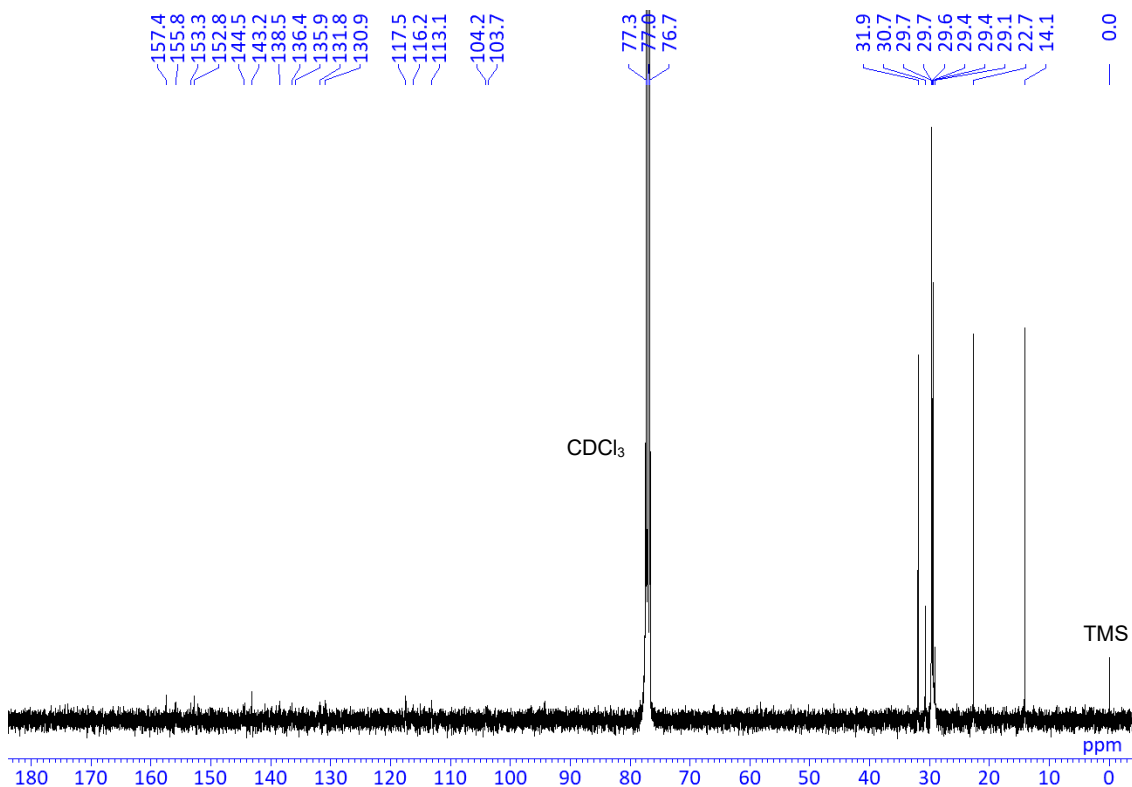


Chart S32. ¹³C NMR spectrum of P-BAz-5F in CDCl₃, 100 MHz.

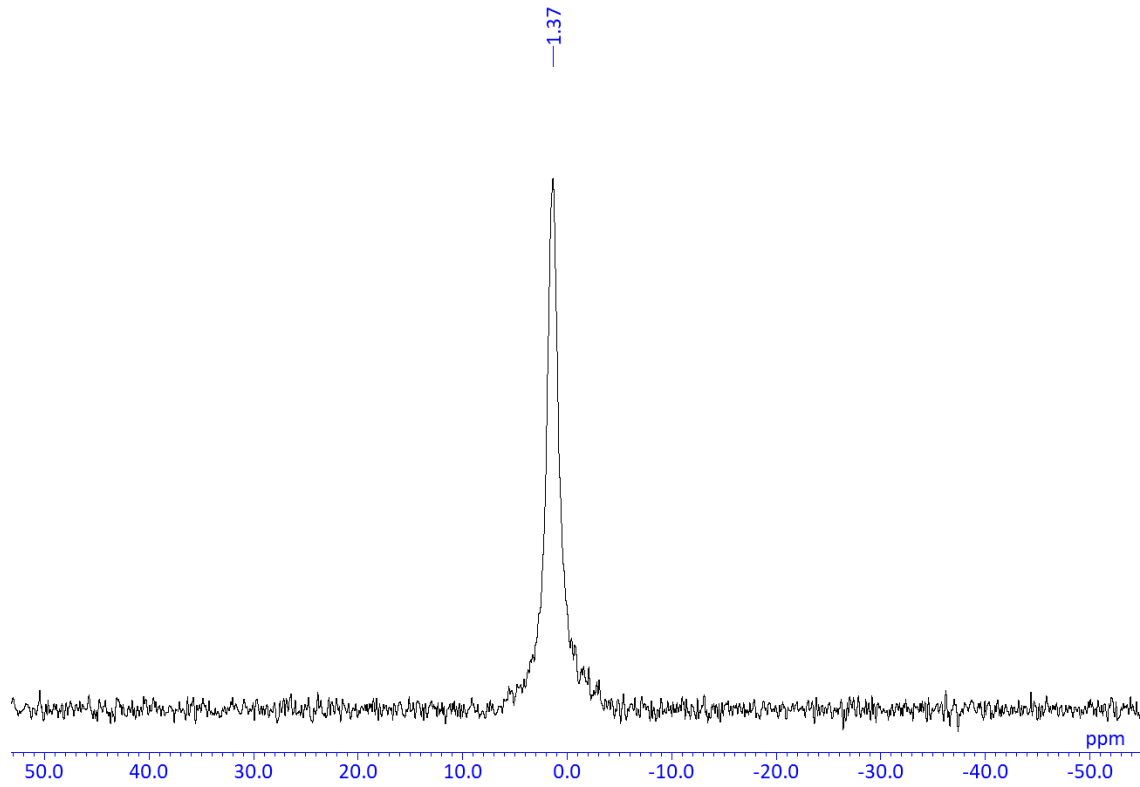
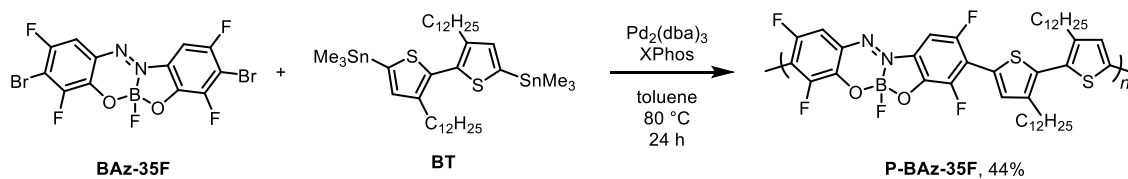


Chart S33. ¹¹B NMR spectrum of **P-BAz-5F** in CDCl₃, 128 MHz.

Synthesis of P-BAz-35F



A mixture of **BAz-35F** (47.2 mg, 0.10 mmol), 5,5'-bis(trimethylstannyl)-3,3'-didodecyl-2,2'-bithiophene (**BT**) (82.9 mg, 0.10 mmol), Pd₂(dba)₃ (2.7 mg, 0.0030 mmol), XPhos (2.9 mg, 0.0060 mmol) was placed in a round-bottom flask equipped with a magnetic stirring bar. After degassing and filling N₂ three times, toluene (2.0 mL) was added to the mixture. The reaction was carried out at 80 °C for 24 h. After the reaction, the obtained polymer was redissolved in a small amount of toluene, and then the product was purified by flash column chromatography on SiO₂. The obtained polymer was redissolved in a small amount of toluene, and then the product was reprecipitated from MeOH. The high molecular weight of the polymer was fractionated by HPLC. The obtained fraction was redissolved in a small amount of toluene, and then the product was reprecipitated from MeOH. The polymer collected by filtration was dried *in vacuo* to afford **P-BAz-35F** (35.8 mg, 44%)

$M_n = 13,400$, $M_w = 20,800$, $M_w/M_n = 1.6$. ¹H NMR (CDCl₃, 400 MHz) δ 7.89 (s, 1H), 7.78 (s, 1H), 7.61 (d, $J = 11$ Hz, 1H), 7.51 (d, $J = 8.5$ Hz, 1H), 2.68 (br, 4H), 1.65 (br, 4H), 1.24 (br, 36H), 0.87 (t, $J = 6.1$ Hz, 6H) ppm; ¹³C NMR (CDCl₃, 100 MHz) δ 155.4, 154.4, 152.9, 152.0, 147.6, 146.7, 145.1, 143.9, 143.7, 134.9, 134.4, 134.1, 133.3, 129.6, 111.4, 99.6, 31.9, 30.8, 29.7, 29.7, 29.6, 29.4, 29.4, 29.0, 22.7, 14.1 ppm; ¹¹B NMR (CDCl₃, 128 MHz) δ 1.37 ppm.

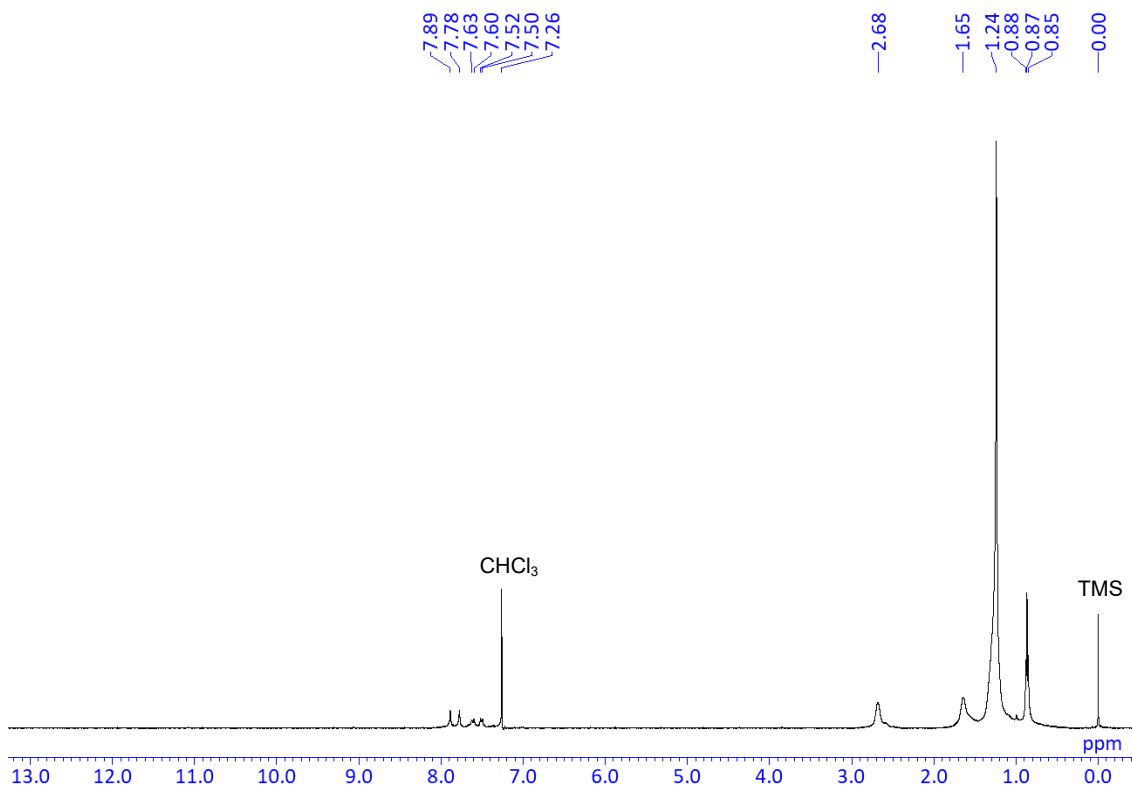


Chart S34. ¹H NMR spectrum of **P-BAz-35F** in CDCl₃, 400 MHz.

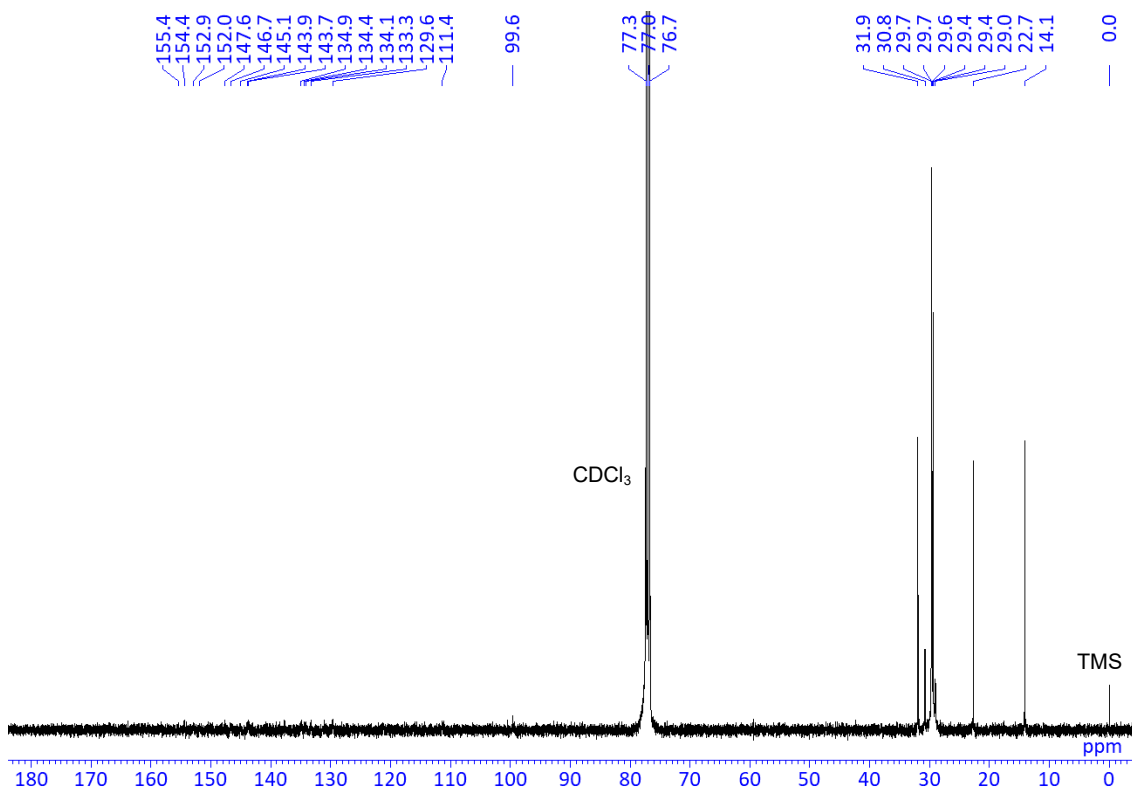


Chart S35. ¹³C NMR spectrum of **P-BAz-35F** in CDCl₃, 100 MHz.

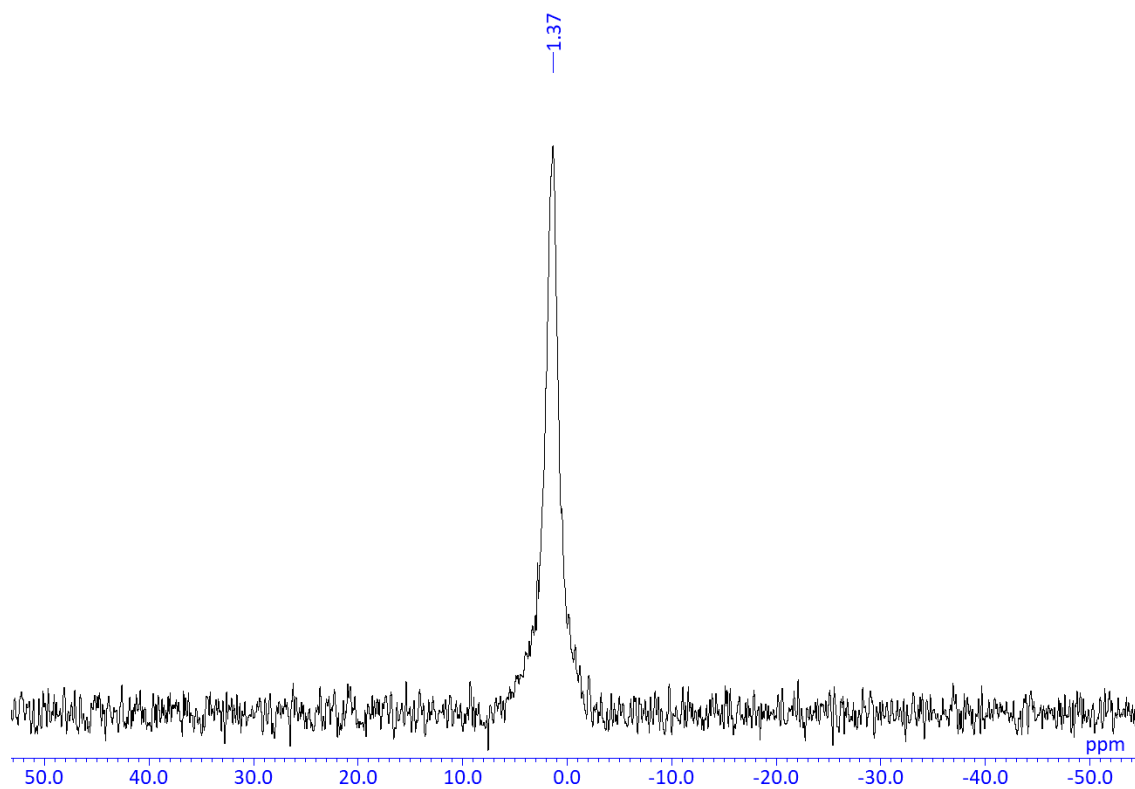


Chart S36. ^{11}B NMR spectrum of **P-BAz-35F** in CDCl_3 , 128 MHz.

Enlarged views of UV-vis-NIR absorption spectra

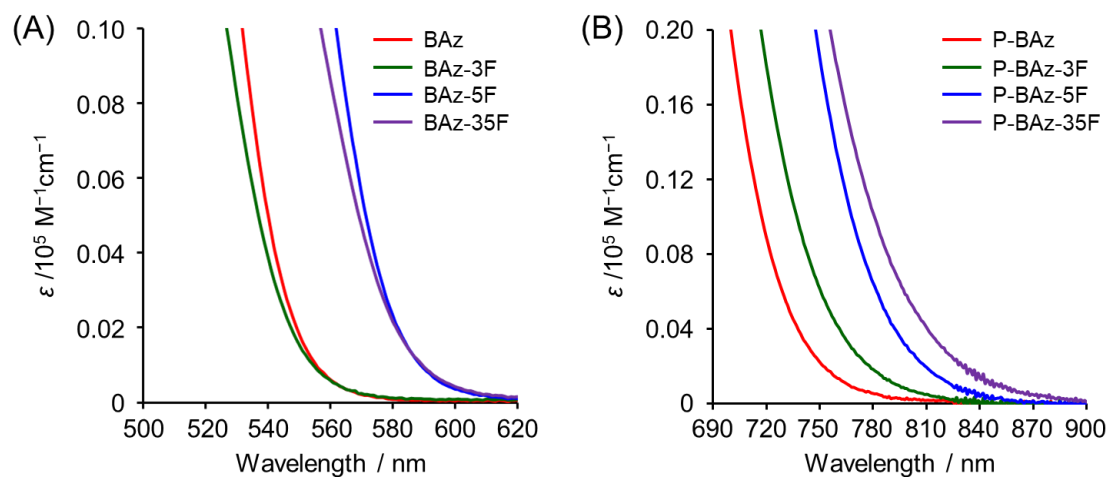


Figure S1. Enlarged views at edge of UV-vis absorption spectra of (A) BAZ monomers and (B) polymers in chloroform ($1.0 \times 10^{-5} \text{ M}$ for monomers, $1.0 \times 10^{-5} \text{ M}$ per repeating unit for polymers) for estimation of optical energy gaps.

Solvent effect of monomers

Lippert–Mataga plots

The Lippert–Mataga plots were constructed by using the relation below.

$$\nu = [2(\mu_e - \mu_g)^2 / hca^3] \Delta f + \nu^0$$

$$\Delta f = [(\epsilon - 1) / (2\epsilon + 1)] - [(n^2 - 1) / (2n^2 + 1)]$$

ν : Stokes shift

ν^0 : Stokes shift in the absence of solvent

μ_g : dipole moments in the ground state

μ_e : dipole moments in the excited state

a : Onsager cavity radius

Δf : orientation polarizability

ϵ : solvent dielectric constant

n : solvent refractive index

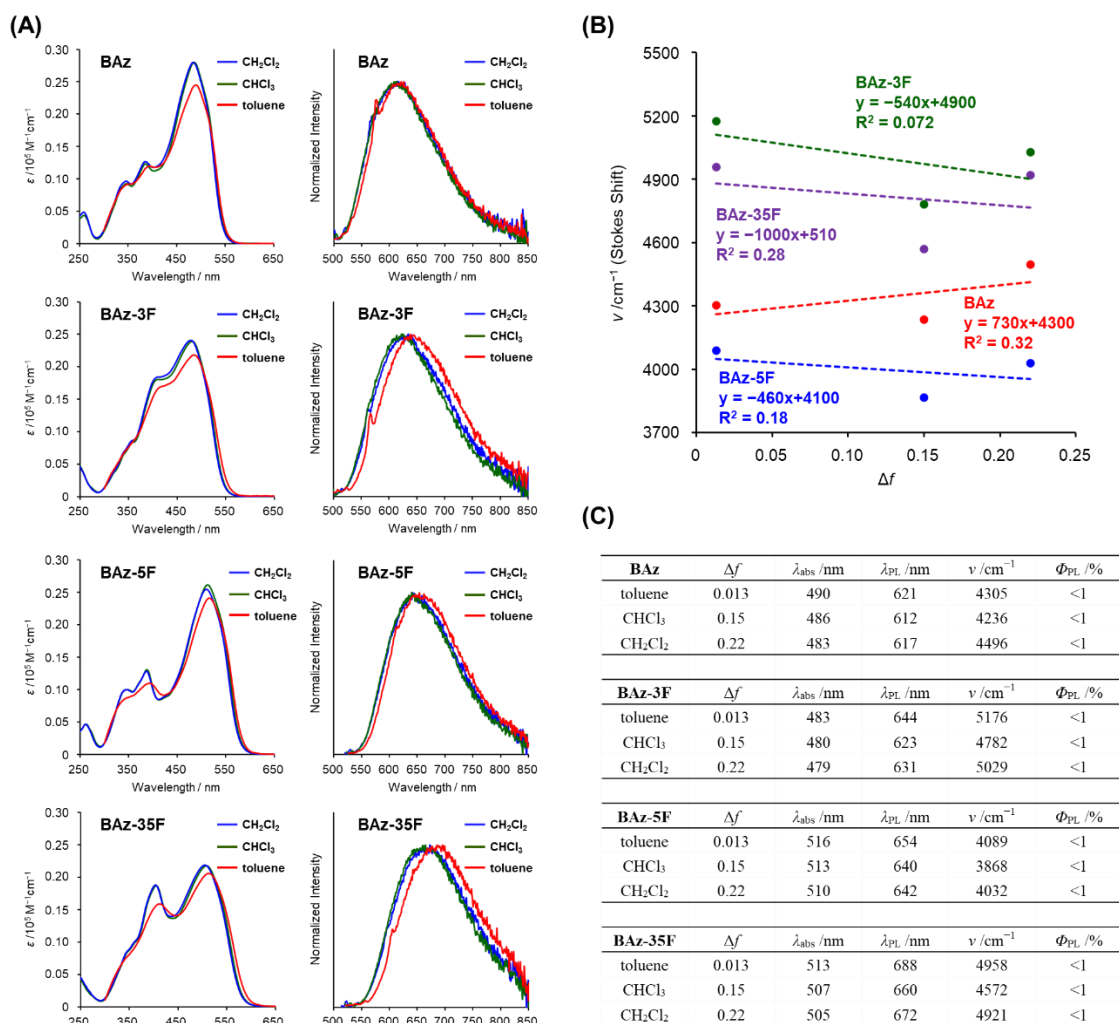


Figure S2. (A) UV-vis absorption (left) and PL spectra (right), (B) Lippert–Mataga plots and (C) spectroscopic data of **BAz**, **BAz-3F**, **BAz-5F** and **BAz-35F** in the diluted solutions (1.0×10^{-5} M) at room temperature, excited at the wavelength of the absorption maxima.

Solvent effect of polymers

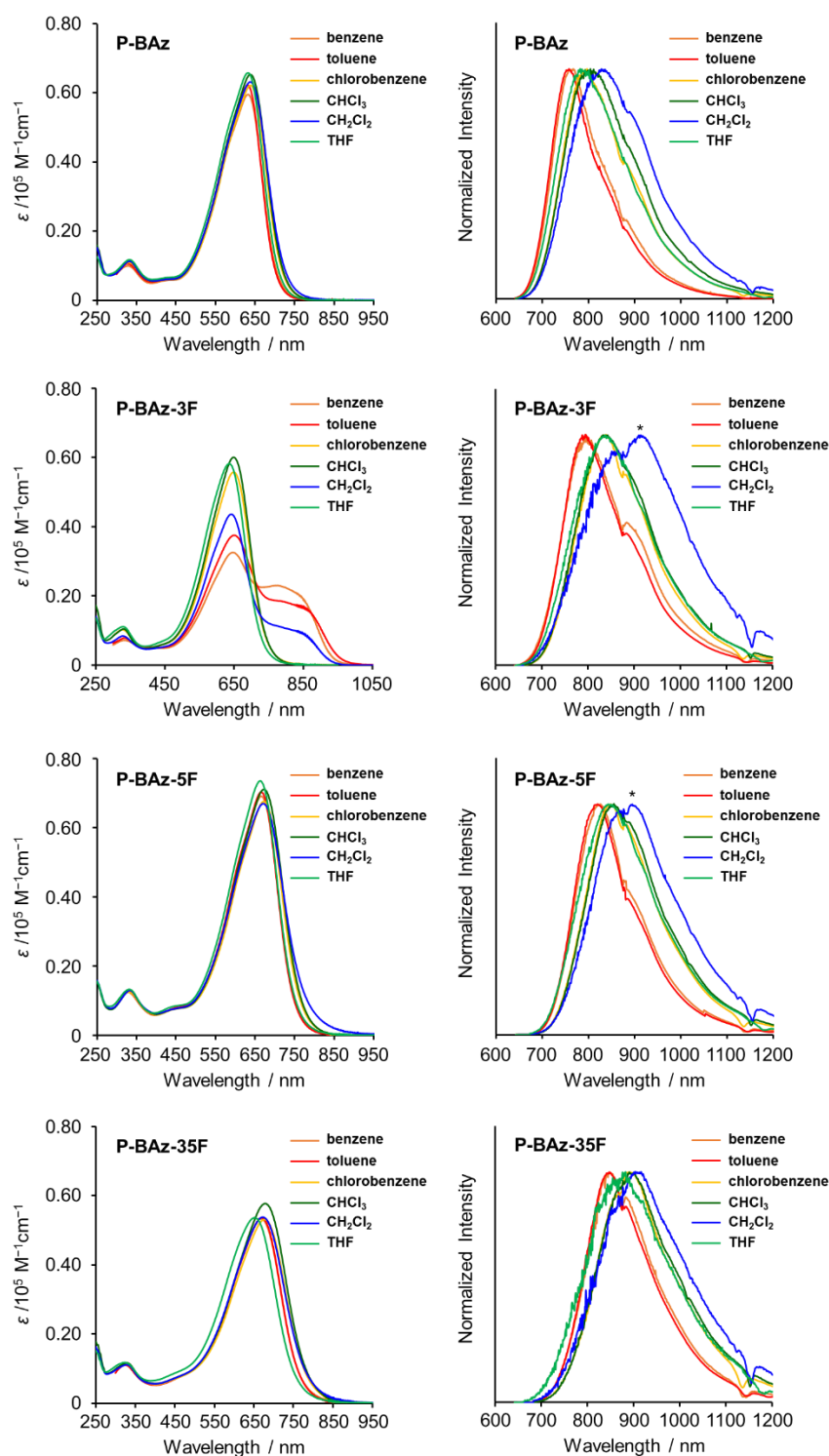


Figure S3. UV-vis-NIR absorption (left) and PL spectra (right) of **P-BAz**, **P-BAz-3F**, **P-BAz-5F** and **P-BAz-35F** in the diluted solutions (1.0×10^{-5} M per repeating unit, solvent/ $\text{CHCl}_3 = 99/1$ v/v) at room temperature, excited by absorption maxima. An asterisk denotes a noise peak.

Table S1. Spectroscopic data of **P-BAz** and **P-BAz-3F**

solvent	P-BAz				P-BAz-3F			
	λ_{abs}^a /nm	$\lambda_{\text{PL}}^{a,b}$ /nm	ν^c /cm ⁻¹	$\Phi_{\text{PL}}^{a,d}$ /%	λ_{abs}^a /nm	$\lambda_{\text{PL}}^{a,b}$ /nm	ν^c /cm ⁻¹	$\Phi_{\text{PL}}^{a,d}$ /%
benzene	633	767	2760	22	648	795	2853	4
toluene	631	758	2655	23	643	794	2958	8
chloro- benzene	638	797	3127	11	650	839	3466	6
CHCl ₃	637	804	3261	7	649	838	3475	4
CH ₂ Cl ₂	637	831	3665	2	650	863	3797	<1
THF	632	786	3100	5	650	837	3437	2

^a In solvent/CHCl₃ = 99/1 v/v (1.0×10⁻⁵ M)

^b Excited by λ_{abs}

^c Stokes shift; ν (cm⁻¹) = 1/(λ_{abs} (nm))×10⁷ - 1/(λ_{PL} (nm))×10⁷

^d Absolute PL quantum efficiency excited at λ_{abs} .

Table S2. Spectroscopic data of **P-BAz-5F** and **P-BAz-35F**

solvent	P-BAz-5F				P-BAz-35F			
	λ_{abs}^a /nm	$\lambda_{\text{PL}}^{a,b}$ /nm	ν^c /cm ⁻¹	$\Phi_{\text{PL}}^{a,d}$ /%	λ_{abs}^a /nm	$\lambda_{\text{PL}}^{a,b}$ /nm	ν^c /cm ⁻¹	$\Phi_{\text{PL}}^{a,d}$ /%
benzene	666	826	2908	10	667	848	3200	5
toluene	666	821	2835	11	670	846	3105	7
chloro- benzene	672	848	3088	5	678	892	3539	2
CHCl ₃	672	853	3158	3	677	897	3623	2
CH ₂ Cl ₂	671	867	3369	1	672	913	3928	<1
THF	663	846	3263	2	650	848	3592	<1

^a In solvent/CHCl₃ = 99/1 v/v (1.0×10⁻⁵ M)

^b Excited by λ_{abs}

^c Stokes shift; ν (cm⁻¹) = 1/(λ_{abs} (nm))×10⁷ - 1/(λ_{PL} (nm))×10⁷

^d Absolute PL quantum efficiency excited at λ_{abs} .

Lippert–Mataga plots of polymers

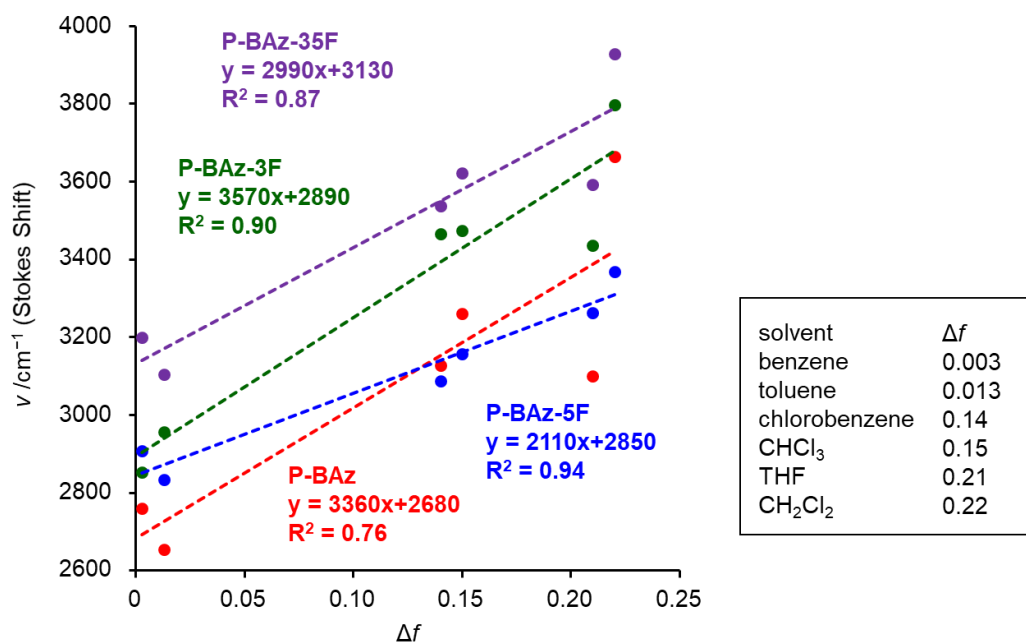


Figure S4. Lippert–Mataga plots of **P-BAz**, **P-BAz-3F**, **P-BAz-5F** and **P-BAz-35F** in the diluted solutions (1.0×10^{-5} M) at room temperature including THF data. Plotted data are listed in Tables S1 and S2.

Variable temperature absorption spectra and PL spectra

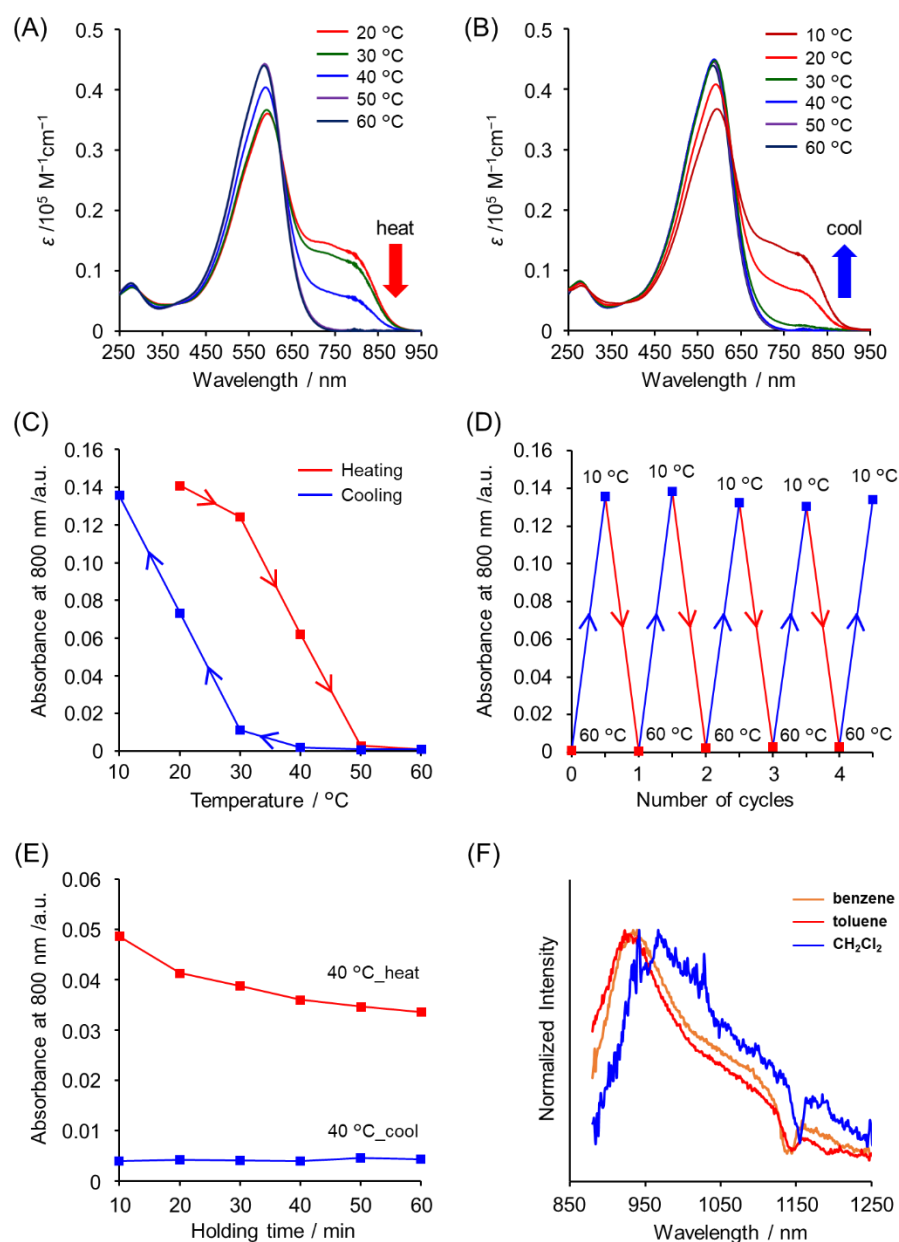


Figure S5. (A–E) Variable temperature UV–vis–NIR absorption spectra of **P-BAz-3F** in toluene/CHCl₃ = 99/1 v/v (1.0×10^{-5} M per repeating unit). (A) Heating profiles with 10 min holding time at each temperature. (B) Cooling profiles with 10 min holding time at each temperature. (C) Monitoring absorbance at 800 nm of Figures S5A and S5B. (D) Reversibility of spectrum variation monitoring absorbance at 800 nm between at 60 °C and 10 °C with 10 min holding time at each temperature. (E) Monitoring absorbance at 800 nm during holding 40 °C under heating or cooling process. (F) PL spectra in solvent/CHCl₃ = 99/1 v/v (1.0×10^{-5} M per repeating unit) excited at 772 nm.

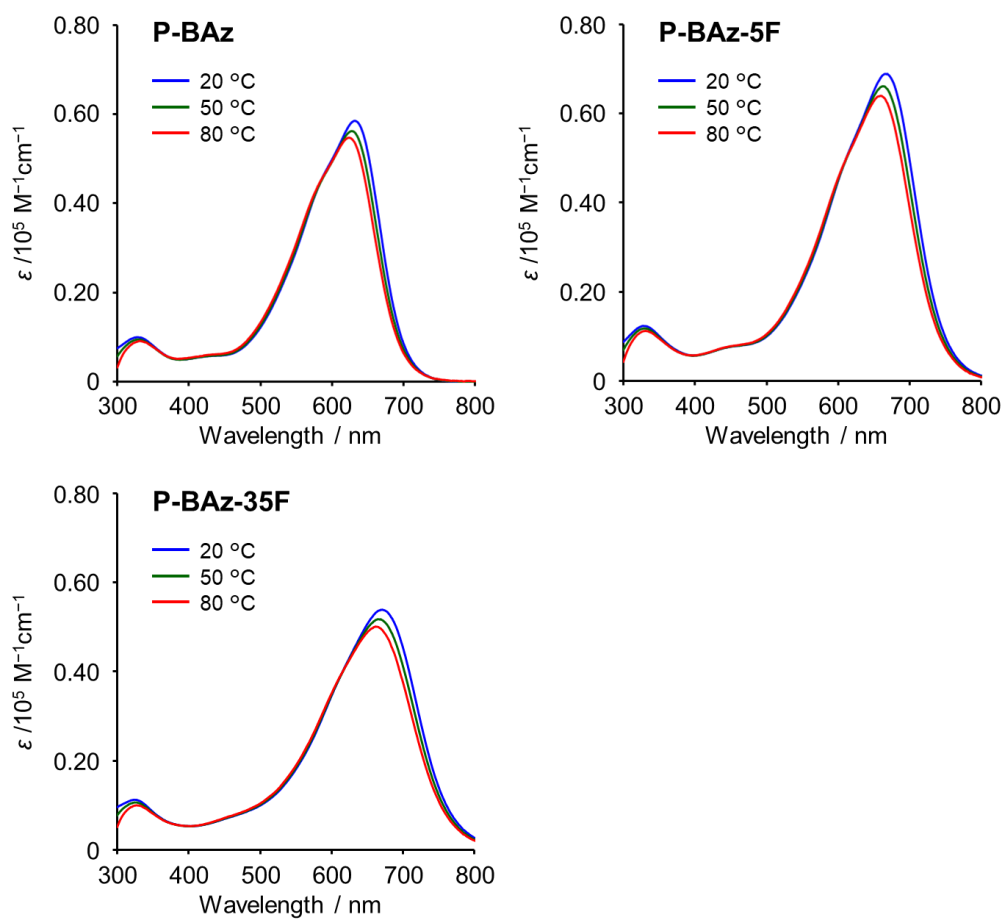



Figure S6. Variable temperature UV–vis–NIR absorption spectra of **P-BAz**, **P-BAz-5F** and **P-BAz-35F** in toluene (1.0×10^{-5} M per repeating unit).

Single crystal X-ray structure analysis of BAz

Intensity data were collected on a Rigaku R-AXIS RAPID imaging plate area detector with graphite monochromated MoK α radiation ($\lambda = 0.71069 \text{ \AA}$). The structures were solved and refined by full-matrix least-squares procedures based on F^2 (SHELX-2014).^[9]

Table S3. Crystallographic data of **BAz**

Empirical formula	C ₁₂ H ₆ BBr ₂ FN ₂ O ₂	 <p style="text-align: center;">BAz CCDC # 2054961</p>
Formula weight	399.82	
Temperature (K)	93(2)	
Wavelength (Å)	0.71075	
Crystal system, space group	Triclinic, $P-1$	
Unit cell dimensions	a=6.9614(13) b=7.2752(14) c=14.275(3) $\alpha=95.280(7)$ $\beta=97.895(7)$ $\gamma=115.814(8)$	
Volume (Å ³)	635.3(2)	
Z, calculated density (g cm ⁻³)	2, 2.090	
Absorption coefficient	6.392	
F(000)	384	
Crystal size (mm)	0.30 × 0.20 × 0.10	
θ range for data collection	3.155-27.58	
Limiting indices	$-9 \leq h \leq 9$, $-9 \leq k \leq 9$, $-18 \leq l \leq 18$	
Reflections collected (unique)	5835/3969 [$R(\text{int})=0.0878$]	
Completeness to theta	0.994	
Max. and min. transmission	1.000, 0.063	
Goodness-of-fit on F^2	1.054	
Final R indices [$I > 2\sigma(I)$] ^a	$R_1 = 0.0778$, $wR_2 = 0.2084$	
R indices (all data)	$R_1 = 0.1155$, $wR_2 = 0.2387$	

^a $R_1 = \Sigma(|F_0| - |F_c|) / \Sigma|F_0|$. $wR_2 = [\Sigma w(F^2_0 - F^2_c)^2 / \Sigma w(F^2_0)^2]^{1/2}$. $w = 1 / [\sigma^2(F^2_0) + (ap)^2 + bp]$, where $p = [\max(F^2_0, 0) + 2F^2_c] / 3$.

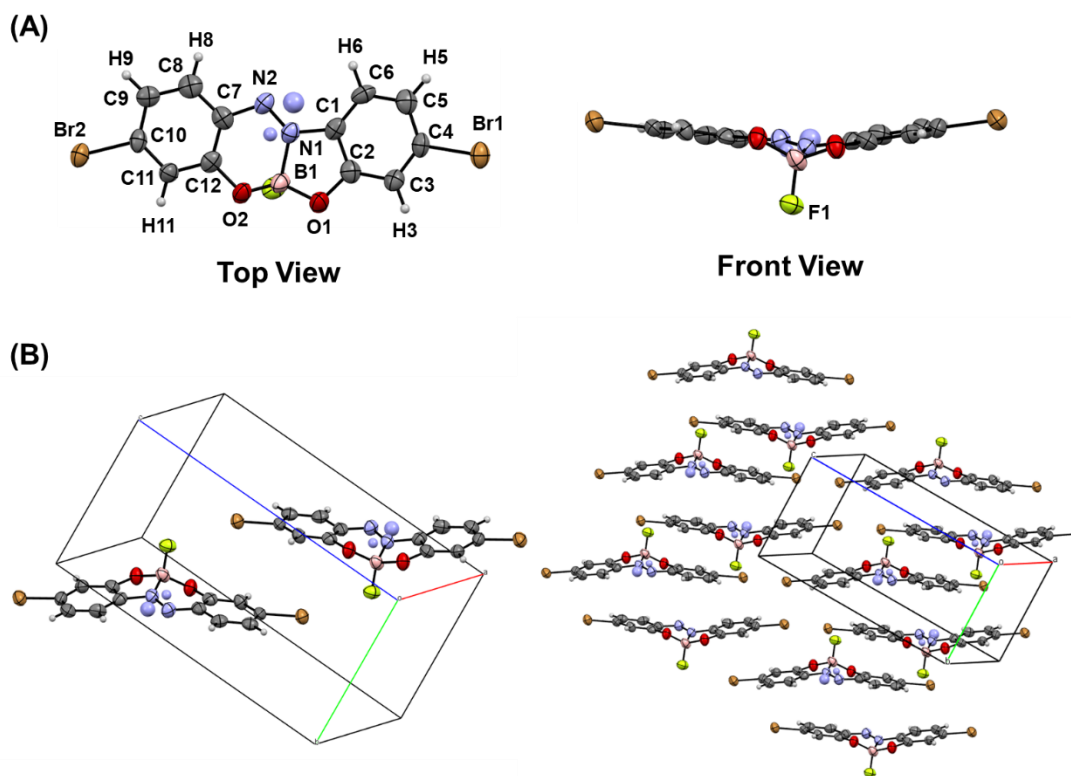
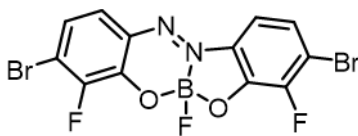


Figure S7. (A) ORTEP drawings and (B) packing diagrams of **BAz**. Thermal ellipsoids are scaled to the 50% probability level.

Single crystal X-ray structure analysis of BAz-3F

Intensity data were collected on a Rigaku Saturn 724+ with MicroMax-007HF CCD diffractometer with Varimax Mo optics using graphite-monochromated MoK α radiation. The structures were solved and refined by full-matrix least-squares procedures based on F^2 (SHELXL-2014/7).^[9]

Table S4. Crystallographic data of **BAz-3F**

Empirical formula	C ₁₂ H ₄ BBr ₂ F ₃ N ₂ O ₂	 <p style="text-align: center;">BAz-3F</p> <p style="text-align: center;">CCDC # 2054962</p>
Formula weight	435.80	
Temperature (K)	143(2)	
Wavelength (Å)	0.71075	
Crystal system, space group	Monoclinic, <i>P</i> 21/ <i>c</i>	
Unit cell dimensions (Å)	a=8.659(6) b=7.316(5) c=20.883(14)	
Unit cell dimensions (°)	α =90 β =93.436(10) γ =90	
Volume (Å ³)	1320.5(16)	
Z, calculated density (g cm ⁻³)	4, 2.192	
Absorption coefficient	6.181	
F(000)	832	
Crystal size (mm)	0.17 × 0.10 × 0.05	
θ range for data collection	3.2-27.4	
Limiting indices	-10 ≤ <i>h</i> ≤ 11, -9 ≤ <i>k</i> ≤ 9, -26 ≤ <i>l</i> ≤ 27	
Reflections collected (unique)	10304/1835 [<i>R</i> (int)=0.0859]	
Completeness to theta	0.994	
Max. and min. transmission	1.000, 0.798	
Goodness-of-fit on F^2	1.009	
Final <i>R</i> indices [<i>I</i> > 2 σ (<i>I</i>)] ^a	<i>R</i> ₁ = 0.0570, w <i>R</i> ₂ = 0.1042	
<i>R</i> indices (all data)	<i>R</i> ₁ = 0.0950, w <i>R</i> ₂ = 0.1189	

^a $R_1 = \Sigma(|F_0| - |F_c|) / \Sigma|F_0|$. $wR_2 = [\Sigma w(F^2_0 - F^2_c)^2 / \Sigma w(F^2_0)^2]^{1/2}$. $w = 1 / [\sigma^2(F^2_0) + (ap)^2 + bp]$, where $p = [\max(F^2_0, 0) + 2F^2_c] / 3$.

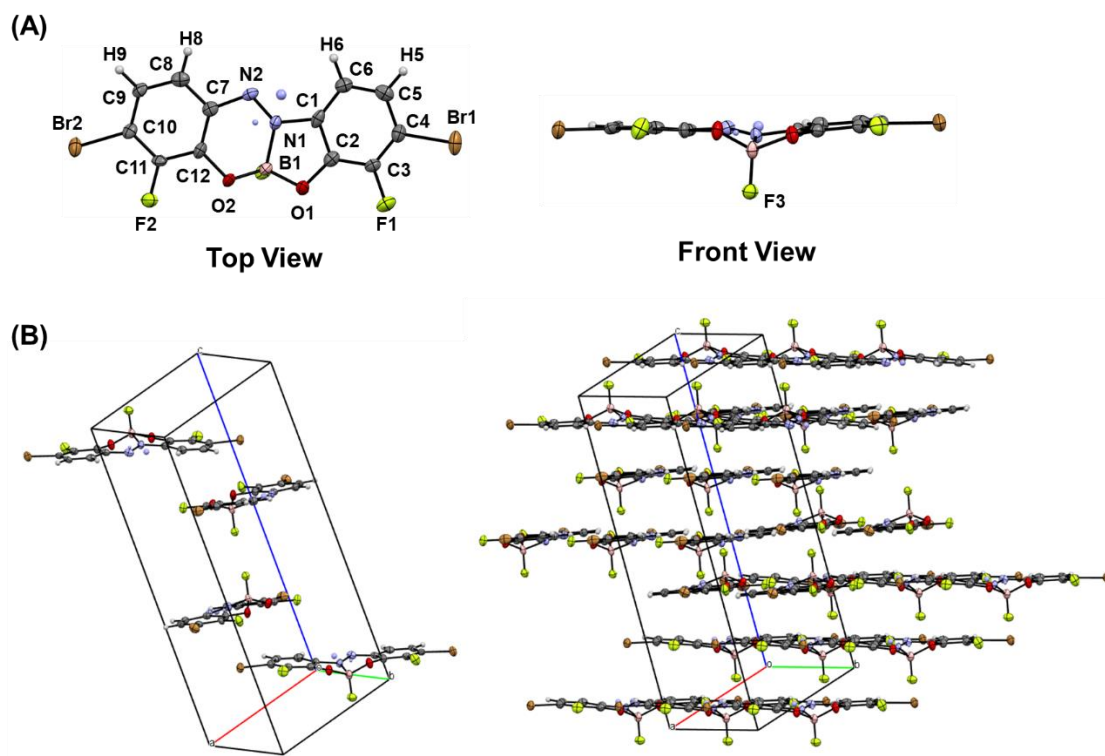


Figure S8. (A) ORTEP drawings and (B) packing diagrams of **BAz-3F**. Thermal ellipsoids are scaled to the 50% probability level.

Intermolecular interaction in BAz and BAz-3F crystals

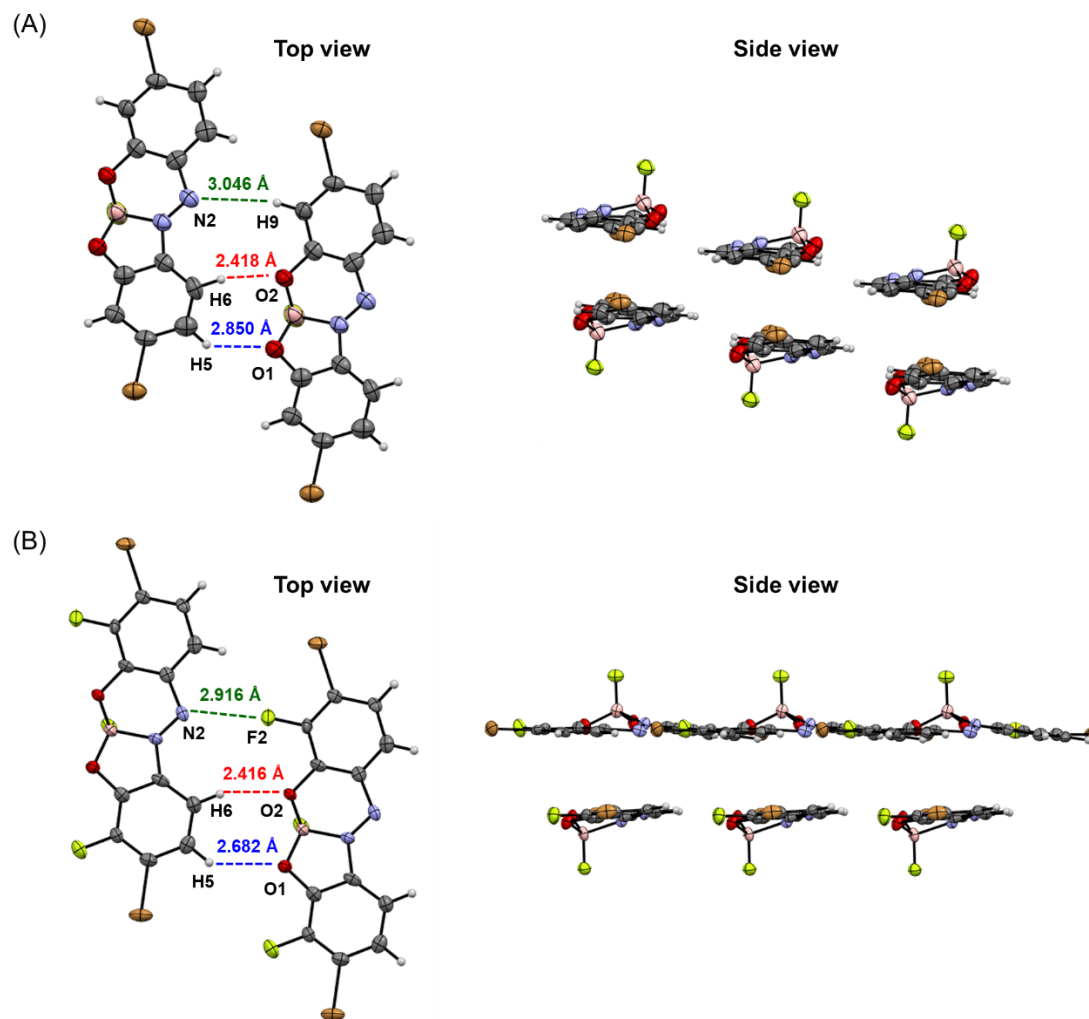


Figure S9. Intermolecular interaction between two fractions in crystal and packing diagrams of (A) **BAz** and (B) **BAz-3F**. Thermal ellipsoids of ORTEP drawings are scaled to the 50% probability level.

Cyclic voltammetry

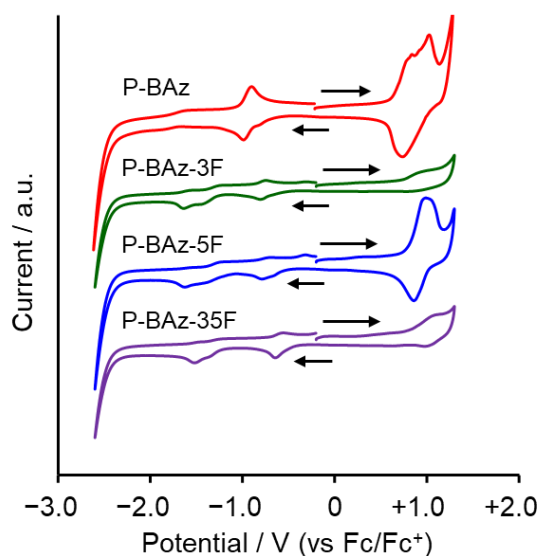


Figure S10. Cyclic voltammograms of BAz polymers in dichloromethane (1.0×10^{-3} M for monomers, 1.0×10^{-3} M per repeating unit for polymers) containing $n\text{Bu}_4\text{NPF}_6$ (0.10 M) at room temperature with a scan rate of 0.1 V s^{-1} (positive scan). The black arrows denote sweep directions (positive scan).

Table S5. Energy levels of molecular orbitals of BAz polymers

	$E_{\text{onset}}^{\text{ox} a} / \text{V}$	$E_{\text{HOMO}}^b / \text{eV}$
P-BAz	0.63	-5.43
P-BAz-3F	0.71	-5.51
P-BAz-5F	0.81	-5.61
P-BAz-35F	0.78	-5.58

^a In dichloromethane (1.0×10^{-3} M for monomers, 1.0×10^{-3} M per repeating unit for polymers) containing $n\text{Bu}_4\text{NPF}_6$ (0.10 M) at room temperature with a scan rate of 0.1 V s^{-1} (positive scan).

^b $E_{\text{HOMO}} = -(4.8 - E_{\text{onset}}^{\text{ox}})$ (eV),^[10] $E_{\text{LUMO}} = E_{\text{HOMO}} + E_{\text{g,opt}}$.

Computational details for theoretical calculation

The Gaussian 16 program package^[11] was used for computation. We optimized the structures of the **BAz**, **BAz-3F**, **BAz-5F**, **BAz-35F**, **BAz-BT**, **BAz-3F-BT**, **BAz-5F-BT** and **BAz-35F-BT** in the ground S_0 states and calculated their molecular orbitals. The density functional theory (DFT) was applied for the optimization of the structures in the S_0 states at B3LYP/6-311G(d,p) level. We calculated the energy of the transitions with optimized geometries in the S_0 states by time-dependent (TD) DFT at B3LYP/6-311G(d,p) level.

Results of representative transitions of BAz complexes

Table S6. Results of representative transitions of BAz monomers from TD-DFT calculations

	Energy gap / eV	Wavelength / nm	Oscillator Strength	transition	Assignment (Weight) (Contribution)
BAz	2.6788	462.83	0.5457	$S_0 \rightarrow S_1$	HOMO \rightarrow LUMO (0.68044) (93%)
	3.0733	403.42	0.0833	$S_0 \rightarrow S_2$	HOMO-1 \rightarrow LUMO (0.68790) (95%)
	3.2301	383.84	0.1318	$S_0 \rightarrow S_3$	HOMO-2 \rightarrow LUMO (0.62041) (77%)
BAz-3F	2.6461	468.55	0.3538	$S_0 \rightarrow S_1$	HOMO \rightarrow LUMO (0.63267) (80%)
	2.8772	430.92	0.0780	$S_0 \rightarrow S_2$	HOMO-1 \rightarrow LUMO (0.64190) (82%)
	3.0293	409.28	0.3814	$S_0 \rightarrow S_3$	HOMO-2 \rightarrow LUMO (0.61079) (75%)
BAz-5F	2.5189	492.21	0.4818	$S_0 \rightarrow S_1$	HOMO \rightarrow LUMO (0.68645) (94%)
	2.8937	428.47	0.0560	$S_0 \rightarrow S_2$	HOMO-1 \rightarrow LUMO (0.69340) (96%)
	3.1901	388.65	0.2089	$S_0 \rightarrow S_3$	HOMO-2 \rightarrow LUMO (0.61019) (74%)
BAz-35F	2.4877	498.39	0.3374	$S_0 \rightarrow S_1$	HOMO \rightarrow LUMO (0.66468) (88%)
	2.7311	453.97	0.0465	$S_0 \rightarrow S_2$	HOMO-1 \rightarrow LUMO (0.68785) (95%)
	3.0268	409.63	0.4316	$S_0 \rightarrow S_3$	HOMO-2 \rightarrow LUMO (0.64342) (83%)

Table S7. Results of representative transitions of BAz model compounds from TD-DFT calculations

	Energy gap / eV	Wavelength / nm	Oscillator Strength	transition	Assignment (Weight) (Contribution)
BAz-BT	2.1932	565.31	1.5942	$S_0 \rightarrow S_1$	HOMO \rightarrow LUMO (0.70518) (99%)
BAz-3F-BT	2.1116	587.16	1.6778	$S_0 \rightarrow S_1$	HOMO \rightarrow LUMO (0.70642) (99%)
BAz-5F-BT	2.0652	600.36	1.5958	$S_0 \rightarrow S_1$	HOMO \rightarrow LUMO (0.70607) (99%)
BAz-35F-BT	1.9857	624.38	1.6409	$S_0 \rightarrow S_1$	HOMO \rightarrow LUMO (0.70675) (99%)

Molecular orbitals of BAz complexes

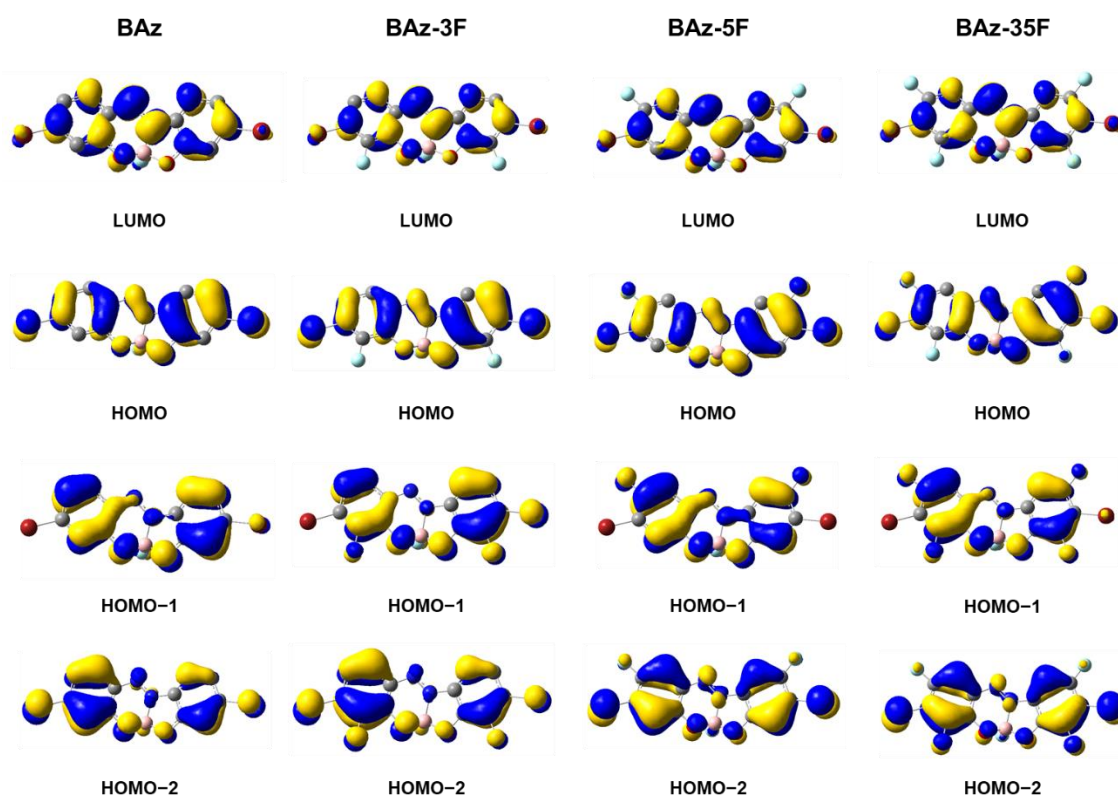


Figure S11. Selected Kohn–Sham orbitals of **BAz** monomers obtained with DFT calculations (isovalue = 0.03). Hydrogens were omitted for clarity.

Selected Kohn–Sham orbitals of model compounds

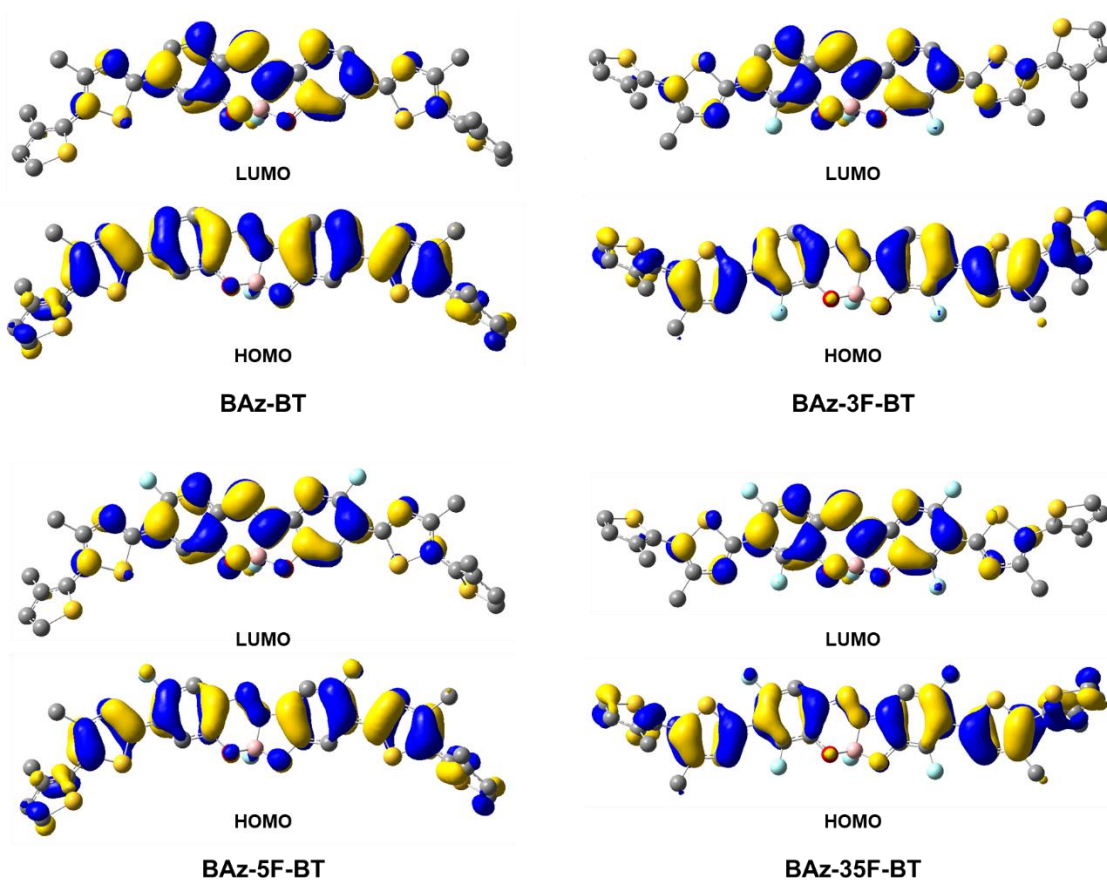


Figure S12. Selected Kohn–Sham orbitals of model compounds **BAz-BT**, **BAz-3F-BT**, **BAz-5F-BT** and **BAz-35F-BT** obtained with DFT calculations (isovalue = 0.025). Hydrogens were omitted for clarity.

References

- [1] T. Higashi, ABSCOR. Program for Absorption Correction.; Rigaku Corporation: Japan, **1995**.
- [2] G. M. Sheldrick, SHELX-97. Programs for Crystal Structure Analysis.; University of Göttingen: Germany, **1997**.
- [3] K. Wakita, Yadokari&XG. Program for Crystal Structure Analysis.; **2000**.
- [4] L. J. Farrugia, *J. Appl. Cryst.* **1997**, *30*, 565.
- [5] A. B. Pangborn, M. A. Giardello, R. H. Grubbs, R. K. Rosen, F. J. Timmers, *Organometallics* **1996**, *15*, 1518–1520.
- [6] M. Gon, K. Tanaka and Y. Chujo, *Angew. Chem. Int. Ed.* **2018**, *57*, 6546–6551.
- [7] R. Yoshii, K. Tanaka, Y. Chujo, *Macromolecules* **2014**, *47*, 2268–2278.
- [8] X. Guo, Q. Liao, E. F. Manley, Z. Wu, Y. Wang, W. Wang, T. Yang, Y.-E. Shin, X. Cheng, Y. Liang, L. X. Chen, K.-J. Baeg, T. J. Marks, X. Guo, *Chem. Mater.* **2016**, *28*, 2449–2460.
- [9] G. M. Sheldrick, *Acta Cryst.* **2015**, *C71*, 3–8.
- [10] a) J. Pommerehne, H. Vestweber, W. Guss, R. F. Mahrt, H. Bässler, M. Porsch, J. Daub, *Adv. Mater.* **1995**, *7*, 551–554; b) C. M. Cardona, W. Li, A. E. Kaifer, D. Stockdale, G. C. Bazan, *Adv. Mater.* **2011**, *23*, 2367–2371.
- [11] Gaussian 16, Revision A.03, M. J. Frisch, G. W. Trucks, H. B. Schlegel, G. E. Scuseria, M. A. Robb, J. R. Cheeseman, G. Scalmani, V. Barone, G. A. Petersson, H. Nakatsuji, X. Li, M. Caricato, A. V. Marenich, J. Bloino, B. G. Janesko, R. Gomperts, B. Mennucci, H. P. Hratchian, J. V. Ortiz, A. F. Izmaylov, J. L. Sonnenberg, D. Williams-Young, F. Ding, F. Lipparini, F. Egidi, J. Goings, B. Peng, A. Petrone, T. Henderson, D. Ranasinghe, V. G. Zakrzewski, J. Gao, N. Rega, G. Zheng, W. Liang, M. Hada, M. Ehara, K. Toyota, R. Fukuda, J. Hasegawa, M. Ishida, T. Nakajima, Y. Honda, O. Kitao, H. Nakai, T. Vreven, K. Throssell, J. A. Montgomery, Jr., J. E. Peralta, F. Ogliaro, M. J. Bearpark, J. J. Heyd, E. N. Brothers, K. N. Kudin, V. N. Staroverov, T. A. Keith, R. Kobayashi, J. Normand, K. Raghavachari, A. P. Rendell, J. C. Burant, S. S. Iyengar, J. Tomasi, M. Cossi, J. M. Millam, M. Klene, C. Adamo, R. Cammi, J. W. Ochterski, R. L. Martin, K. Morokuma, O. Farkas, J. B. Foresman, and D. J. Fox, Gaussian, Inc., Wallingford CT, 2016.